



Some pages of this thesis may have been removed for copyright restrictions.

If you have discovered material in Aston Research Explorer which is unlawful e.g. breaches copyright, (either yours or that of a third party) or any other law, including but not limited to those relating to patent, trademark, confidentiality, data protection, obscenity, defamation, libel, then please read our [Takedown policy](#) and contact the service immediately (openaccess@aston.ac.uk)

PROGRAMMED FATIGUE OF A LOW
CARBON STEEL

by

A.E. INCKLE A.I.M.

A THESIS SUBMITTED TO THE UNIVERSITY OF
ASTON IN BIRMINGHAM FOR THE
DEGREE OF DOCTOR OF PHILOSOPHY

OCTOBER 1971

669.0192
INC

-3 JAN 72 146233

SUMMARY

Fatigue crack propagation has been investigated in single edge notched mild steel specimens under constant and programmed loading conditions. Results have been analysed by the fracture mechanics approach and the Palmgren-Miner summation. Fracture surfaces were examined with a Cambridge Stereoscan scanning electron microscope.

In tests where both load rises and load drops were included, the cumulative cycle ratio was always slightly greater than unity, irrespective of block size, load level, rate of load change or sequence. When the programme consisted only of load rises, the cumulative cycle ratio decreased below unity. These results have been explained in terms of residual stresses developed at the crack tip during load changes. The fracture mechanics analysis was found to provide a satisfactory method of data correlation, provided the effects of material and experimental variables were fully appreciated. However, no single value of slope of the $\log \Delta K - \log da/dN$ relationship will apply to all materials and conditions. In the absence of residual stresses due to manufacturing processes, computer integration of the constant amplitude fracture mechanics data will provide a satisfactory method of life prediction.

Fractographic observations showed that striation spacings were often larger than the macroscopic crack growth rate. This effect was discussed in terms of discontinuous crack front movement. Striation spacing measurements were not therefore useful as a technique of correlating macroscopic crack growth rate with the microscopic observations. However, two distinct modes of fracture were observed to occur. The first (designated stage IIa) was structure sensitive, whilst the second (designated stage IIb) was structure insensitive. The transition from stage IIa to stage IIb occurred when the radius of the plastic zone ahead of the crack tip reached a value of about four times the mean grain diameter. Under programmed loading conditions, stage IIa was found to occur after a high to low load change even though the prevailing

stress intensity was at the level sufficient to produce stage IIb in a single stress level test. It is suggested that this effect is caused by substantial residual compressive stresses acting in opposition to the applied stress intensity and estimates of the minimum levels of these residual stresses have been made. The mechanisms of residual stress formation and decay have been explained in terms of sizes of plastic zones at the crack tip.

CONTENTS

	<u>Page</u>
1. REVIEW OF PREVIOUS LITERATURE	1
1.1. APPROACHES TO FATIGUE CRACK PROPAGATION	1
1.2. PREVIOUS RESULTS OF FRACTURE MECHANICS APPLIED TO FATIGUE CRACK PROPAGATION	3
1.2.1. Stress Ratio	3
1.2.2. Plasticity Effects	5
1.2.3. Notch Geometry Effects	7
1.2.4. Environmental and Microstructural Effects	8
1.2.5. Summary of Factors Affecting the Fracture Mechanics Analysis	8
1.3. APPLICATION OF CUMULATIVE DAMAGE LAWS TO PROGRAMMED FATIGUE	9
1.3.1. Introduction	9
1.3.2. Cumulative Damage Theories	10
1.3.3. Residual Stress Effects	12
1.3.4. Summary of Cumulative Damage Approaches	15
1.4. SURVEY OF THE RESULTS OF PROGRAMMED LOADING WORK	16
1.5. FRACTOGRAPHIC ASPECTS OF FATIGUE CRACK PROPAGATION	17
1.5.1. Introduction	17
1.5.2. Classification of Fracture Mode	17
1.5.3. Characteristics of Fatigue Fracture Surfaces	18
1.5.4. Mechanisms of Striation Formation	19
1.5.5. Structure Sensitive Fatigue Fracture	21
1.5.6. The Effect of Load Level Changes on Striations	22
1.5.7. Summary of Fractographic Aspects	23
2. OBJECTIVES	25
3. MATERIALS AND EXPERIMENTAL TECHNIQUES	26
3.1. MATERIALS AND HEAT TREATMENT	26
3.2. SPECIMEN DESIGN AND FATIGUE MACHINES	27

	<u>Page</u>
3.3. MEASUREMENT OF CRACK LENGTH BY THE POTENTIAL DROP TECHNIQUE	28
3.4. EXAMINATION OF FRACTURE SURFACES	28
4. EXPERIMENTAL RESULTS	29
4.1. CONSTANT AMPLITUDE TESTING	29
4.1.1. Push-Pull Tests at Zero Mean Stress	29
4.1.2. Three Point Bending Tests	31
4.1.2.1. Small Specimens	31
4.1.2.2. Large EN 3B Specimens	32
4.2. FRACTOGRAPHIC OBSERVATIONS UNDER CONSTANT AMPLITUDE LOADING	33
4.2.1. Slow Crack Growth Rates	33
4.2.2. Fast Crack Growth Rates	34
4.2.3. The Role of Pearlite in the Fatigue Fracture Process	34
4.2.4. Observations of Stage IIa and IIb in Other Materials	35
4.2.5. Quantitative Aspects of Stage IIa and IIb Fracture	36
4.2.6. Striation Spacing Measurements	37
4.3. RESULTS OF PROGRAMMED LOADING TESTS	38
4.3.1. Two Level Tests	39
4.3.2. Multi-Level Tests	40
4.3.3. Crack Growth Data	40
4.3.4. Effect of Rate of Change of Load Level	41
4.4. FRACTOGRAPHIC RESULTS OF PROGRAMMED LOADING TESTS	41
4.4.1. Observations at Low Magnifications	41
4.4.2. Observations at High Magnifications	42
4.4.3. The Extent of "Unstable" Stage IIa	43
4.5. RESIDUAL TENSILE STRESS EFFECTS	44
4.6. LIFE PREDICTION COMPUTER PROGRAMME	45

	<u>Page</u>
5. DISCUSSION	47
5.1. CONSTANT AMPLITUDE RESULTS	47
5.1.1. Fracture Mechanics Data	47
5.1.2. Deviations in the Slope of the Fracture Mechanics Analysis	47
5.1.3. Scatter in Results	49
5.2. CONSTANT AMPLITUDE FRACTOGRAPHY	49
5.2.1. Stage IIa and Stage IIb Fracture Criteria	49
5.2.2. The Nature of Crack Front Movement	52
5.3. PROGRAMMED LOADING	54
5.3.1. The Consistency of the Cumulative Cycle Ratio	54
5.3.2. Mechanisms of Residual Stress Formation and Decay	56
5.3.3. The Magnitude of Residual Stress	58
5.3.4. The Validity of the Palmgren-Miner Hypothesis	58
6. CONCLUSIONS	60
7. SUGGESTIONS FOR FURTHER WORK	62
8. REFERENCES	63
9. ACKNOWLEDGMENTS	69
APPENDIX 1. SURVEY OF THE EXPERIMENTAL RESULTS OF PROGRAMMED LOADING TESTS IN THE LITERATURE	70
APPENDIX 2. NOTCH CUTTING PROCEDURE	74
APPENDIX 3. THE POTENTIAL DROP CRACK GROWTH MEASUREMENT TECHNIQUE	75
APPENDIX 4. PUBLISHED PAPERS	76
APPENDIX 5. EXPERIMENTAL ERRORS	77
APPENDIX 6. LIFE PREDICTION COMPUTER PROGRAMME	79

1. REVIEW OF PREVIOUS LITERATURE

1.1. APPROACHES TO FATIGUE CRACK PROPAGATION

Early fatigue studies were concerned with producing stress-life relationships principally on notched and unnotched rotating bend specimens and until the mid-50's little published work existed on the growth of fatigue cracks. The early crack propagation work of Moore (1), de Forrest (2) and Bennett (3) was limited to the extension of circumferential surface cracks on notched and unnotched cylindrical specimens. In the interpretation of notched specimen data, attention was concentrated on a comparison of the strength reduction factor, K_f (i.e. the ratio of unnotched to notched fatigue limits) with the theoretical elastic stress concentration factor of the notch, K_t . The strength reduction factor was often found to be less than the elastic stress concentration factor and some of the theories put forward to account for this effect have been reviewed by Frost and Dugdale (4).

Eventually, it was realised that in many practical instances cracks, or crack-like material defects were present from an early stage and the majority of life was spent in propagating the crack. This led to a change in the approach and workers began to follow the course of fatigue by examining the progress of through-thickness cracks initiated from sharp notches in a variety of designs of test piece.

As a result, several crack propagation laws have been presented (5,6,7,8) which may be expressed in the form;

$$\frac{da}{dN} = f(\sigma, a, C) \quad (1)$$

where da/dN is the rate of crack growth, σ the alternating stress and C a constant incorporating mean stress. In a review of crack growth relationships, Paris and Erdogan (9) pointed out that most of these approaches were applicable only to data collected from a limited range of crack growth rate and suggested that only the fracture mechanics approach could satisfactorily account for a wide range of fatigue crack growth data.

This approach to fatigue crack propagation had previously been suggested by Paris et al (8) based on the Irwin stress intensity factor concept (10). The stress intensity factor, K , was shown to represent the effects of externally applied load and geometry on the intensity of the stress field at the crack tip. It was also suggested that the distribution of elastic stress around the crack tip in plane extension problems always had the same functional form and differed only by the stress intensity factor. Thus it was reasoned that the stress intensity factor of the crack tip stress field should control the fatigue crack propagation process.

The stress intensity factor was linearly dependent on the load and contained a geometric factor related to crack length or other geometric property of the body. Finite width correction factors for a wide variety of specimen designs have since become available (11). A good correlation was found between the linear stress intensity factor and the log of the rate of crack growth for different loading configurations (8), an example of which is shown in fig.1.

On the basis of experimental data available in the literature Paris and Erdogan (9) suggested a power law of the form

$$\frac{da}{dN} = C (\Delta K)^m \quad (2)$$

where ΔK is the stress intensity range, m a dimensionless constant and C a constant incorporating other variables including mean stress. Their observations suggested that m was equal to 4 for a wide range of aluminium alloys and high strength steels. Subsequent theoretical treatments (12-16) have justified this relationship although the exact value of m is questionable.

Several limitations of the approach became apparent at this stage. Firstly, the inherent assumption that the minor variables could be incorporated into the constant C was an over-simplification. The effects of mean stress have since been shown to vary for different materials (17). Secondly, the relationship between ΔK and da/dN was assessed in terms of a log - log plot which tended to disguise experimental scatter. Thirdly,

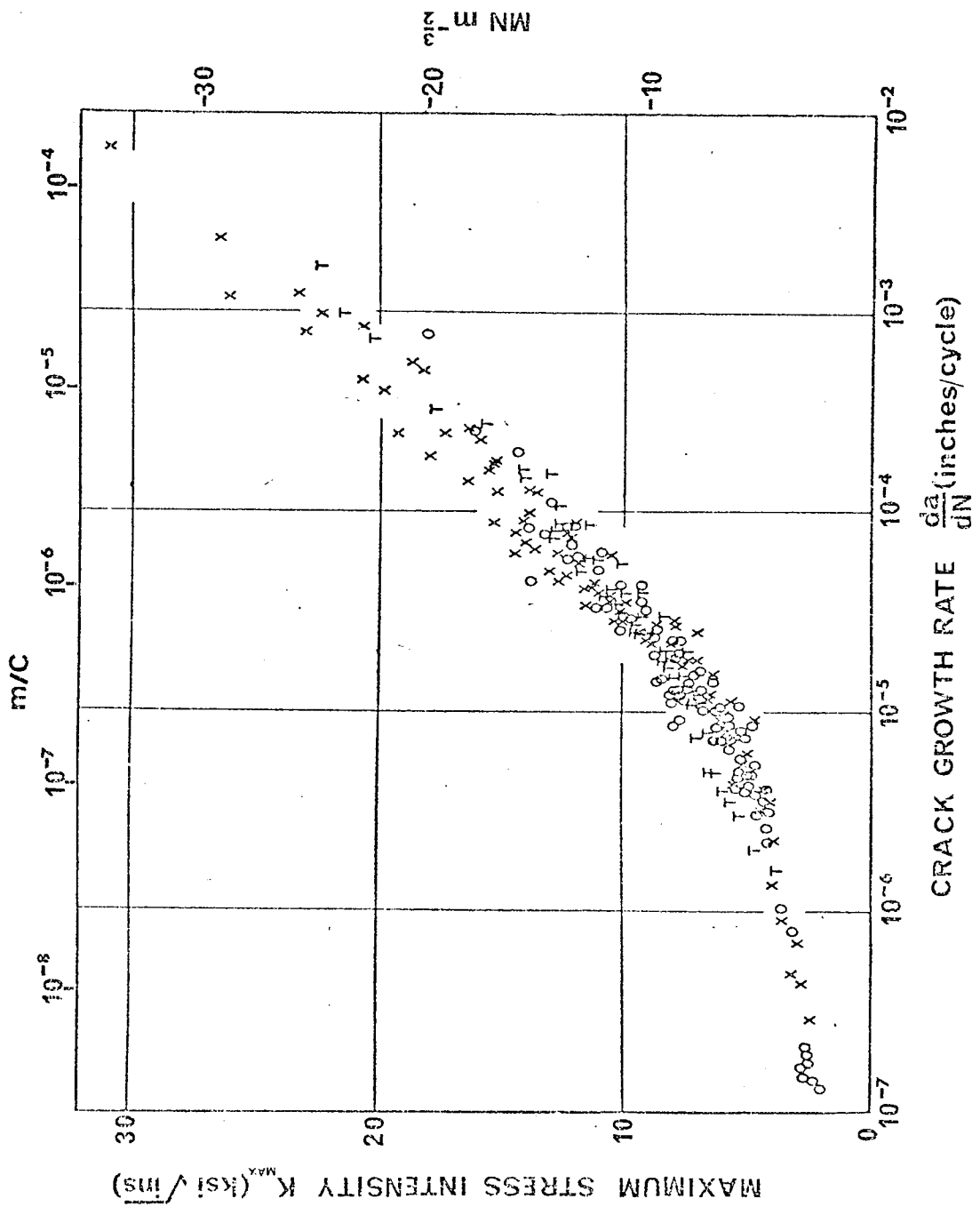


Fig. 1 (ref. 5)

by assuming a continuum approach, no account was taken of the possible effects of microstructure. Finally, the observations of Frost (18) that a critical stress was required to re-commence propagation of a pre-existing crack, pointed strongly to the presence of a minimum value of ΔK at slow crack growth rates, below which propagation would not occur.

Nevertheless, the fracture mechanics approach has become a widely accepted means of interpreting fatigue data, principally because of its simplicity and ability to include the geometrical aspects of the problem. In this respect it is a significant step forward.

1.2. PREVIOUS RESULTS OF FRACTURE MECHANICS APPLIED TO FATIGUE CRACK PROPAGATION

Obviously the concept of a simple fatigue crack growth relationship has far reaching implications and, since the original proposal, a wealth of crack growth data has become available. Unfortunately the results are by no means as well defined as one might have hoped. Indeed, evidence of confusion was apparent in Paris and Erdogan's original paper and the discussion to that paper clearly pointed to the need for further work. This section reviews the important aspects of the problem in the light of recently published work and attempts to demonstrate that a clearly defined trend is becoming apparent.

The most important factors to be considered are:-

- (1) The stress ratio, (R). (i.e. ratio of minimum to maximum alternating stresses)
- (2) Bulk tensile properties of the material
- (3) Plasticity effects, with particular reference to the fracture mode transition and the instability effect as the critical stress intensity for fast fracture is approached.
- (4) Notch geometry
- (5) Environmental and microstructural effects.

1.2.1. Stress Ratio

Recent work (19,20) has demonstrated a dependence of m and C on the

value of stress ratio for a wide variety of materials. The effects varied from the relatively insensitive pure aluminium, copper and mild steel to the very sensitive high strength aircraft aluminium alloys, the value of m increasing with R .

Several semi-empirical approaches accounting for the effect of mean stress have been suggested (21,22) but the most generally applicable relationship so far proposed is that due to Forman, Kearney and Engle (23), which takes into account both the effects of stress ratio and the approach of instability as the maximum value of stress intensity approaches the critical stress intensity of the material (K_c). The relationship hinges on the criterion that as K_c is approached the rate of crack growth approaches infinity. Their relationship has the form:

$$\frac{da}{dN} = \frac{C_1 (\Delta K)^m}{(1-R) K_c - \Delta K} \quad (3)$$

The data of McEvily and Illg (7) for aircraft aluminium alloys fitted this equation well. Other workers (24) have also found results from aluminium alloys to give a good fit to equation (3).

The majority of fatigue crack propagation work has been carried out under conditions of positive mean stress with the stress ratio, R , equal to or greater than zero. Gurney (25) examined crack propagation relationships in a series of mild steels with increasing yield stresses under conditions of pulsating tension and zero mean stress, and found that between 10% and 35% of the compressive part of the cycle was effective in propagating the crack, the contribution decreasing with increasing yield stress. The results were also analysed in terms of fracture mechanics using only the tensile portion of the cycle to calculate the stress intensity factor. The data for the material with the lowest yield stress fell into a scatter band which showed quite clearly that as the alternating stress range increased, both m and C changed systematically. The exact reason for this was not clear, and Gurney chose to ignore the effect since the higher yield stress materials showed

much narrower scatter bands.

The main experimental difficulty when systematically investigating the contribution of the compressive portion of the cycle is in maintaining accurate specimen alignment under all loading conditions, and there is clearly a need for systematic work to clarify this aspect of the problem.

In conclusion it may be stated that it is essential to include a consideration of the stress ratio in the fracture mechanics analysis, particularly when comparing data from a variety of sources. However, the effect of mean stress will vary according to the material under consideration.

1.2.2. Plasticity Effects

At fast crack growth rates of the order of 10^{-4} inches (2500 nm) per cycle and above, where the stress intensity factor begins to approach the critical stress intensity factor for static fracture, an increase in m value on the $\log \Delta K$ - $\log da/dN$ relationship is often observed. Several investigators have clearly demonstrated that as instability is approached, components of ductile fracture are observed in association with the fatigue mode. Clark (26) found that in some high strength steels and aluminium alloys the point of transition to faster crack growth rates correlated well with the onset of sub-critical cracking in monotonic loading tests, allowing for the effect of frequency. Fracture surface observations demonstrated quite clearly the presence of ductile fracture associated with the fatigue mode. Carman and Katlin (27) found similar effects in maraging steels.

In some circumstances, deviations at fast crack growth rates may not be observed. For example if the data is collected over a rather limited crack growth rate range it is likely that the slope transition will be lost due to the insensitivity of the log-log plot. Brothers and Yukawa (28) did not usually observe a transition to faster crack growth rates in the majority of their tests on low alloy steels. In the one instance in which the transition was observed, the range of crack growth rate data considered

was larger than in any of the other tests.

Another cause of difficulty is the inability of many fatigue machines to maintain the correct stroke under conditions of fast crack growth, particularly at high frequencies. Under these conditions the load level may begin to fall off and data collected in this region should be rejected. Generally, it can be concluded that the effects of instability on the log-log relationship appear to be well documented and clearly understood.

Confusion appears to have arisen over the effect of the fracture mode transition from 90° plane strain to 45° plane stress. Several relationships defining the transition have been proposed (29-31), all emphasising the importance of the material thickness, yield stress, and plastic zone size. There is evidence to suggest that the fracture mode transition can cause:

- (a) Reduction in crack growth rate (32 - 34)
- (b) Acceleration in crack growth rate (30)
- (c) No effect (35 - 37).

Wilhelm (32) re-examined previously published crack propagation data for a variety of materials including aircraft aluminium alloys, titanium alloys and high strength steels. He analysed these results by plotting graphs of linear stress intensity range (ΔK) and log crack growth rate (da/dN). He showed that, above crack growth rates of about 10^{-5} inches (250 nm) per cycle, a particularly large decrease in the slope of his relationship occurred. This was attributed to the change in fracture mode from plane strain to plane stress. Wilhelm did not, however, attempt to account for stress ratio effects in his analysis, and a detailed examination of his results shows that over the range of materials considered the R value varied from -0.2 to +0.85.

The results of Hudson et al (38-40) have been re-analysed here, taking due account of stress ratio. This work formed the basis of the arguments developed by Wilhelm, but in the present work the results were plotted

in terms of log stress intensity versus log crack growth rate. Figs. 2-9 show quite clearly that R is principally affecting C values in a manner that could give rise to Wilhelm's interpretation. In figures 8 and 9 the stress ratio varies only between 0 and 0.1 but the trend is the reverse of that proposed by Wilhelm. He also cited the results of McEvily and Illg but these have been re-analysed by Forman et al (23). Their results also showed that when the effects of stress ratio were recognised, adequate straight line representations could be drawn without any evidence of a transition due to the fracture mode being apparent.

The log-linear relationship used by Wilhelm was first used by Paris et al (8) to correlate stress intensity, crack growth rate data. They also found a curved relationship of the type shown in fig.1, but did not consider that the fracture mode transition was responsible for the pronounced knee. Since this type of relationship is known to show a knee and because Wilhelm did not account for the stress ratio effect, he drew the erroneous conclusion that the fracture mode transition was having a very large retarding effect on the crack extension rate. In addition, the experimental work he carried out to verify his views was far from conclusive.

Other evidence (33-37) also suggests that the fracture mode transition is of secondary importance in affecting the slope of the $\Delta K - da/dN$ relationship, due to the inherent insensitivity of the log-log plot. It would seem reasonable to conclude that plane stress conditions reduce the rate of crack growth only slightly, and that this is due to the dissipation of strain into the larger volume of plastic material at the crack tip. Much more marked is the effect of instability causing acceleration of crack growth rates at higher stress intensities.

1.2.3. Notch Geometry Effects

Another important factor to be considered, particularly at slow crack growth rates, is the influence of the notch on the log stress intensity-log crack growth rate data. There is ample evidence (25, 30, 41-44) to

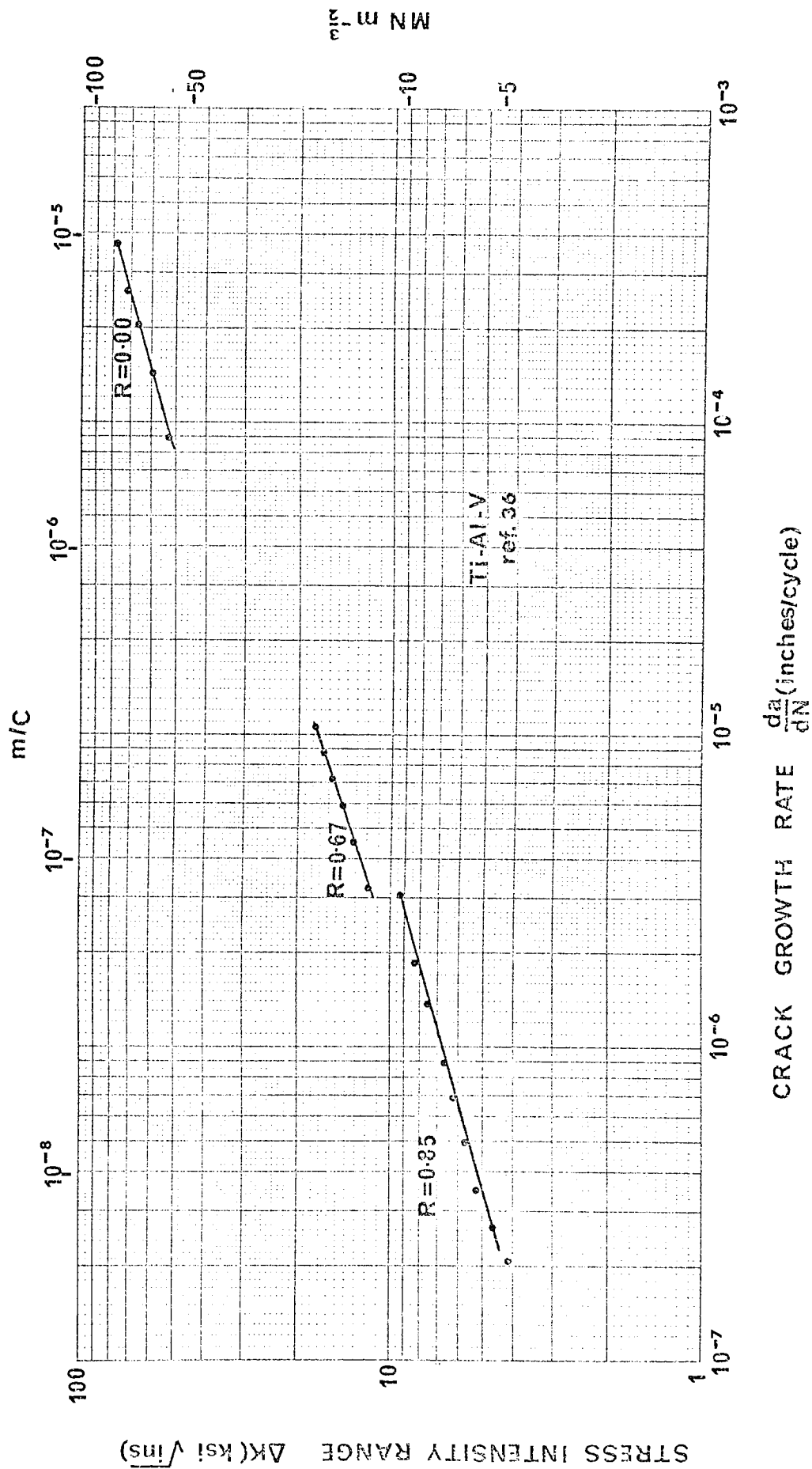


Fig. 2 DATA RE-ANALYSIS

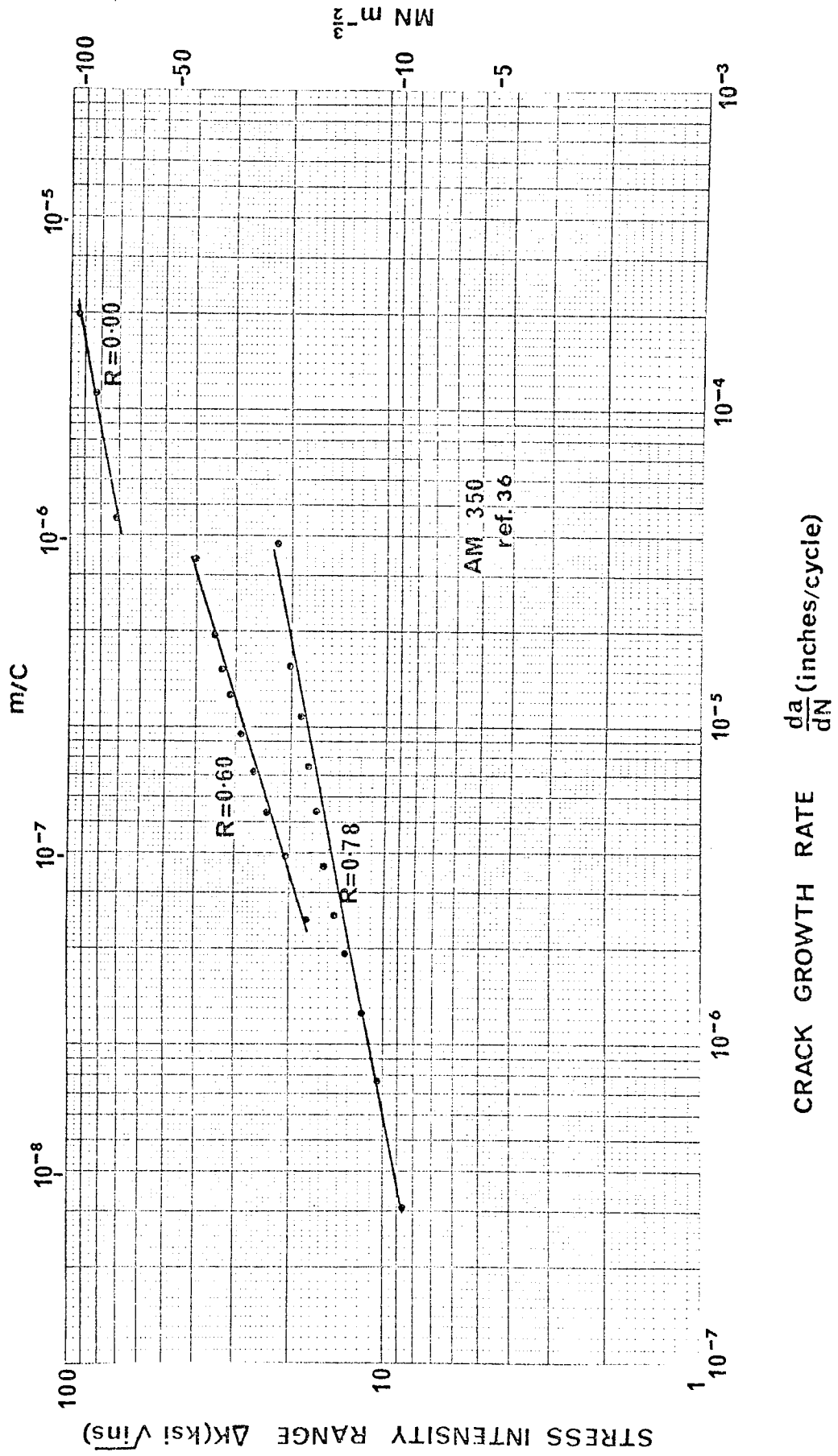
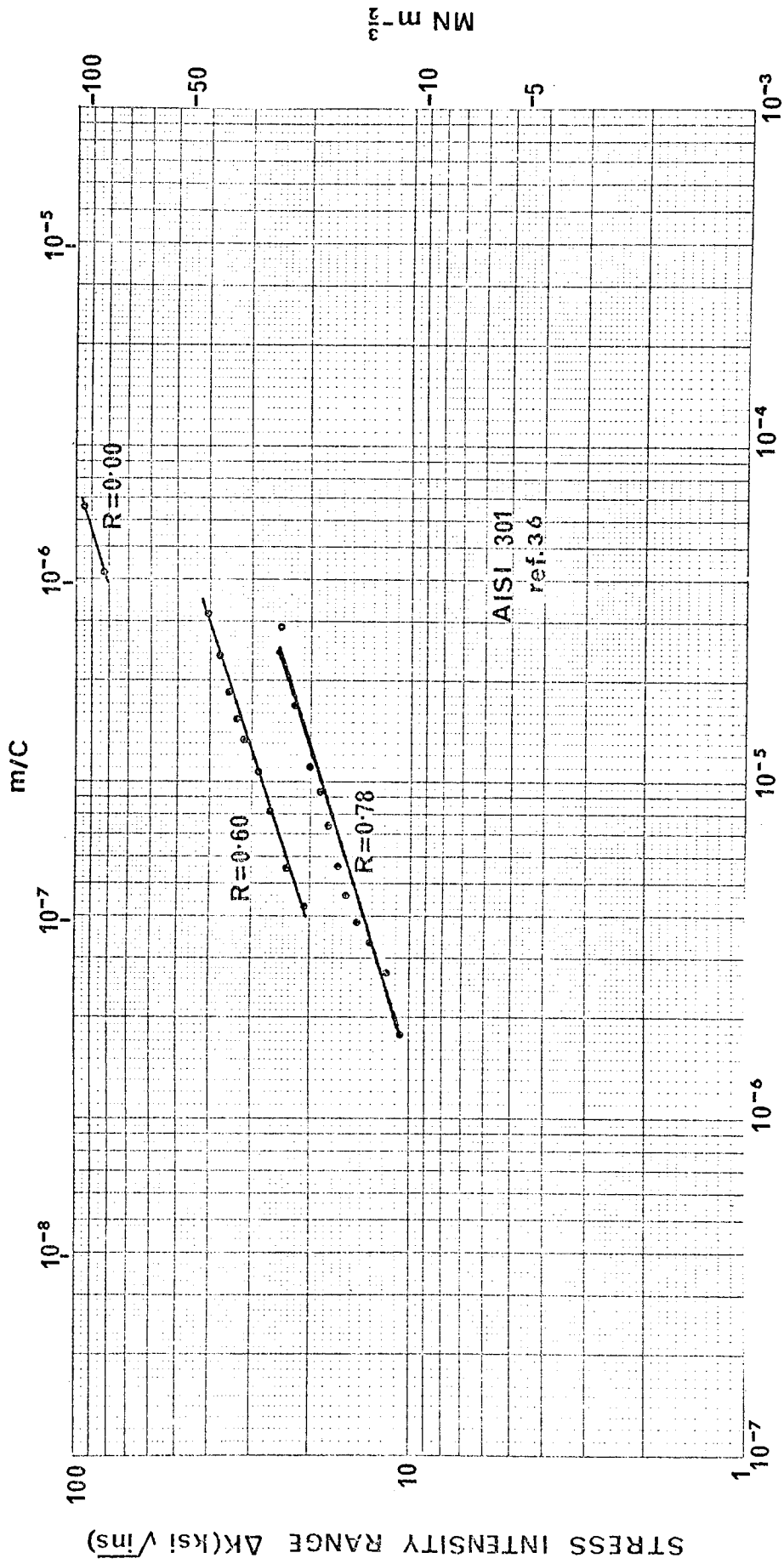


Fig.3 DATA RE-ANALYSIS



CRACK GROWTH RATE $\frac{da}{dN}$ (inches/cycle)

Fig.4 DATA RE-ANALYSIS

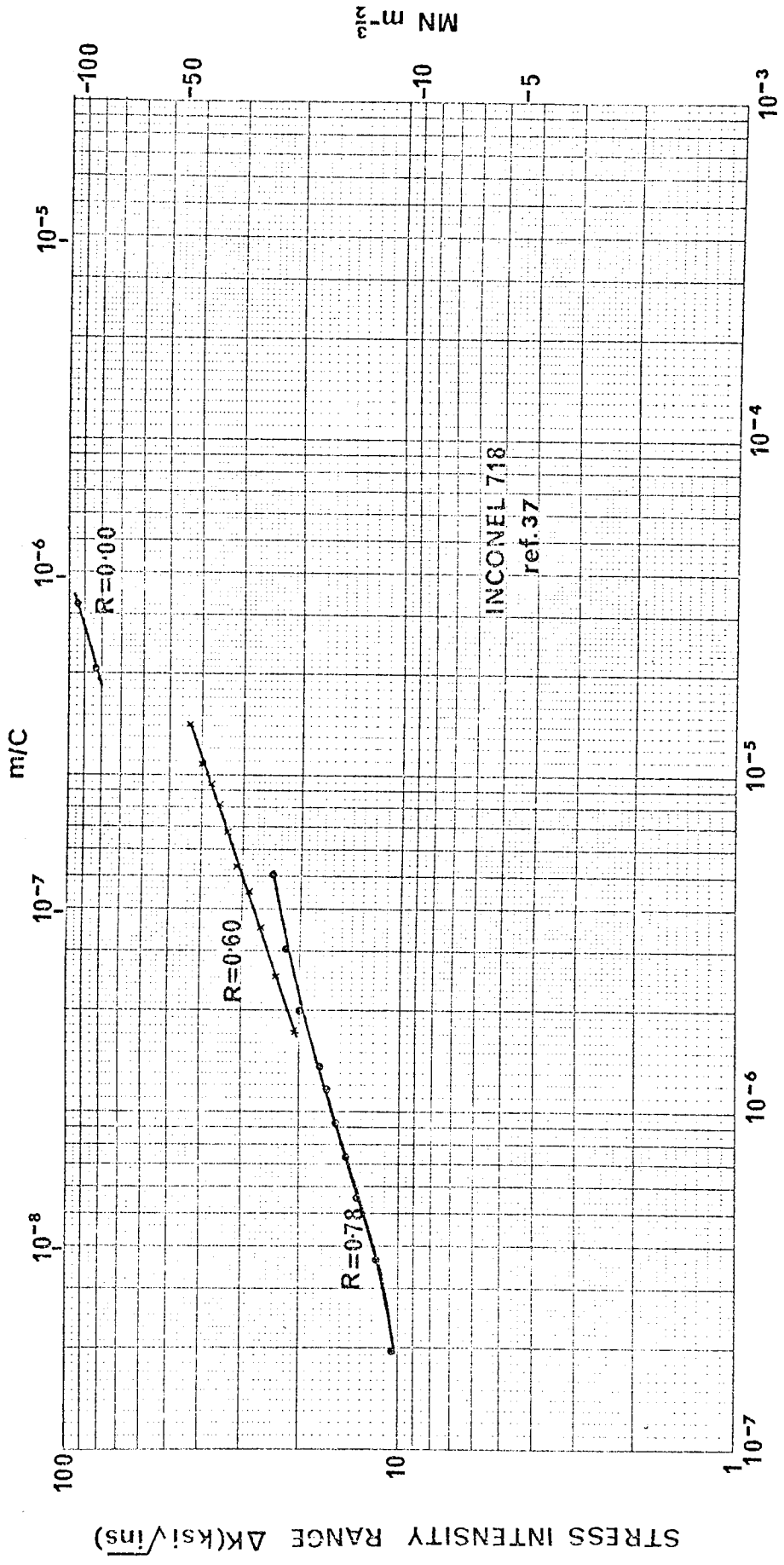


Fig.5 DATA RE-ANALYSIS

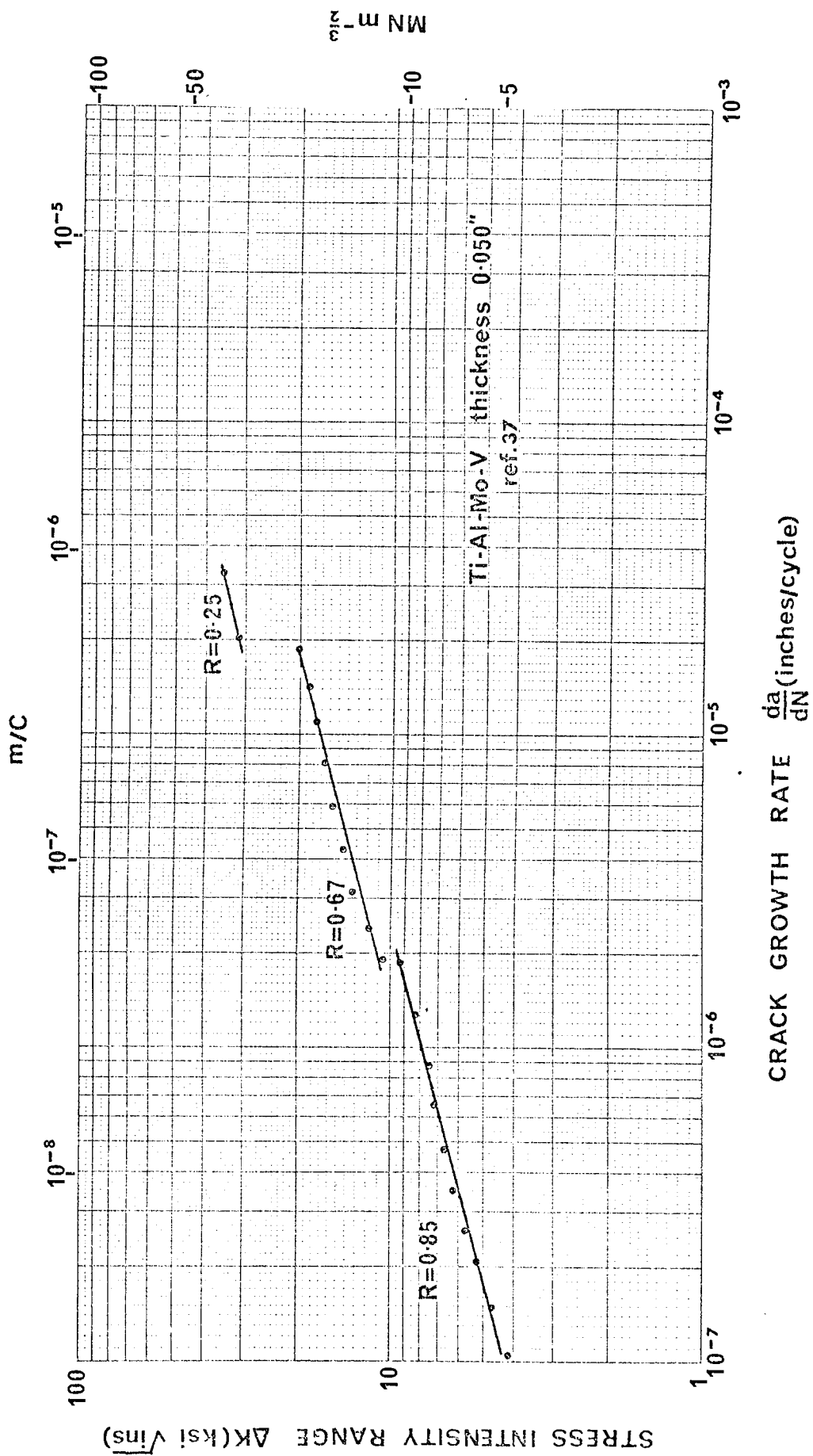


Fig.6 DATA RE-ANALYSIS

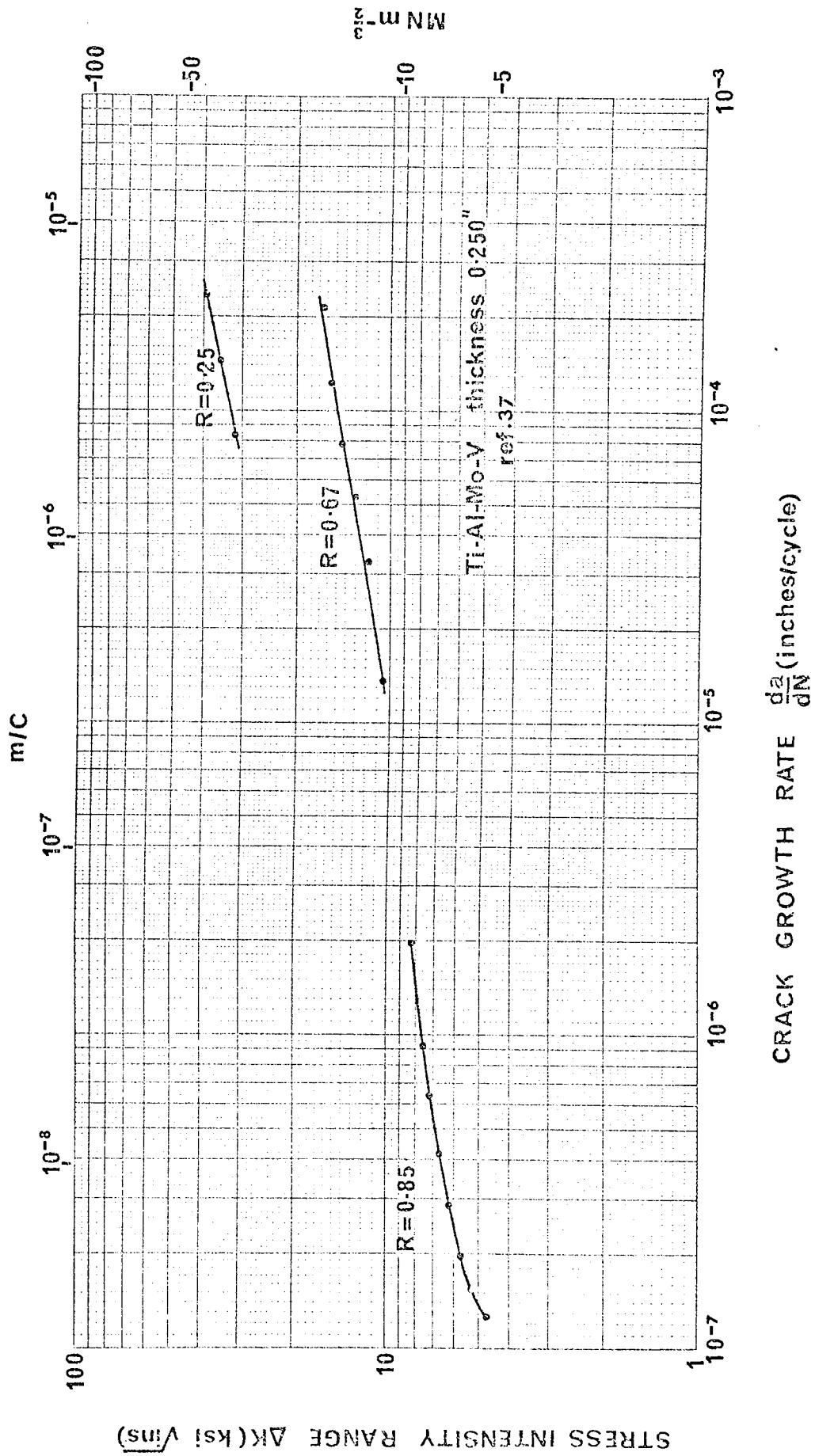


Fig.7 DATA RE-ANALYSIS

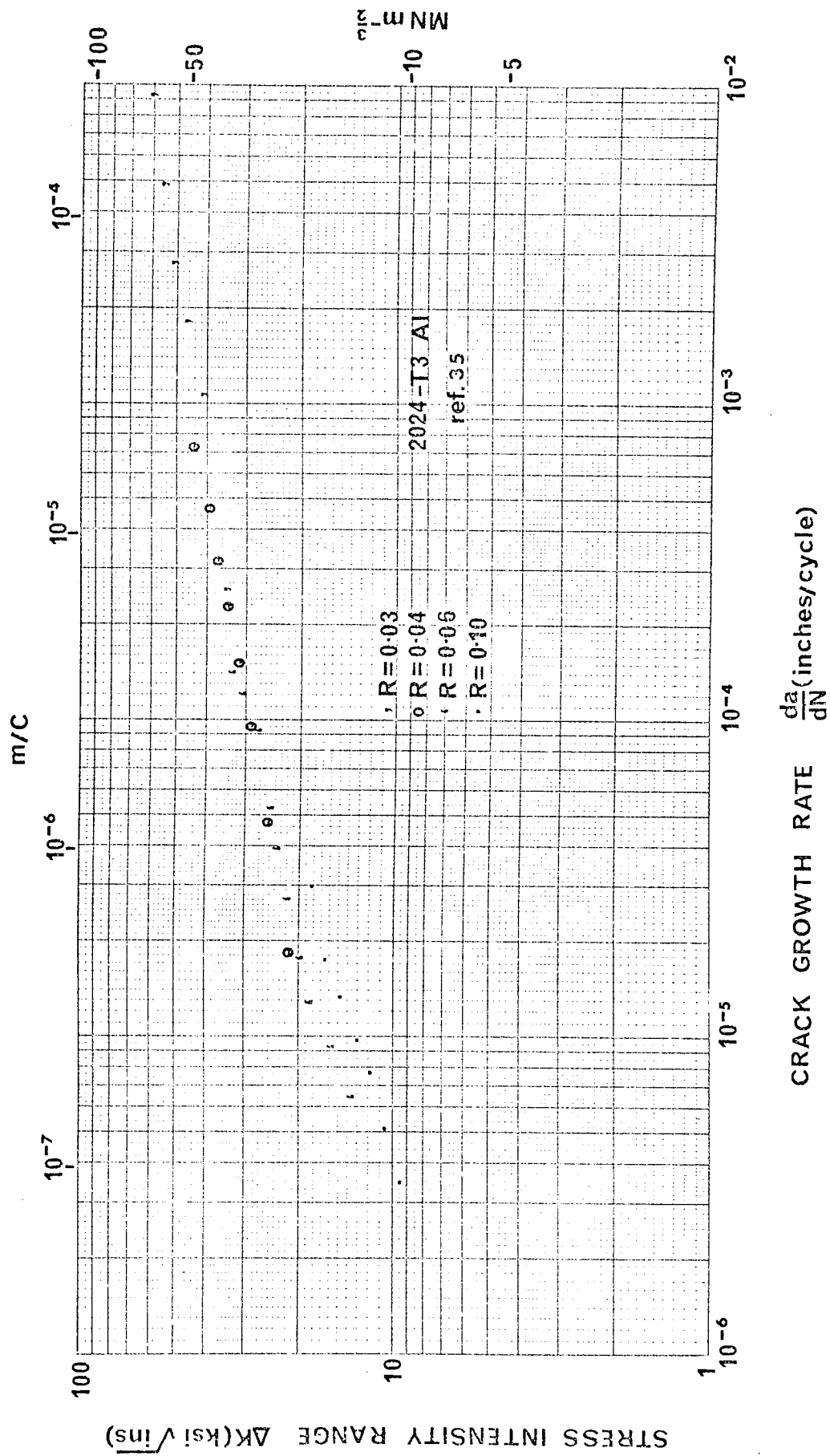


Fig.8 DATA RE-ANALYSIS

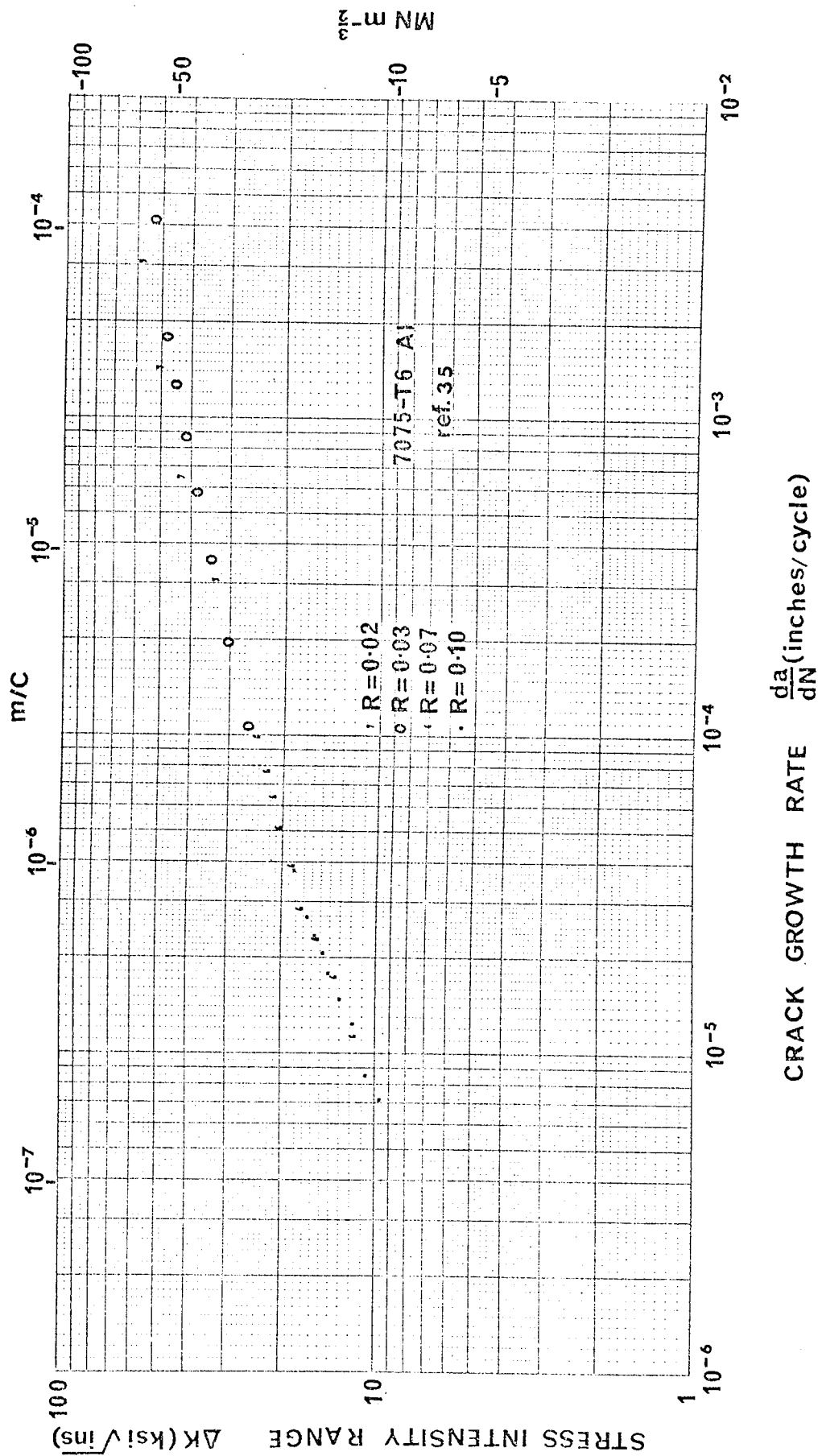


Fig.9 DATA RE-ANALYSIS

suggest that the additional stress concentration of the notch causes an increase in the slope of log stress intensity-log crack growth rate relationship in the early stages of crack growth. This effect is more marked at low applied stress levels since the crack spends a greater proportion of total life near the notch root.

1.2.4. Environmental and Microstructural Effects

Hartman (45) and Bradshaw and Wheeler (46) found that aircraft aluminium alloys were sensitive to moisture in the test environment, the effect being a maximum at low applied stress intensity levels. Wei (47) considered the mechanism to be a hydrogen embrittlement effect occurring by a water-metal reaction at the crack tip, and not an environment transport mechanism. Thus, as crack tip plasticity increased at the longer crack lengths, the effects of hydrogen released into the sub-microscopic cavities became relieved. Frost (48) found a slight detrimental effect of moisture on fatigue crack propagation in mild steel under mean tension stress, but not at zero mean stress.

Hence, increases in m value at slow crack growth rates may also be closely related to the environment. Moreover, recent work (49) has shown that at slow crack growth rates where the theoretical plastic zone size at the crack tip is small relative to the micro-structure, the crack path can become structure sensitive.

Some attempt has been made to account for microstructural variables through properties obtained from the unidirectional tensile test (34, 50). Both approaches emphasise the use of the elastic modulus as a normalising factor when comparing the data from a variety of sources. The equations of McEvily and Johnston (34) also indicate that increases in tensile strength do not cause proportionate improvements in fatigue resistance.

1.2.5 Summary of Factors Affecting the Fracture Mechanics Analysis

The stress ratio is the largest single source of scatter in the log stress intensity - log crack growth rate plot and the relationship of Forman et al (23) seems most able to take account of

this effect. When comparing the results from a variety of materials, improvement in correlation results from including the yield stress, elastic modulus and plasticity parameters in equations relating crack propagation rate to the stress intensity factor.

Of the factors that can cause slope transitions at constant stress ratios on the log stress intensity-log crack growth rate relationship it has been shown that instability will cause crack acceleration at high stress intensities. Notch geometry, environment and microstructure may all play a part in producing slope transitions to higher m values at slow crack growth rates. The fracture mode transition is considered to have only a minor retarding effect on the rate of crack propagation, which is not normally visible on the insensitive log-log plot.

Where crack growth rates vary between 10^{-7} and 10^{-4} inches (2.5 - 2500 nm) per cycle the data can generally be represented quite adequately by a straight line, but no single value of m or C will apply to all materials and conditions as first proposed by Paris. It is in this region that the crack growth rate is relatively insensitive to metallurgical variables, and the fracture mechanics approach is therefore not well suited to the assessment of microstructure on fatigue properties.

The most fruitful area for further research into the metallurgical control of fatigue crack propagation undoubtedly lies in the early stages where the crack growth rates are usually below 10^{-7} inches (2.5 nm)/cycle. Little information is available in this region due to the time involved in testing and the complicating effects of non-propagating cracks and clearly much more detailed work is required.

If the limitations described above are taken into account the fracture mechanics approach to fatigue can be useful, its principal advantage being the ability to account for the geometrical aspects of the problem.

1.3. APPLICATION OF CUMULATIVE DAMAGE LAWS TO PROGRAMMED FATIGUE

1.3.1. Introduction

For some time, it has been recognised that cycling at more than one

stress level can cause changes in the expected life, predicted from a conventional constant amplitude S-N curve. However, the problem of predicting life under complex loading histories has not yet been solved satisfactorily. Any relationship proposed should accurately represent the experimental findings and from a designer's point of view, be simple to apply and require a minimum of experimental data for its application. In this section, a selection of cumulative damage laws applicable principally to programmed fatigue will be discussed. Emphasis will be placed on the assumptions concerning the damage criterion, since it is the questionability of the physical soundness of these assumptions that often results in restricted application of many of the relationships. It will be shown that despite the ingenuity of some of the theories proposed, the original Palmgren-Miner hypothesis still remains the most widely used design criterion.

1.3.2. Cumulative Damage Theories

The first attempt to provide a generally applicable cumulative damage law was made by Palmgren (51). He suggested that failure would occur under programmed loading conditions when the sum of the fractional lives at each stress level (i.e. the cumulative cycle ratio) reached unity. This is expressed as:

$$\sum \frac{n_i}{N_i} = 1 \quad (4)$$

where n_i is the number of cycles at the i th stress level and N_i is the failure life at the same level.

Miner (52) later restated this relationship and demonstrated by means of repeated multi-level load tests on unnotched rotating bending specimens of aluminium alloy, that the value of cumulative cycle ratio ranged from 0.61 to 1.45, and gave an average value of approximately 1.

The Palmgren-Miner relationship has become widely accepted as a simple design criterion, its principal advantage being that only a knowledge of the conventional S-N curve is necessary for its application.

Its principal weakness lies in the assumption that the damage criterion D , at any instant is equal to the cycle ratio, (i.e. $D = \sum n_i / N_i$). Also equation (4) does not take into account the possibility of "interaction" between different stress levels changing the rate of damage progress, nor does it allow for any change in the rate of damage accumulation with changing stress level (stress dependency). Furthermore, it does not account for the possible effects of stressing below the nominal fatigue limit at some intermediate stage in the testing.

Richart and Newmark (53), and later Marco and Starkey (54) proposed that the Palmgren-Miner damage criterion should be raised to an exponent x which varied (empirically) according to the applied stress level. This resulted in a series of damage curves of the type shown in fig.10, and gave shorter life predictions than the Palmgren-Miner rule.

A variety of other proposed cumulative damage laws have been reviewed by Kaechele (55) who concluded that they offered no improvement in physical understanding or theoretical techniques of life prediction. Manson (56) and Grover (57) have suggested approaches considering crack propagation aspects of the problem but these also suffer from similar criticisms. Gatts (58) defined damage in terms of a deterioration in strength in an attempt to base life prediction on a more realistic assessment of damage, but his approach was restricted in application. More recently, Brook and Parry (59) using unnotched specimens of a turbine steel measured changes in damping characteristics throughout the life of their specimens. From a knowledge of the rate of change of damping at a given instant they were able to accurately predict the remaining life at a given stress level.

Paris (60) has discussed the possibility of applying fracture mechanics to programmed fatigue. He suggested that the crack growth relationship of equation(2) could be integrated if the finite width correction factor, Y was assumed constant, and K was expressed in terms of stress and crack length. Alternatively numerical integration at each stress level using

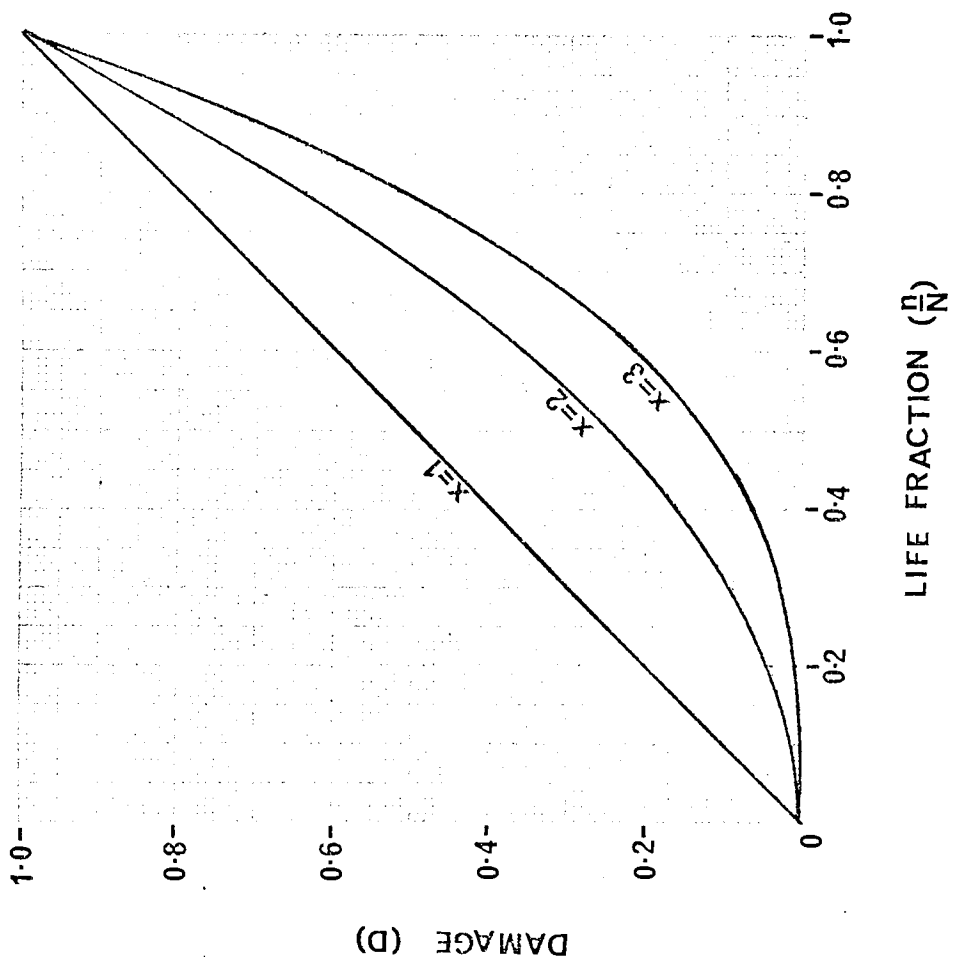


Fig.10 MODIFIED MINER RULE

a computer could provide a more accurate and convenient technique.

It should be emphasised that the assumption that equation(2) applies over the full range of crack growth rates considered, and the interaction of one stress level upon the other can be neglected, leads to a situation equivalent to the Palmgren-Miner rule, provided the failure criterion is stress independent.

Very little subsequent work applying fracture mechanics to complex load histories appears to have been carried out. Smith (61) working with centrally notched panels of 7075 - T6 aluminium alloy compared constant amplitude sinusoidal load tests with broad and narrow band random loading. Graphs of log rms stress intensity against log crack growth rate gave a straight line relationship over two orders of magnitude of crack growth rate but the m value for sinusoidal loading was greater than the m value for random loading. Integration of the experimentally determined crack growth relationship was carried out to determine the number of cycles to failure for random loading and compared with the number of cycles to failure for sinusoidal loading. The latter gave consistently shorter lives and the cumulative cycle ratio for the random loading was therefore always greater than one.

1.3.3. Residual Stress Effects

Edwards (62) attempted to account for residual stress effects during the period of fatigue crack initiation in mildly notched (i.e. $K_t \leq 3$) test pieces. During fatigue with a mean tensile load, localised yield occurs in the vicinity of the stress concentration if the product of the peak alternating stress and the theoretical elastic stress concentration factor of the notch exceeds the yield point of the material. He argued that this effect occurred on the first cycle, causing a reduction in the mean stress in the immediate vicinity of the notch. Thereafter the point of fatigue crack initiation would be subjected to a mean stress below that applied to the bulk of the specimen and the fatigue life would tend to be increased. Similarly if a specimen was given a tensile preload prior to

fatiguing at zero mean stress, there would be a strong possibility of compressive yield occurring due to the additive effects of residual compressive stress (due to the preload) and the compressive portion of the cycle. This would raise the local mean stress into the tensile region and shorten the expected life.

It has been found that, programme loaded notched aluminium specimens subjected to a mean tension stress tend to give cumulative cycle ratios greater than unity. Edwards argued that when the high stress caused localised yielding, subsequent cycling at a lower stress would take place at a reduced local mean stress, compared with the reference constant amplitude test at the same level; providing localised yield did not occur at the lower stress under constant amplitude conditions. Therefore under programmed conditions, fatigue damage accumulation would be slower at the lower stresses and the cumulative cycle ratio would exceed unity.

It is important to emphasise that the residual stress effects discussed above were considered to exert their maximum influence in the vicinity of the notch (i.e. during the crack initiation stage). The effectiveness of these residual stresses during the crack propagation stage were expected to decrease as the crack grew away from the notch, at a rate dependent on the geometry of the test piece. Using these ideas, Edwards developed a cumulative damage law taking full account of residual stress effects.

In the case of more sharply notched specimens, when the majority of the life is spent in crack propagation, the effects discussed above are less likely to predominate, since localised yield at the crack tip occurs at all stress levels in the finite life range, giving rise to a plastic zone ahead of the crack tip. However Schijve (63) and Hudson and Hardrath (38) demonstrated that with aircraft aluminium alloys using a two-level loading programme, crack arrest occurred when the load level changed from high to low, the effect being greater the larger the initial stress level. Schijve found that the reversed sequence produced a slight

acceleration before returning to the expected growth rate for the particular stress level. Hudson and Hardrath however were not able to detect any effect in the reversed direction.

This relatively localised effect is probably associated with the plastic zone ahead of the advancing crack. On changing from a high to low level the "non-equilibrium" plastic zone is forced into compression by the reduced applied stress, thereby causing the observed retardation. However, when the sequence is reversed any residual tensile stresses developed will be rapidly exhausted in enlarging the plastic zone to the new "equilibrium size" for the high stress level, and little effect will therefore be observed.

The magnitude of the residual stress induced at a load change can be calculated approximately from a knowledge of the stress strain curve and the stress concentration factor (64). However, the effectiveness of residual stress on the overall fatigue life (in both the initiation and propagation stages) is controlled directly by the ability of the material to support the induced residual stress under the action of cyclic loading. Pattinson and Dugdale (65) induced residual stresses in unnotched bars of mild steel and aluminium, by overstraining in bending. Using strain gauge techniques they found that cycling at stresses below the fatigue limit caused rapid decay of residual stress in mild steel up to about 10^5 cycles and thereafter a slower progressive reduction up to 10^7 cycles. In aluminium alloys, cycling below the endurance limit had no effect on the residual stress, which remained unaffected up to 10^7 cycles. For lives in excess of 10^7 cycles at the same stress level, progressive decay occurred. However, this effect may have been due to a change in testing machine, and no explanation of these effects was offered.

Residual stress effects are less likely to be retained if cycling at low stress levels in the finite life region causes localised yielding. Rosenthal and Sines (66) showed that, for mildly notched samples, the softened condition of 61S aluminium alloy could not support the residual

stress induced by preloading, whereas the same material in the precipitation hardened condition did. In mild steel, Forrest (67) found that marked cyclic strain softening occurred during the fatigue of mildly notched samples. Considerable plastic flow was found to develop at alternating stress levels as low as 75% of the initial yield point when the failure life occurred at about 10^6 cycles. For aluminium alloys a much reduced effect was observed. This cyclic softening effect which is particularly marked in mild steel could explain the effects observed by Pattinson and Dugdale (65).

Thus residual stresses can have an important effect on fatigue life, and on the basis of the information available it would appear that aluminium alloys are better able to support residual stresses than mild steel.

1.3.4. Summary of Cumulative Damage Approaches

Simple modifications to the cycle ratio or S-N curve are not a satisfactory method of deriving a generalised cumulative damage relationship, because the exact damage process is very loosely defined and is only represented by a life factor that takes no account of changes in the mechanical properties of the material. This is particularly true in the case of unnotched specimens, where up to 95% of life is expended in initiating the fatigue crack. Theories which are based on assumptions concerning the exact damage process during this stage, are not adequate for a generalised approach. It is therefore not surprising that these expressions only apply under specific conditions. Clearly the best approach in this situation is that of Brook and Parry (59) where measurements of actual changes in physical properties of the material are considered. Similarly, fatigue tests under cyclic strain control can also provide a better physical basis for cumulative damage analysis. In this context the recent work of Topper et al (68, 69), in simulating the behaviour of notched specimens with unnotched specimens, has been shown successful for the prediction of crack initiation at mild notches.

When the majority of the life is spent propagating the crack, the nature of the damage process is different and more easily defined. A knowledge of the crack growth relationship for a material will go some way towards the prediction of life but, as with the initiation stage, a knowledge of the magnitude and extent of residual stress effects is essential. Commonly used methods of estimating residual stresses employ strain gauge techniques, X-ray diffraction and graphical procedures based on the stress-strain curve. No attempt appears to have been made to use fracture surface observations as a method of residual stress estimation.

The application of fracture mechanics to variable amplitude fatigue has received little attention, and although the use of a simple stress intensity crack growth rate relationship for variable load history summation is equivalent in form to the Palmgren-Miner approach, it does provide a useful starting point into which the effects of residual stress due to loading interactions can be incorporated.

Only by obtaining a more realistic view of the nature of the damage mechanisms associated with the fatigue process can more reliable fatigue life relationships be determined.

1.4. SURVEY OF THE RESULTS OF PROGRAMMED LOADING WORK

A detailed analysis of the published results of variable load history experiments has been carried out in terms of the cumulative cycle ratio, full details of which are given in Appendix 1. Many inconsistencies have emerged and only in the case of non-ferrous notched test-pieces does the stress ratio appear to exert a consistent effect on the value of cumulative cycle ratio. It is likely that many of the anomalies can be explained in terms of residual stress effects, particularly those induced by specimen preparation procedures. Factors such as block size, frequency and life range appear to exert only secondary effects on the cumulative cycle ratio. Little crack propagation work has been carried out and there is clearly a need for more work, particularly on steels.

In many papers, complex situations have been examined without an

adequate knowledge of the elementary effects of simple programmed loads. It is therefore essential that a systematic approach be adopted and particular attention paid to specimen preparation if meaningful results are to be obtained.

1.5. FRACTOGRAPHIC ASPECTS OF FATIGUE CRACK PROPAGATION

1.5.1. Introduction

Early investigations of fatigue fracture surfaces using optical techniques were limited by a small depth of focus and by the maximum useful magnification that could be attained. Rapid progress was made with the advent of electron microscopy and its associated replica techniques. The principal disadvantages with transmission electron microscopy were difficulties of interpretation due to the presence of artefacts in the replica and a restriction on the area of fracture that could be examined at any one time. More recently the scanning electron microscope has become available. This enables direct examination of the complete fracture surface and renders tedious replication processes unnecessary. With a depth of focus 300 times better than the optical microscope, accurate three dimensional fractographs can be produced, the maximum resolution being limited to about 200 \AA . At the present time the full potential of the instrument does not appear to have been realised in fatigue research.

1.5.2. Classification of Fracture Mode

Forsyth (70) suggested that fatigue crack propagation should be divided into two stages. Stage I fracture developed from the surface as a slip band groove at approximately 45° to the tensile axis, in the direction of maximum shear stress. As the crack grew inwards, the ratio of shear to tensile stress decreased until eventually the crack path turned to 90° with respect to the load axis, to become a Stage II crack.

The extent of each mode was dependent on the prevailing experimental conditions. Stage I was promoted by unnotched specimens, low alternating stresses, the absence of tensile mean stress, corrosive conditions and

single crystals. Stage II predominated in sharply notched specimens where multiple slip conditions were operative. The transition to stage II was often observed to occur at a grain boundary which acted as an obstruction to dislocation movement. In unnotched specimens, often greater than 90% of life could be spent developing a stage I crack across one or two grains, whilst in sharply notched specimens ($K_t \geq 4$) stage I was an insignificant proportion of the total life.

At long crack lengths when the plastic zone size becomes large with respect to specimen thickness the stage II crack plane turns over to about 45° with respect to the principal stress axis establishing a plane stress condition. This has been referred to as stage III crack propagation(71).

1.5.3. Characteristics of Fatigue Fracture Surfaces

At high magnifications stage I fracture is often flat in appearance with lines running parallel to the direction of crack growth and usually occupies a small proportion of the fracture surface. A detailed discussion of stage I fracture has been given elsewhere (72).

At low magnifications fatigue service failures often exhibit lines referred to as beach markings. These are probably caused by periods of crack arrest during which the fracture surface is corroded or oxidised. This gives rise to a fracture surface containing concentric rings of varying colours indicating the intermittent nature of crack progress and Jacoby (73) has cited examples of colour changes associated with programme loaded specimens.

At high magnifications, striations or ripple markings are the principal characteristic of stage II fatigue fracture surfaces in a wide range of materials (74-77). These consist of regular markings running in a direction approximately normal to the direction of crack growth. In certain circumstances particularly at high strains there is often observed a one to one correlation between striations and applied load cycles and the striation spacing becomes a direct measure of the macro-

scopic crack growth rate (37, 75, 78-80). In low carbon steels, a one to one correlation is not always observed particularly at slow crack growth rates (76). Hertzberg and Paris (37) emphasised that striations do not necessarily cover the whole fracture surface. In higher carbon materials striations occur less frequently (72) and may be absent altogether (77,81). Fracture surface rubbing, slip in the wake of the advancing crack and a vacuum environment in aluminium alloys may obliterate striations (82, 83).

More information is required at low strains since it is in this region that there is less likelihood of a one to one correlation. Under these circumstances Plumbridge and Ryder (84) have pointed out that one load cycle may produce one striation but every load cycle will not necessarily produce a striation.

1.5.4 Mechanisms of Striation Formation

Jacoby (85) has noted that striations have been observed on the fracture surfaces of Al, Be, Zn, Fe, Ti, Mg, Ni, Mo, Ta, Zr, Cu, Cr, Nb and some of their alloys. In addition McEvily et al (86) observed well defined striations on polymers and it would therefore appear that a specific lattice structure is not a pre-requisite to their presence.

Stubbington and Forsyth (87) observed that in aluminium-zinc-magnesium alloys under corrosion conditions the more usual "ductile" type of striations became brittle in character. Ductile striations were found to lie on curved plateaux that were parallel to the general fracture surface. Brittle striations lay on crystallographic facets, usually (100) planes at considerable angles to the main fracture plane. These observations led Forsyth (88) to suggest a mechanism of striation formation based on an alternating process of cleavage and ductile rupture, where the morphology of the striation was controlled by the relative proportions of each. The chief objection to this theory was the necessity for cleavage in a face-centred-cubic material.

Laird and Smith (89) proposed a mechanism of striation formation

based on observations of crack tip deformation under high strain fatigue in pure aluminium and nickel. They found crack propagation to be a continuous process and suggested that crack extension and crack tip blunting occurred on the tensile portion of the cycle. During the subsequent compression cycle, crack tip re-sharpening occurred and formed a stress concentration for the next tensile cycle. Laird (90) later modified details of the blunting process to the form shown in figure (11). During the resharpener process, two "ears" were formed, their subsequent extension being influenced by the structure ahead of the crack tip. Non symmetrical extension of the "ears" was shown to account for various observed striation profiles and secondary cracks running below the main fracture surface. Although this mechanism took some account of the effects of microstructure it was based principally on continuum considerations.

Hertzberg (91) suggested that the mechanism of striation formation was crystallographic in nature. Striations were proposed to form as a result of an alternating slip process on (111) planes in a $\langle 110 \rangle$ direction. This mechanism suggested that the main fracture plane should be close to a (100) type, exactly that which Stubbington and Forsyth (87) had found during the corrosion fatigue of an aluminium-zinc-magnesium alloy.

It could be argued that it is incorrect to base striation mechanisms on crystallographic considerations because of the presence of striations in amorphous polymers. However, McMillan and Hertzberg (71) pointed out that a striation forms as the result of a stress pattern at the crack tip and in a polymer there is no restriction on the manner in which it may deform. In metals, there are a restricted number of possible slip systems and the striation will form when slip systems are most favourably oriented with respect to the crack tip stress field. If this is not the case, then a poorly defined striation will result.

On the evidence available, the mechanism of striation formation at high strains appears well represented by the continuum mechanism of Laird

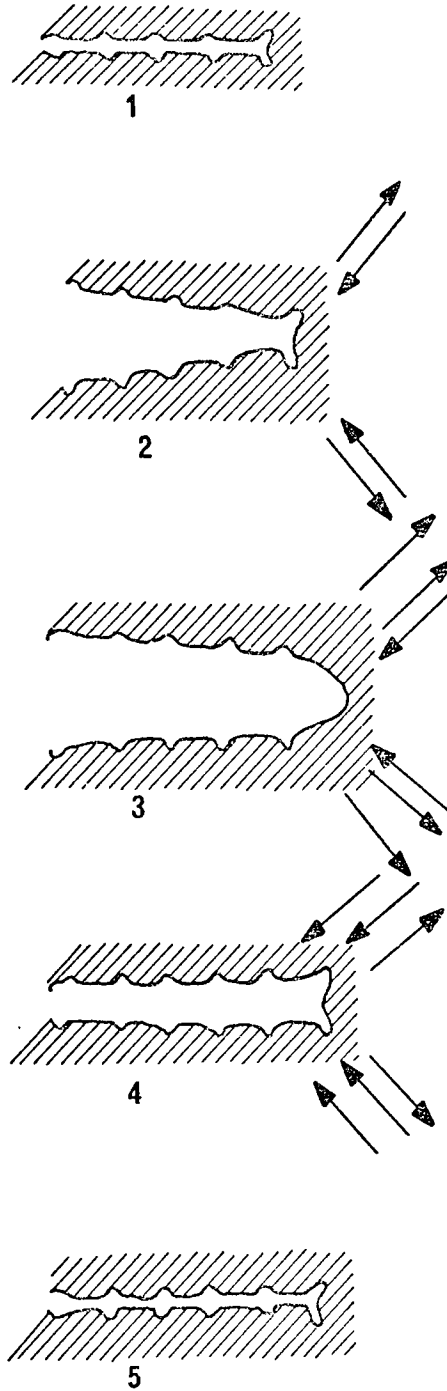


FIG. II THE PLASTIC BLUNTING PROCESS OF FATIGUE CRACK
PROPAGATION (AFTER LAIRD REF. 90)

and Smith. However, at lower strains crystallographic factors may become important, depending on the material under consideration.

1.5.5. Structure Sensitive Fatigue Fracture

The term structure sensitive is applied here to fatigue fractures where details of the underlying micro-structure, particularly grain boundaries, are visible in addition to the striations.

Forsyth (88) noted that under corrosion conditions, the brittle striations were associated with river markings reminiscent of cleavage, and the main plane of the fracture was close to (100) type planes. Pelloux (92), using etch pit techniques on 2024-T3 aluminium alloy, found that below crack growth rates of about $10,000 \overset{\circ}{\text{Å}}$ per cycle ductile striations formed on fracture planes close to the (100) type. These results led him to suggest that when the plastic zone ahead of the crack tip covered only a few grains the deformation became confined to a limited number of crystallographic planes. Jacoby (85) has shown grain boundaries separating adjacent packets of ductile striations in aluminium alloys. Meyn (82) found a change from "brittle" to ductile fatigue cracking at crack growth rates of the order of $5,000 \overset{\circ}{\text{Å}}$ per cycle in 2024-T3 aluminium.

Broek and Bowles (93), whilst investigating the effects of cold deformation and ageing on 2024 aluminium alloy, carried out several programmed load tests with high to low sequences. In one particular instance the load sequence caused a very sharp crack retardation, the macroscopic crack growth rate being reduced to about $25 \overset{\circ}{\text{Å}}$ per cycle. Close examination of their fractographs suggests that river patterns may have become apparent immediately after the load drop, although the authors made no comment on this point.

Williams and Smith (94) observed river type patterns lying on (100) and (110) planes during stage II fracture of body centred cubic β brass. As grain boundaries were crossed, more river markings were generated. Eventually this mode gave way to non-structure sensitive ductile

striations at a constant peak stress of 41 ksi. The transition often occurred rapidly over a few cycles. River patterns of a similar nature have also been observed in 13% manganese steel (95).

Golland and James (96) found grain boundary cracking in zone refined iron with a very low oxygen content. The addition of silicon promoted transgranular fracture and they suggested that grain boundary fracture might be a characteristic of the material rather than an embrittlement effect. Miller (77) observed grain boundary fracture and ductile dimples in martensitic 4340 steel, but there was no evidence of striations, although faint indications characteristic of slip were present on the grain boundary facets. Hoepfner (97) found grain boundaries on the fatigue fracture surface of electrolytic tough pitch copper, near the root of the notch. In coarse grained specimens, ductile striations were promoted some distance away from the notch, and generally, coarse grain sizes decreased the tendency to form grain boundary fracture. However, no distinct change was observed in propagation rate at the transition from grain boundary to the more usual fatigue mode.

Dahlberg (98) carried out a series of tests in various humidities with martensitic 4340 steel and concluded that grain boundary fatigue fracture was favoured by low loads and high relative humidity. Evans et al (99) examined the effects of residual impurities on the fatigue fracture of commercial and vacuum refined 1½% nickel, chromium, molybdenum steel in the hardened and tempered condition. All tests were carried out in vacuum, and it was concluded that the elements arsenic, antimony, tin and phosphorus were instrumental in promoting grain boundary fracture in the commercial steel, although on the basis of the striation spacing the crack growth rate was not affected.

The presence of crystallographic features in fatigue fracture therefore appears to be favoured by small plastic zones ahead of the advancing crack (i.e. low strains), corrosive environments and impurity elements.

1.5.6. The Effect of Load Level Changes on Striations

Although evidence was presented in section 1.3.3. for crack retardation

at a high to low load change, no indication was given as to the exact effect on the micromechanisms of fracture. Jacoby (85) showed evidence that peak loads in aluminium alloys increased the striation spacing associated with the peak load, but that the subsequent striations were reduced in size.

The situation appears to be different in high strain fatigue. McMillan and Hertzberg (71) found that a load drop caused an increase in striation spacing associated with that cycle, even though a decrease in macroscopic crack growth rate was observed. It was concluded that there may have been complicating effects due to the overlapping of plastic zones between peak loads and they subsequently carried out a further series of experiments with more widely spaced peak loads. In this case the striation spacings immediately before and immediately after the peak load application were approximately equal after which the spacing slowly decreased to a minimum before returning to the spacing characteristic of the applied load. This was taken as evidence of the effectiveness of the crack tip resharpener process and subsequent reduction of crack growth was presumed to occur in the plastic zone. It is also noteworthy that no crack arrest was considered to have occurred.

McMillan and Pelloux (100) found varying load range to exert a greater effect on striation spacing than mean load. Generally, high to low sequences promoted longer life, but the exact effect on striation spacing was not clear from their fractographs. Low to high sequences promoted an immediate increase in the striation spacing at the changeover, after which the striations became characteristic of the new load level. This localised increase was interpreted in terms of changes in characteristic crack tip root radius, but equally it may have been a residual tensile stress effect associated with the plastic zone.

1.5.7. Summary of Fractographic Aspects

Correlation of striation spacing with the macroscopic crack growth rate in stage II is not always possible. Conditions are most favourable

at high strains particularly in aluminium alloys. In some instances the striation spacing may not reflect the macroscopic crack growth rate since other fracture processes may be occurring simultaneously. The evidence from steels is less systematic and is difficult to generalise.

The mechanism of striation formation at high strains is probably best represented by the Laird-Smith model, but at lower strains crystallographic mechanisms of striation formation are more likely to be operative. Environment is also an important factor that can change or obliterate the striation detail of the fracture. The absence of striations from the fracture surface does not therefore necessarily imply that fatigue was not operative.

Fatigue fractures of steels, brass, copper and aluminium alloys may reveal microstructural details such as grain boundaries. However the transition from structure sensitive to structure insensitive fracture does not appear to affect the macroscopic crack growth rate. Conditions favouring structure sensitivity are low stresses and high humidity. Aluminium-zinc-magnesium alloys appear to pass through three phases: (i) crystallographic river patterns with brittle striations at slow crack growth rates, if the humidity is high, (ii) ductile striations formed on crystallographic facets and, (iii) at high strains ductile striations on non-crystallographic planes. Impurities have also been shown to promote grain boundary cracking, particularly in steels, although grain boundary fracture might well be an inherent property of low carbon irons under fatigue conditions.

2. OBJECTIVES

This review has indicated the need to provide a simple and reliable guide for designing against fatigue under complex loading histories. Little information is available on the applicability of even the Palmgren-Miner relationship to the fatigue crack propagation situation.

With these considerations in mind, the following objectives were set in the present investigation.

1. To produce consistent constant amplitude fatigue crack propagation data to be analysed by the fracture mechanics approach.
2. To obtain information on mechanisms of crack growth from fracture surface observations.
3. To carry out simple block programme tests, analysing the results by the Palmgren-Miner and fracture mechanics approaches.
4. To determine the mechanisms of fracture at load level changes.
5. To develop a theory that will explain the experimental observations in physical terms.
6. To produce a computer programme to predict variable load history life from the constant amplitude experimental data.

By providing a physical understanding of the mechanisms involved, it was intended that the results of this work would then form a basis for future random loading studies simulating actual service conditions.

3. MATERIALS AND EXPERIMENTAL TECHNIQUES

3.1. MATERIALS AND HEAT TREATMENT

The majority of the work was carried out using a low carbon steel with a low inclusion content. The material was prepared from a Swedish iron base, vacuum melted and cast into 112 lb ingots 4" by 4" in cross-section and hot rolled into strips 3" wide by $\frac{1}{2}$ " thick. Other materials used were commercial EN 3B received in the bright drawn condition, oxygen free high conductivity copper and stainless steel. Table 1 gives details of the materials' analysis.

Care was taken to ensure that specimens were tested in a micro-structurally uniform and stress free condition. Specimen blanks of the low carbon steel were normalised prior to machining at 890°C for 20 minutes. After final machining, the sides of the specimens were polished to a 1 micron diamond finish and stress relieved in vacuum at 650°C for 1 hour. The grain size after this sequence was about 25 microns, as determined on a Quantimet B. EN 3B blanks were stress relieved at 650°C for 3 hours, prior to machining, to avoid distortion. After final machining the sides of the specimens were polished to 600 grade emery and stress relieved in vacuum at 650°C for 3 hours. In this case the final grain size was 28 microns. Figures 12 and 13 show longitudinal micro-sections of the low carbon and EN 3B materials respectively in the final heat treated condition. Table 2 lists the tensile properties of both steels in the normalised and stress relieved condition.

MATERIAL	LOWER YIELD STRESS tsi(MN/m ²)	ULTIMATE TENSILE STRENGTH ₂ tsi(MN/m ²)	ELONGATION %	REDUCTION IN AREA %
Low Carbon Steel	11.5 (178)	22.8 (352)	60	65
EN 3B	19.4 (300)	29.8 (460)	50	63

TABLE 2. TENSILE PROPERTIES OF LOW CARBON AND EN3B STEELS.

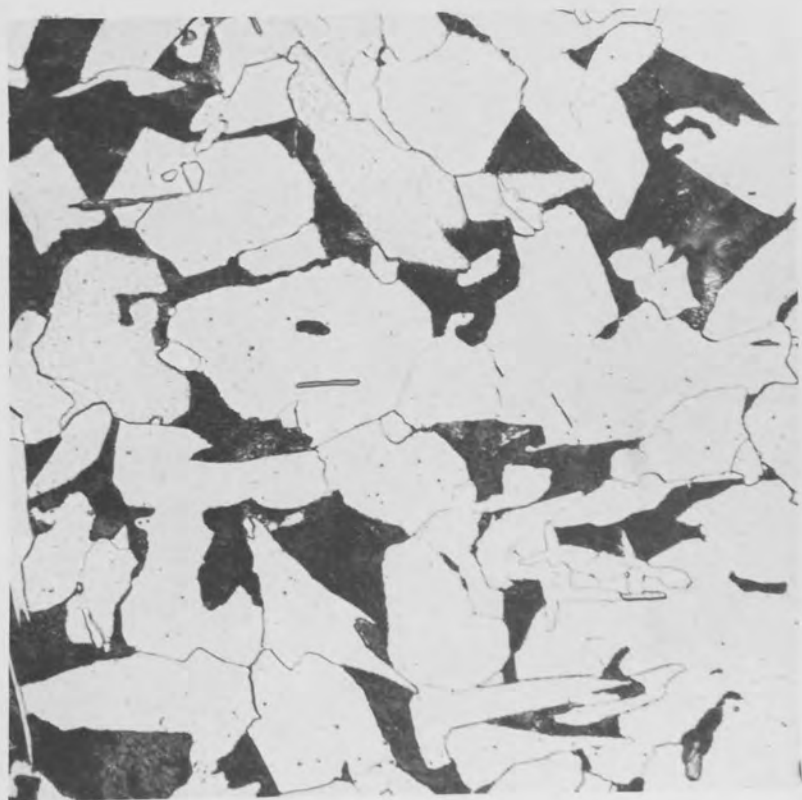
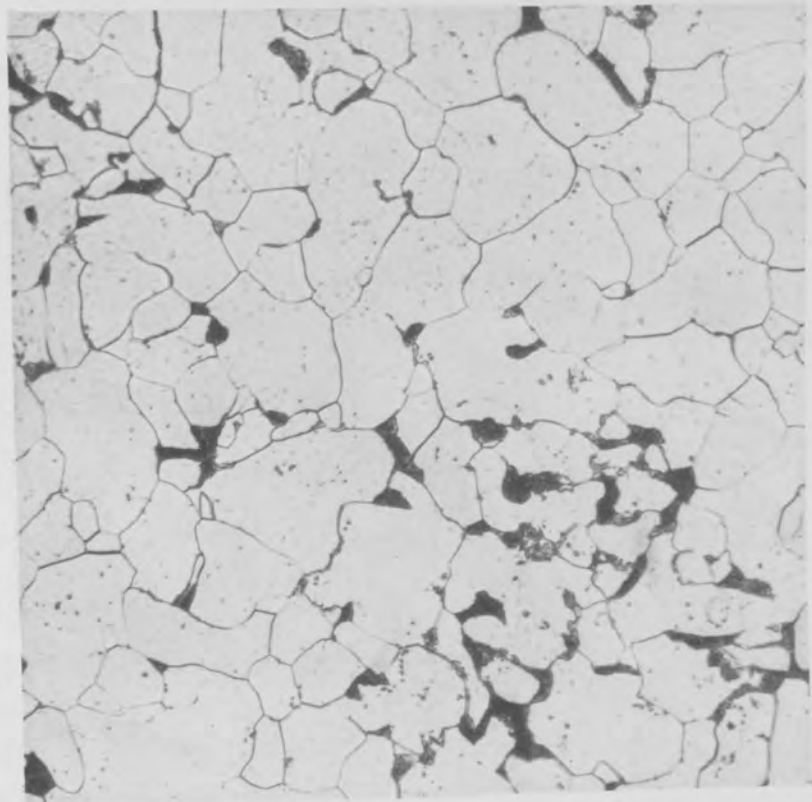
MATERIAL	C	Si	S	P	Mn	Ni	Cr	Mo	Cu	O	N	Nb	As	Sb	Bi	Sn
Low Carbon Steel	.08	.06	.013	.002	.38	.08	.01	.01	.019	.005	.001		.005	<.002	.002	<.002
Commercial EN3B	.17	.26	.039	.011	.64	.18	.12	.02	.25	.002	.008		.032	.006	<.005	.026
OFHC Copper				<.002		.002			>99.9	ND			<.001	<.002	<.001	
Stainless Steel	.06	.50	.016	.025	1.51	9.9	17.6	.34	<.02			.70	.015	<.01	<.01	<.01

ND = Not Detected

TABLE 1. COMPOSITIONS (WT. %) OF EXPERIMENTAL MATERIALS

Fig. 12. Microstructure of Vacuum Melted
0.08% Carbon Steel.
x 500 Mag.
(Neg. 6388)

Fig. 13. Microstructure of Commercial
EN 3B Steel.
x 500 Mag.
(Neg. 6389)



3.2. SPECIMEN DESIGN AND FATIGUE MACHINES

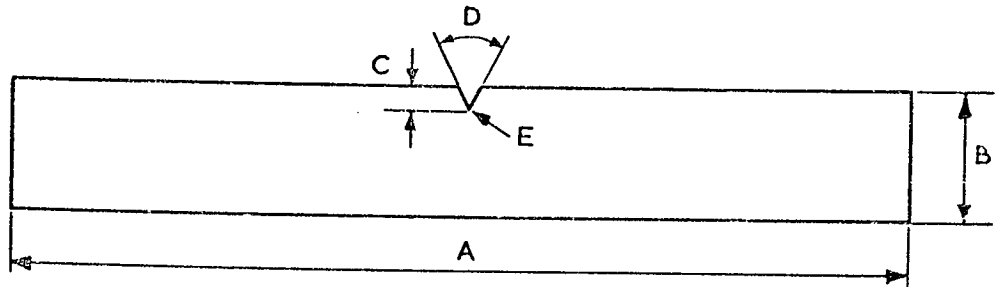
The main part of the work was carried out with small single-edge-notched specimens, details of which are shown in fig. 14. The dimensions were limited by the maximum load capacity of the fatigue machine available, which was an Amsler 2 ton Vibrophore equipped for push-pull and three point bending. The notch dimensions were chosen to give a theoretical K_t value of 10 (101) to ensure that greater than 95% of life would be spent propagating the crack. Details of notch cutting tools and procedures are outlined in Appendix 2.

Crack lengths were measured from both sides of the specimen with two Vickers travelling microscopes and auxiliary lighting was employed only whilst the crack length was being measured. Figs. 15 and 16 show the testing arrangement for push-pull and three point bending respectively.

A standard Vibrophore programmed loading attachment was used for the multilevel tests. This is a simple electrical device which operates the load indicator on the Vibrophore by means of a screwed nut and servo-motor arrangement. The interval and magnitude of load level changes are controlled by metal contact strips attached to a cylindrical drum driven in one direction by a second constant speed servo-motor. The important feature of the equipment is that load level changes always take place at a constant rate over several hundreds of cycles.

In order to investigate the effect of the rate of load level change on fatigue life it was necessary to use an MTS closed loop servo-hydraulic machine. The machine available had a 42 ton load cell which necessitated the use of much larger but geometrically similar test pieces. These were manufactured from the EN3B material and dimensions are given in fig. 14.

A three-point bending rig from a 10 ton Amsler Vibrophore was modified to fit the MTS machine, and the complete testing arrangement is illustrated in fig. 17.



SPECIMEN	A	B	C	D	E	THICKNESS	
	ins (mm)	ins (mm)	ins (mm)			ins	(mm)
SMALL (Vib)	4.8 (122)	.700 (17.8)	.040 (1.0)	45°	.002 (.05)	.220	(5.6)
LARGE (MTS)	15.0 (381)	3.000 (76)	.165 (4.2)	45°	.002 (.05)	.944	(24.0)

FIG. 14. SPECIMEN DIMENSIONS.

Fig. 15. Push-Pull Arrangement on the
Two Ton Vibrophore.
(Neg. 2162)

Fig. 16. Three Point Bending Arrangement
on the Two Ton Vibrophore.
(Neg. 4893)

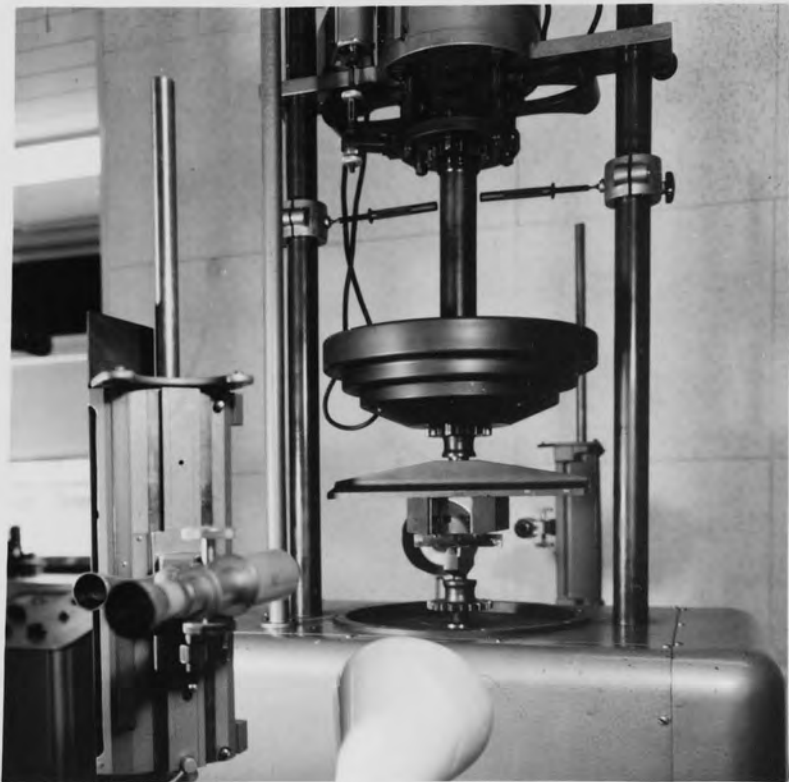


Fig. 17. Three Point Bending Arrangement
on the MTS Machine.
(Neg. 3680)



3.3. MEASUREMENT OF CRACK LENGTH BY THE POTENTIAL DROP TECHNIQUE

In certain selected programmed loading tests the potential drop technique was employed in addition to the travelling microscopes. This enabled more accurate observation of the crack progress at load level changes. The method, which has been described in detail by Gilbey and Pearson (102), consists of passing an electric current through the specimen and measuring the change in potential drop from probes located on both sides of the crack. Full details of the system are given in Appendix 3.

3.4. EXAMINATION OF FRACTURE SURFACES

A Cambridge Instruments Stereoscan Mark IIA scanning electron microscope was used to examine the fatigue fracture surfaces, at an electron gun potential of 30 KV. Specimens were examined at 45° and 90° with respect to the electron beam and a large stage was utilised for the examination of fractures produced on the MTS machine. Fractographs were recorded on 35 mm Ilford FP4 film.

4. EXPERIMENTAL RESULTS

4.1. CONSTANT AMPLITUDE TESTING

Before carrying out programmed loading experiments it was essential to study the results of constant amplitude tests. The small specimens were employed for all tests except those to determine the effect of the rate of change of load level.

Certain parts of the work have been published and copies of the relevant papers are included in appendix 4 (see refs. 49, 103, 104).

4.1.1. Push-Pull Tests at Zero Mean Stress

Fatigue tests were carried out initially at zero mean stress at three principal alternating stress levels on the 2 ton Amsler Vibrophore. Results were interpreted in terms of stress-log cycles to failure and also by fracture mechanics. Failure was defined as the point at which the Vibrophore could no longer maintain the alternating load.

Fig. 18 shows the S-N curve drawn through the mean of the points obtained. There is clearly a large amount of scatter, more than would be normally expected from notched test pieces.

Crack growth-cycles data were plotted on linear scales for each test and a smooth curve drawn through the points. A typical example is shown in fig. 19. The slope of the curve (da/dN) was measured manually at 0.020" (0.5 mm) intervals, but the area in the immediate vicinity of the notch was neglected since localised crack acceleration was sometimes observed in this zone. In some instances crack front slanting occurred and in this situation the smooth curve was drawn through the mean of the two sets of crack length data. Stress intensities for each measured crack growth rate were calculated from the relationship:

$$\frac{\Delta K}{2} = Y\sigma\sqrt{a} \quad (5)$$

where $\Delta K/2$ is the range of stress intensity factor for the tensile portion of the cycle, σ the alternating stress and Y the experimental compliance function (obtained from reference 11).

Correction factors were included to take account of the increase in effective crack length due to the finite size of the plastic zone ahead of the crack tip. The radius of the plastic zone r_y was added on to the crack length and the corrected stress intensity re-calculated. For plane strain conditions r_y was derived from the relationship suggested in reference (10)

$$r_y = \frac{1}{5.6\pi} \left(\frac{K_{\max}}{2\sigma_y} \right)^2 \quad (6)$$

where K_{\max} is the maximum value of stress intensity and σ_y is the static tensile yield stress.

Graphs of $\log \Delta K/2$ versus $\log da/dN$ were drawn in an attempt to test the relationship $\log \Delta K/2 = m \log da/dN + \log C$. The slope (m) and intercept (C) were determined by linear regression analysis using an IBM system/360 model 44 computer. Table 3 summarizes the values of C and m together with the stress-life data and errors are quoted where relevant. A detailed discussion of experimental errors in the present work is given in appendix 5. Fig. 20 shows all of the fracture mechanics data on one graph and again the scatter is very marked.

The possibility of specimen overheating during the tests was investigated as a possible cause of scatter. Copper-constantan thermocouples were attached to several specimens in the immediate vicinity of the notch and in the bulk material well ahead of the propagating crack. Fig. 21 shows a typical temperature-life curve for a high stress test, from a thermocouple located in the bulk of the material. (Temperature readings taken in the immediate vicinity of the notch gave identical results.) It can be seen that the overall temperature rise is about 15^oC.*

Temperature effects were not therefore considered responsible for the observed scatter. However it can be shown by simple mechanics that a small specimen misalignment can create comparatively large bending

*The auxiliary lamp was found capable of raising the temperature of the specimen very rapidly to a level well in excess of the maximum normally attained at the end of the test. For this reason, great care was exercised utilising the lamp which was only illuminated whilst the crack length was being measured.

stresses in a push-pull specimen. Since difficulties of specimen alignment in the Vibrophore grips had been experienced, it was decided to carry out a series of three point bending tests using the same specimens. This loading mode is much less sensitive to misalignment, provided care is taken to grind the edges of the specimen square.

4.1.2. Three point bending tests

4.1.2.1. Small Specimens

The same type of specimen was used for this series of tests as in the push-pull experiments, and the results were analysed in a similar manner. The span, S, between the supports was fixed at 4 times the specimen width and the stress intensity range was calculated from the relationship:

$$\Delta K = \frac{\Delta P Y'}{b \sqrt{w}} \quad (7)$$

where ΔP is the load range, b the specimen thickness and w the specimen width. Equation 7 is an alternative form of the relationship proposed by Srawley & Brown (11):

$$\Delta K = \frac{6 \Delta P Y \sqrt{a}}{b w} \quad \text{for } S = 4 w \quad (8)$$

$$\therefore Y' = 6Y \sqrt{\frac{a}{w}}$$

Equation 7 is more easy to apply since the \sqrt{a} term is included in the Y' function. Tables of Y' against a/w have been published recently (106)

Fatigue tests were carried out at three principal stress levels and fig.22 shows the S-N curve based on a failure crack length of 0.197 ins (5 mm) for all three point bending tests. It can be seen immediately that the level of scatter is remarkably low. Fig. 23 includes all the fracture mechanics data obtained in three point bending tests, and comparison with fig. 20 shows clearly that there is a dramatic reduction in scatter. Table 4 summarises the stress-life and fracture mechanics data for individual tests along with relevant errors, which serve to emphasise the improvement in accuracy.

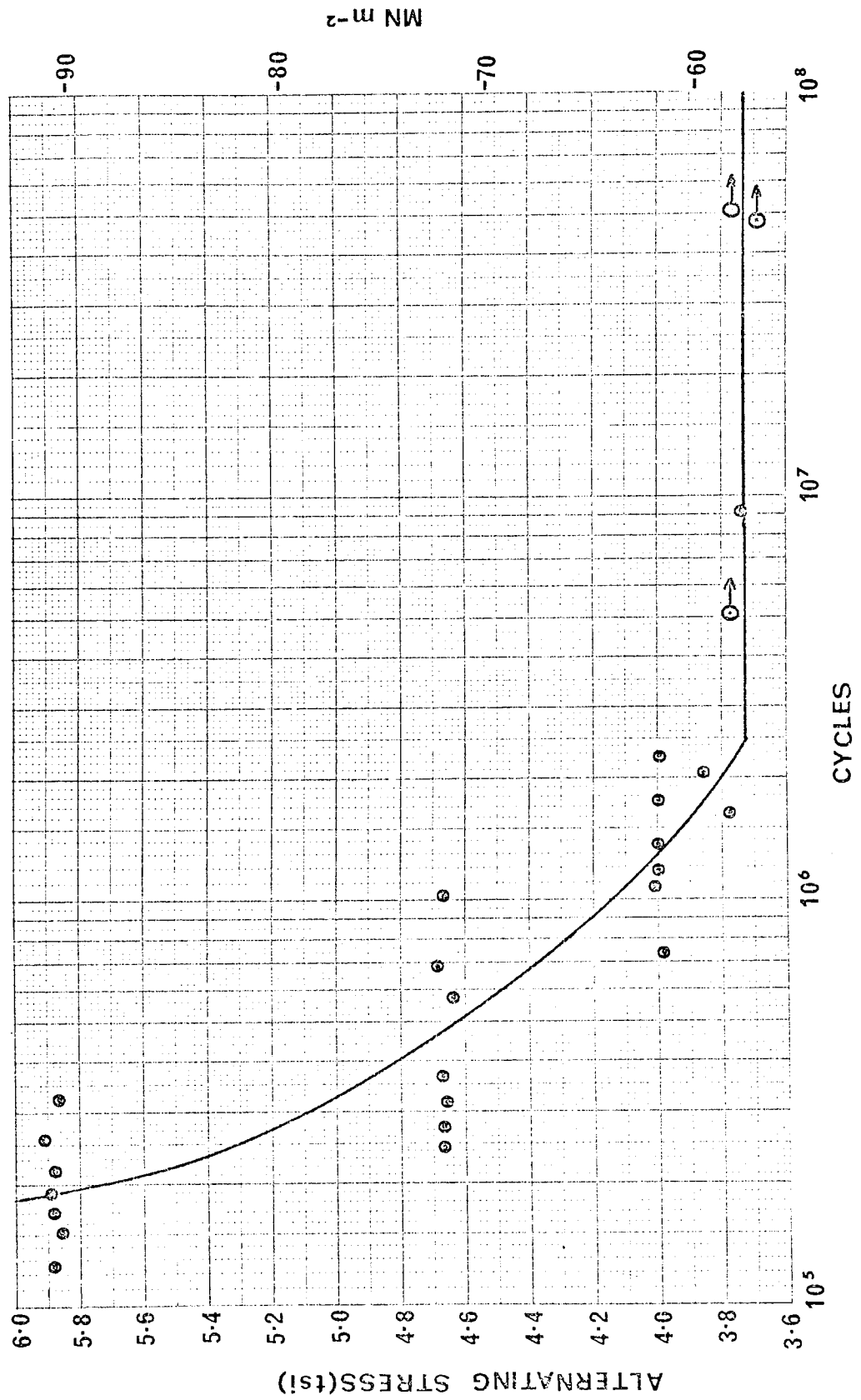


Fig.18 ZERO MEAN STRESS S-N CURVE

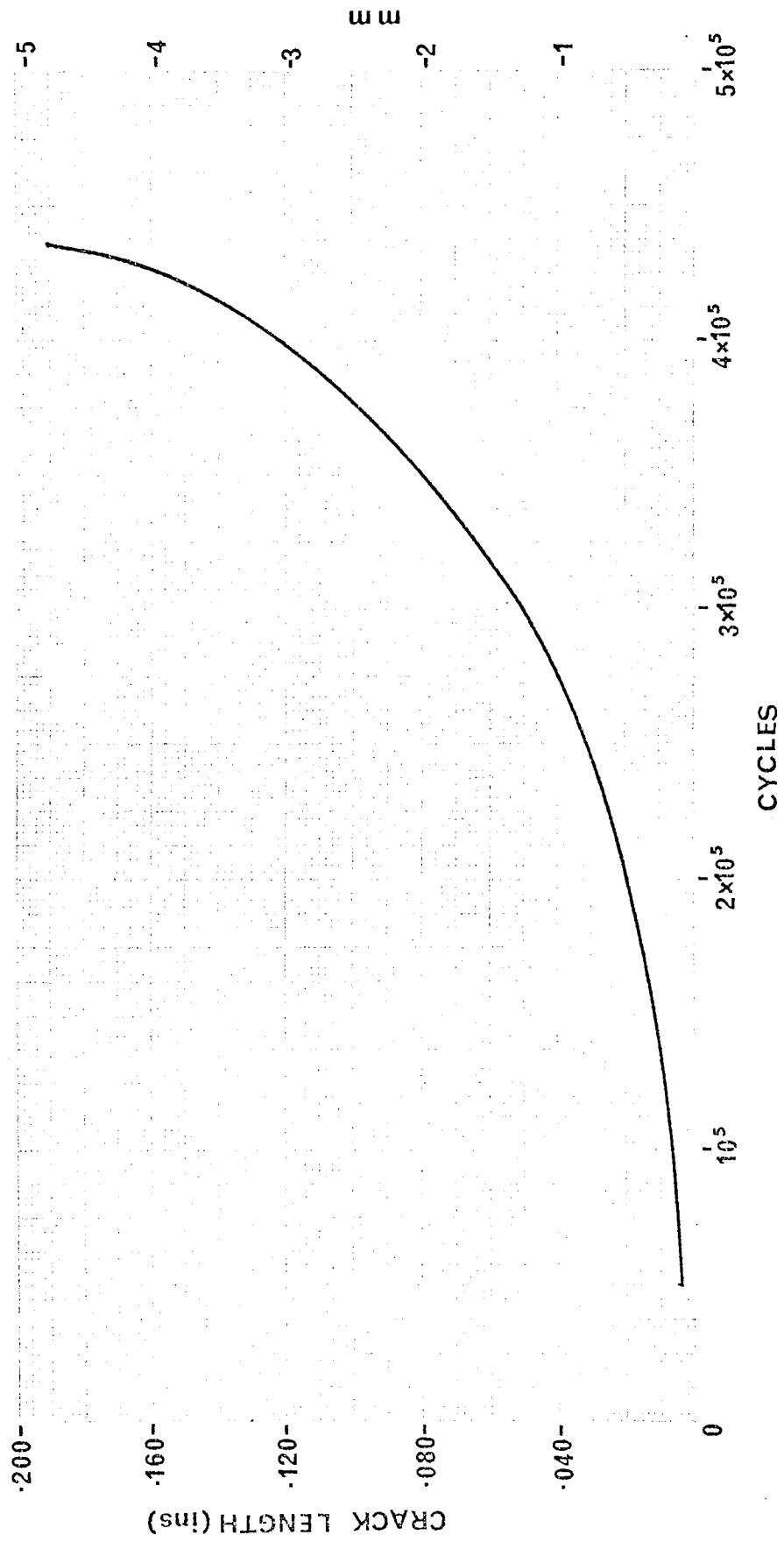


Fig.19 TYPICAL CRACK GROWTH CURVE

SPECIMEN	ALTERNATING STRESS		MEAN LIFE (CYCLES)	STANDARD DEVIATION ON LIFE %	m	STANDARD ERROR ON m %	C Imp. (SI)
	tsi	MN/m ²					
9, 21, 27, 28, 30, 32, 33	5.88	91	2.05×10^5	± 31	3.8	± 9	10^{-20} to 10^{-24} (10^{-11} to 10^{-15})
4, 42, 43, 44, 45, 47, 52	4.67	72	4.96×10^5	± 53	4.2	± 11.5	10^{-20} to 10^{-26} (10^{-9} to 10^{-15})
49, 50, 51, 54, 56, 57	4.00	62	1.39×10^6	± 35	4.5	± 8.1	10^{-22} to 10^{-26} (10^{-10} to 10^{-14})
13	3.78	58	1.63×10^6	-	3.2	± 3.0	10^{-19} (10^{-11})
12	3.86	60	2.04×10^6	-	3.3	± 2.0	10^{-20} (10^{-12})

TABLE 3. SUMMARY OF ZERO MEAN STRESS FATIGUE TEST RESULTS

SPECIMEN	ALTERNATING LOAD		MEAN LIFE (CYCLES)	STANDARD DEVIATION ON LIFE %	m	STANDARD ERROR ON m %	C Imp. (SI)
	lb	N					
66-71	439	1953	1.69×10^5	4.8	3.23	± 3.0	2.1×10^{-20} (1.9×10^{-12})
72	358	1593	3.27×10^5	-	2.74	± 3.5	1.6×10^{-18} (5.2×10^{-12})
73	323	1437	4.74×10^5	-	2.84	± 2.0	6.3×10^{-19} (4.1×10^{-12})
74-77	305	1357	5.53×10^5	1.4	2.60	± 1.5	7.1×10^{-18} (8.9×10^{-12})
78-83	233	1036	1.26×10^6	2.6	2.63	± 5.5	4.0×10^{-18} (6.2×10^{-12})
84	179	796	2.75×10^6	-	2.85	± 5.5	2.0×10^{-19} (1.4×10^{-12})

TABLE 4. SUMMARY OF THREE POINT BENDING FATIGUE TESTS RESULTS (MEAN LOAD = 448 lb (1993N)).

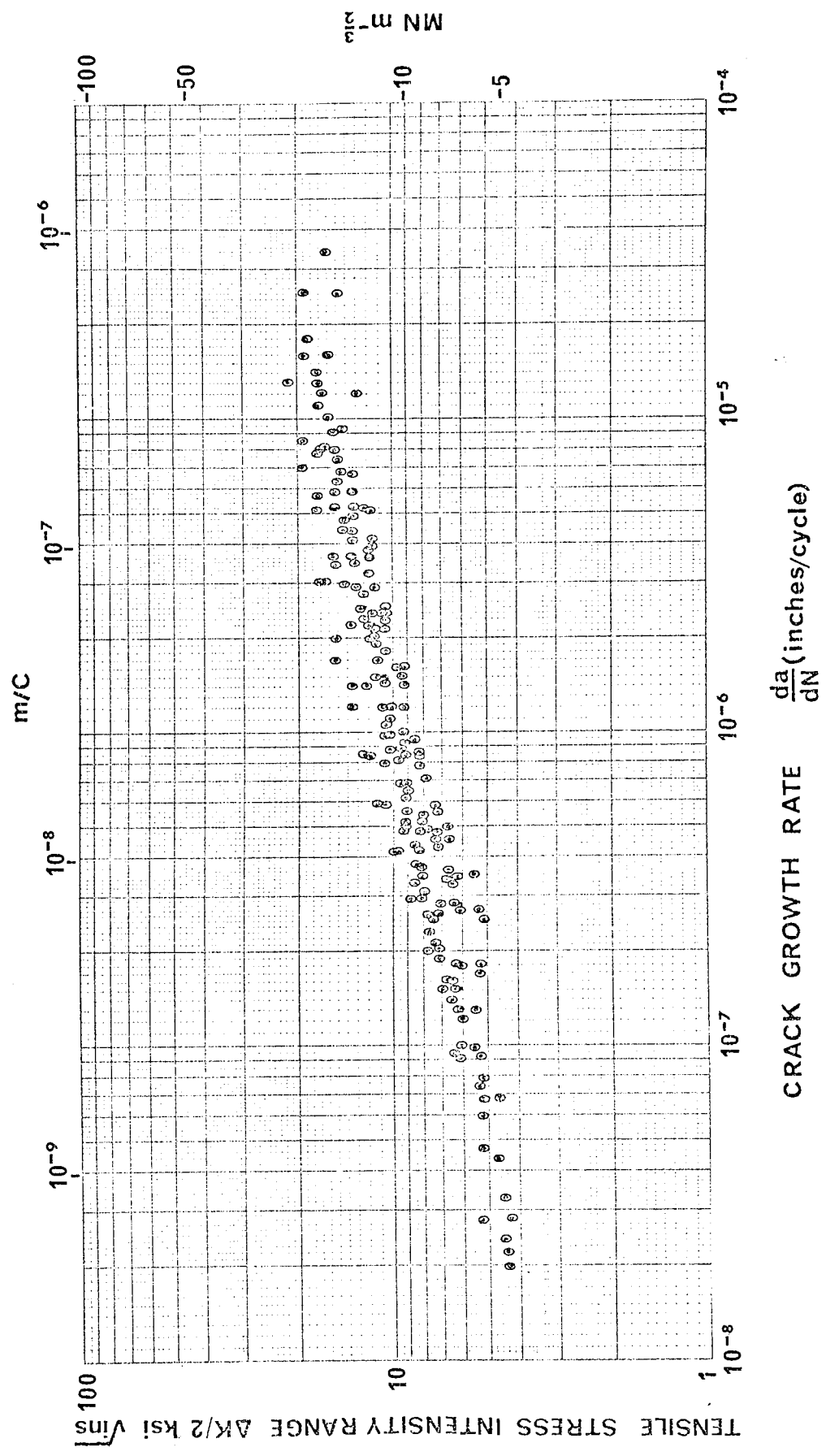


Fig.20 ZERO MEAN STRESS FRACTURE MECHANICS RESULTS

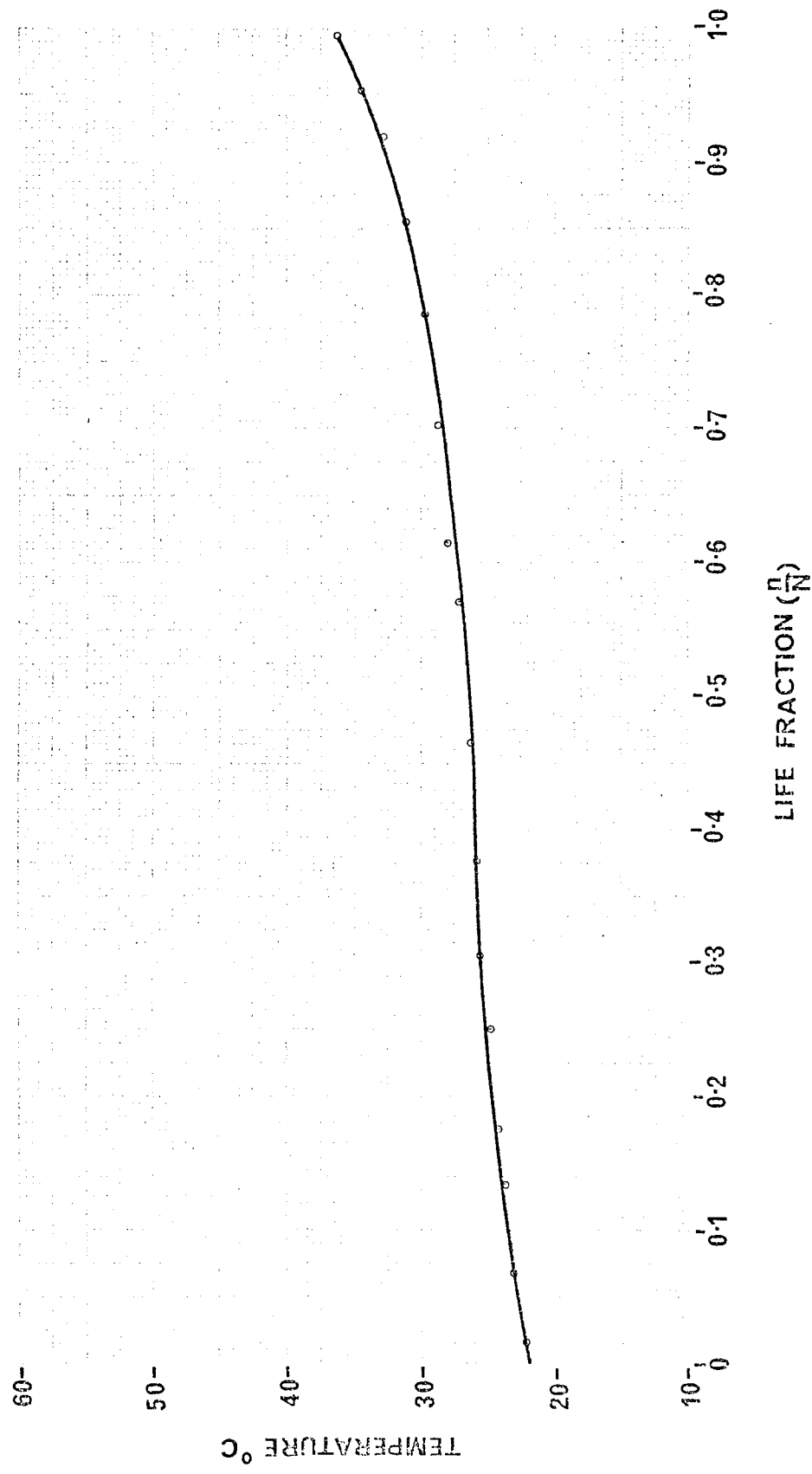


Fig.21 SPECIMEN HEATING CURVE

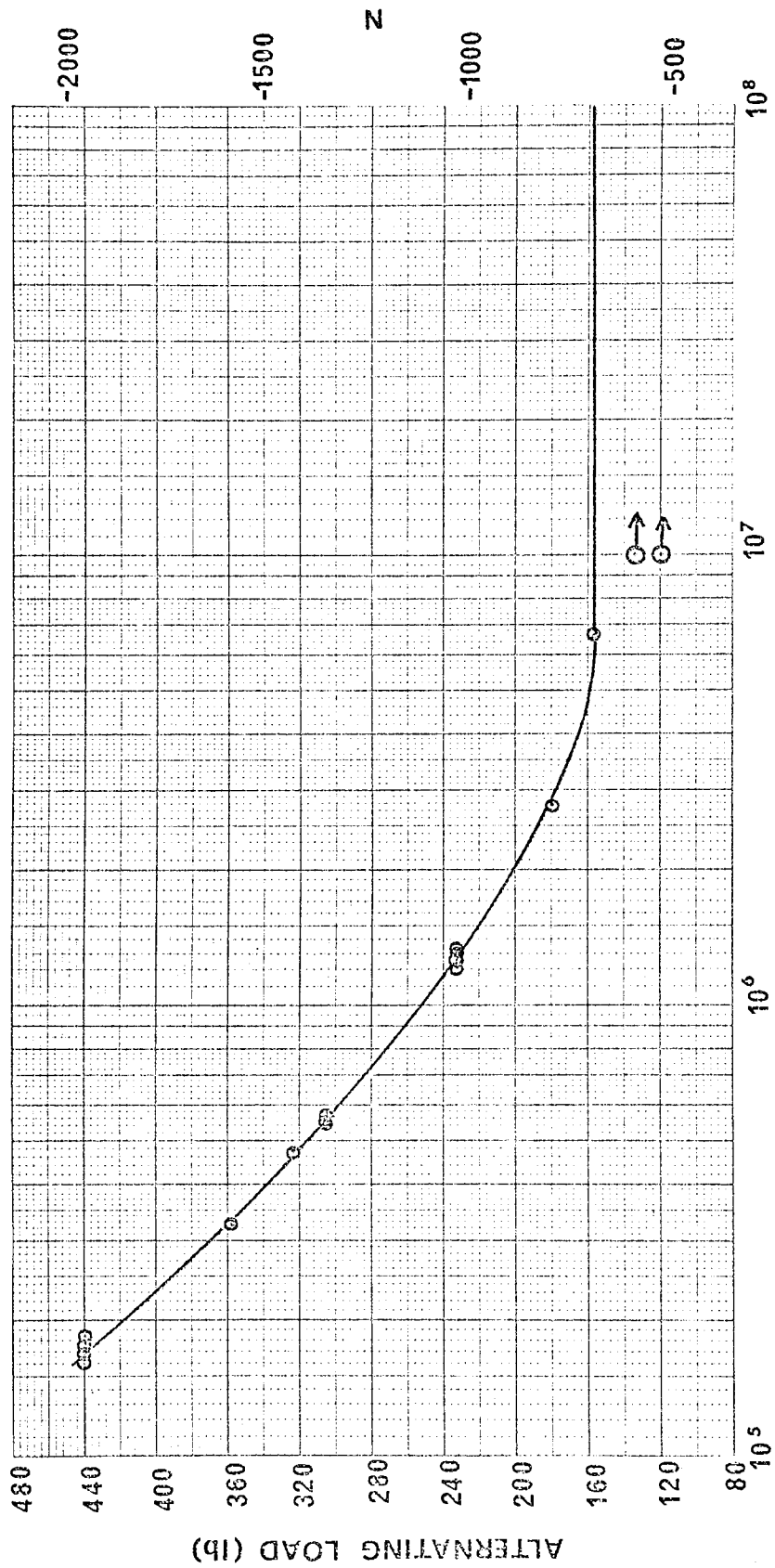


Fig.22 THREE POINT BENDING S-N CURVE

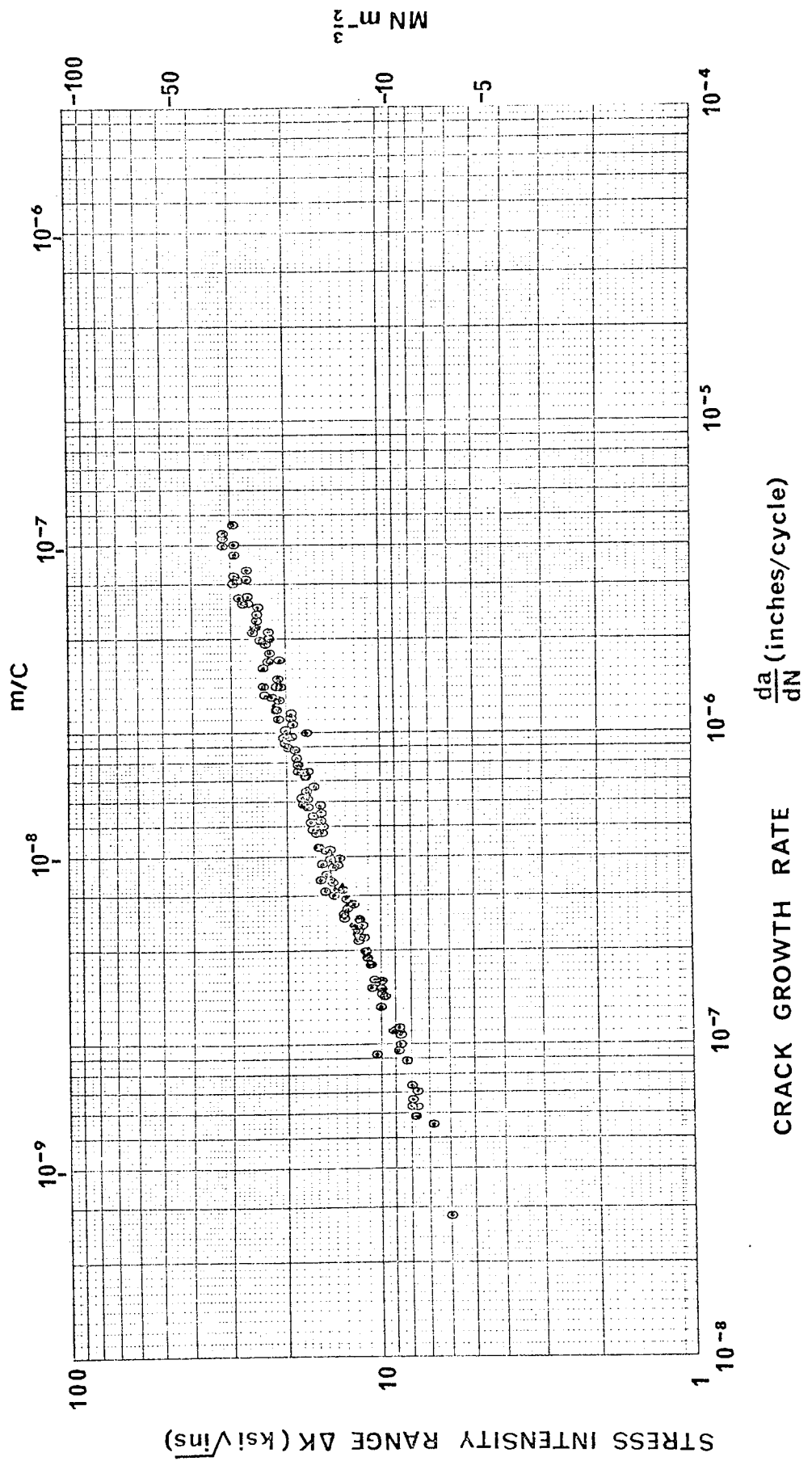


Fig.23 THREE POINT BENDING, FRACTURE MECHANICS RESULTS

The six tests carried out at the highest stress level show significantly higher m values (3.23) than those of the remaining tests (2.60) and since the fracture mechanics analysis took no account of the stress ratio, the results were re-analysed using the relationship of Forman et al (23):

$$\frac{da}{dN} = \frac{C_1 (\Delta K)^m}{(1-R)K_c - \Delta K} \quad (3)$$

where a K_c value of 150 ksi $\sqrt{\text{ins}}$ (165 MN m^{-3/2}) was assumed. Table 5 gives the results, where it can be seen that although the relationship leads to a reduction in m value, the differential still exists.

SPECIMENS	m	STANDARD ERROR ON m %
66 - 71	2.76	±3.5
72	2.35	±3.5
73	2.47	±2.0
74 - 77	2.26	±1.1
78 - 83	2.29	±4.0
84	2.55	±5.5

TABLE 5. FORMAN ET AL ANALYSIS

4.1.2.2. Large EN 3B Specimens

Tests were carried out at two specific stress levels to give lives of approximately 10⁵ cycles and 8 x 10⁵ cycles. Two tests were carried out at each stress level and were again interpreted in terms of stress-life and fracture mechanics. Table 6 lists the experimental results and fig. 24 shows the fracture mechanics data. The m values lie between 2.6 and 2.8 and appear to be stress independent.

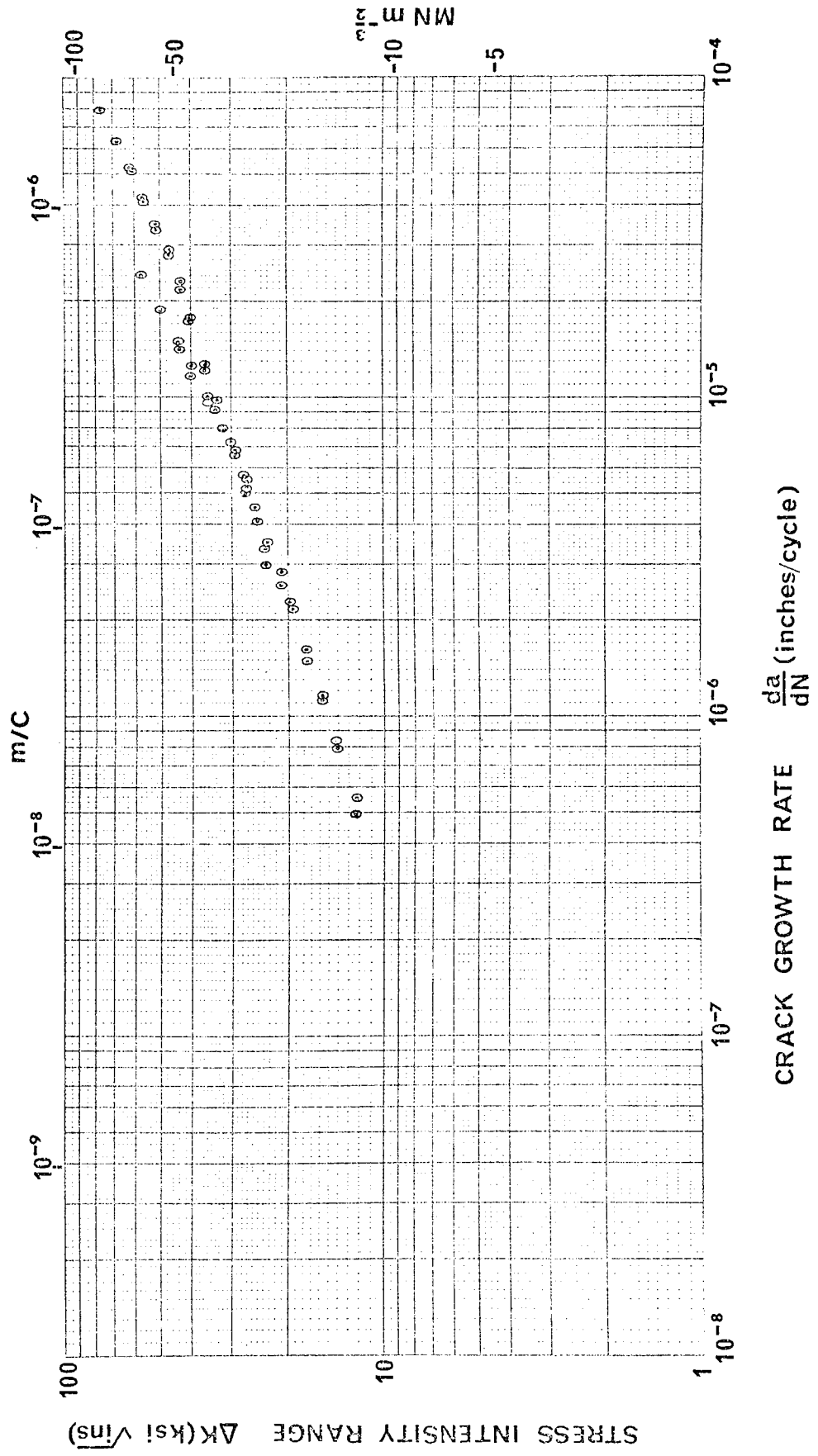


Fig.24 LARGE MTS SPECIMENS, FRACTURE MECHANICS RESULTS

SPECIMEN	ALTERNATING LOAD		LIFE (CYCLES)	m	STANDARD ERROR OF FIT %	C IMP. (SI)	ERROR ON INDEX
	tons	kN					
K7	2.70	26.9	1.32×10^5	2.80	± 2.7	2×10^{-18} (9.8×10^{-12})	± 0.4
K8	1.43	14.3	7.83×10^5	2.74	± 2.3	4×10^{-18} (1.3×10^{-11})	± 0.3
K9	1.43	14.3	8.40×10^5	2.60	± 3.3	1.6×10^{-17} (2.0×10^{-11})	± 0.4
K10	2.70	26.9	1.28×10^5	2.69	± 2.8	6.3×10^{-18} (1.5×10^{-11})	± 0.4

TABLE 6. RESULTS OF MTS FATIGUE TESTS
(MEAN LOAD = 2.75 tons (27.4 kN))

4.2. FRACTOGRAPHIC OBSERVATIONS UNDER CONSTANT AMPLITUDE LOADING

The Cambridge Stereoscan was used to examine the fracture surfaces of specimens fatigued under both push-pull and three point bending conditions. Unless otherwise stated the following observations apply equally to both loading modes. In all cases the fractures produced were of the stage II type. Directions of crack propagation are indicated on each fractograph.

4.2.1. Slow Crack Growth Rates

When the macroscopic crack growth rate was less than approximately 3.2×10^{-7} ins (8 nm) per cycle the fracture was found to show several important distinguishing features. Fig. 25 shows a typical area of fatigue fracture in this region, photographed at an angle of 45° with respect to the electron beam. Feature A is shown in more detail in figs. 26 and 27. It is seen to consist of a series of ridges forming a "hill and valley" type of structure running parallel to the direction of crack growth. Progression markings or striations run across these ridges in a direction approximately parallel to the crack front. Fig. 28 shows a similar area taken with the fracture surface normal to the beam. In this case the hill and valley structure is clearly associated with two adjacent ferrite grains labelled C at the centre of the photomicrograph.

Fig. 25 also shows grain boundary cracking (labelled B) to be associated with this mode of fracture, and another typical area is shown in more detail in figs. 29 and 30. The markings present on the grain boundary facets are similar to the wavy slip traces that are normally observed on electro-polished surfaces of ferrous fatigue specimens and could be confused with striations. They are probably slip traces formed on the freshly exposed fracture surface in the wake of the advancing crack.

4.2.2. Fast Crack Growth Rates

At higher stress intensities, where the crack growth rate exceeds about 2×10^{-6} ins. (50 mm) per cycle, the fracture mode described above gives way to a different mode which is structure insensitive. Figs. 31 to 33 show details of this type of fracture at various magnifications with the specimen at 45° to the beam. It is ragged in appearance and exhibits some surface cracking. At higher magnifications the fatigue striations are clearly visible and cover the majority of the fracture face.

Because of the marked difference between the two modes of fracture they were designated stage IIa (structure sensitive) and stage IIb (structure insensitive).

Several specimens tested at zero mean stress exhibited evidence of damage due to the fracture faces rubbing together. Fig. 34 shows an area of stage IIb fracture, with the associated damage and general attrition labelled D. In some instances lines reminiscent of fatigue striations were observed running across the facets of batter. Not all of the zero mean stress fractures showed this effect which is probably associated with slight mis-alignment of the specimen in the grips. No evidence of battering was observed on any of the three point bending fractures.

4.2.3. The Role of Pearlite in the Fatigue Fracture Process

In order to determine the role of pearlite in the fracture process, fracture surface etching and sectioning was carried out. Etching was achieved by immersing the fracture in a solution of 2% nitric acid in ethyl alcohol for progressively increasing times, followed by examination

on the Stereoscan. Further details concerning the attainment of the optimum etching time (which was 100 seconds) are given in reference (103) which is also included in Appendix 4.

A typical area of stage IIa and stage IIb fracture measuring 0.025 inches (.64 mm) by .013 inches (0.33 mm) was etched for 100 seconds and the number of pearlite colonies revealed were counted. On an area basis stage IIa showed approximately 4% of pearlite whilst stage IIb revealed 10%. The expected pearlite content for this material as established by quantitative metallography on polished and etched micro-sections is about 12%. Figs. 35 and 36 show areas of etched pearlite on IIa and IIb fracture respectively.

Longitudinal sections were next taken through the fracture to determine the location of the crack path with respect to the pearlite colonies. Figs. 37 and 38 show sections taken through stages IIa and IIb fracture respectively. In stage IIa the preferred crack path is around the pearlite colony whilst in stage IIb the crack appears to cut straight through. Thus in stage IIa the pearlite colony will appear in only one of the fracture surfaces and the apparent pearlite density will be half that expected, as was observed.

4.2.4 Observations of stage IIa and IIb in other materials

This part of the work was carried out to determine whether the stage IIa and stage IIb modes of fracture were operative in other materials.

Single edge notched specimens of oxygen free high conductivity copper and 18/8 stainless steel were tested in push-pull on the 2 ton Vibrophore. The results of the fracture surface observations are shown in figs. 39 to 42. It can be seen that at slow crack growth rates near the notch root, there is evidence of grain boundary facets in both materials (figs. 39, 41). At longer crack lengths however the fracture surfaces of both materials (figs. 40, 42) resemble the stage IIb mode. The presence of these grain boundary facets is considered to suggest that the stage IIa mode of fracture is operative at slow crack growth rates although the "hill and valley" feature does not appear to be clearly defined.

Fig. 25. Stage IIa Fracture
x 550 Mag.
Operating Angle 45° .
(Neg. 148/13A)

Fig. 26. "Hill and Valley" Structure
Within a Ferrite Grain.
x 2200 Mag.
Operating Angle 45° .
(Neg. 148/8A)

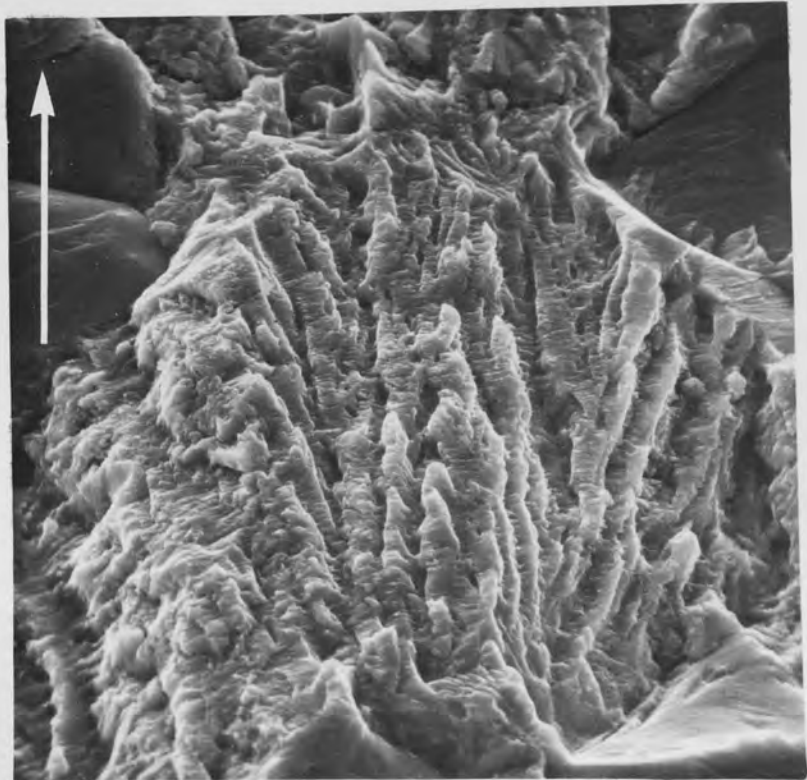
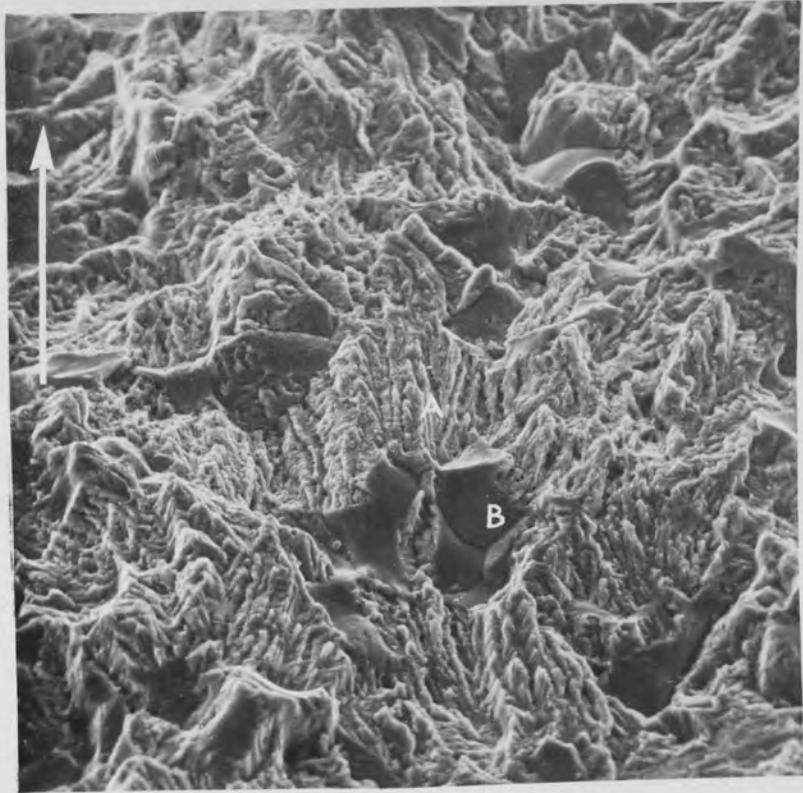


Fig. 27. Striations Running Across the
"Hill and Valley" Structure.
x 11000 Mag.
Operating Angle 45° .
(Neg. 148/2)

Fig. 28. Adjacent Ferrite Grains
Labelled "C" in Stage IIa
Fracture.
x 550 Mag.
Operating Angle 90° .
(Neg. 153/17)



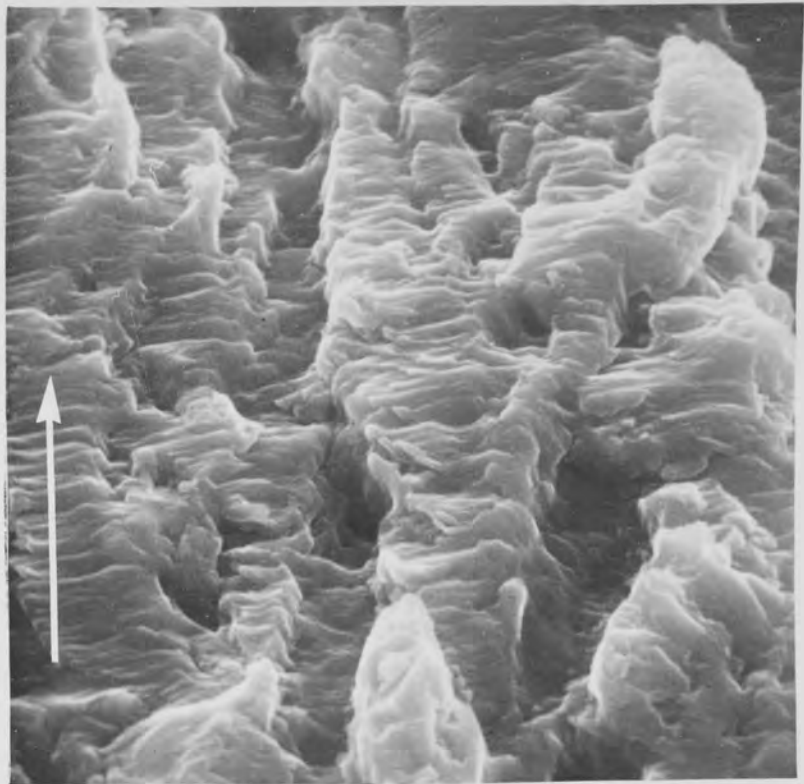


Fig. 29. Grain Boundary Fracture
in Stage IIa.
x 2300 Mag.
Operating Angle 45° .
(Neg. 148/36A)

Fig. 30. Slip Traces on a Grain
Boundary Facet.
x 5300 Mag.
Operating Angle 45° .
(Neg. 148/32A)

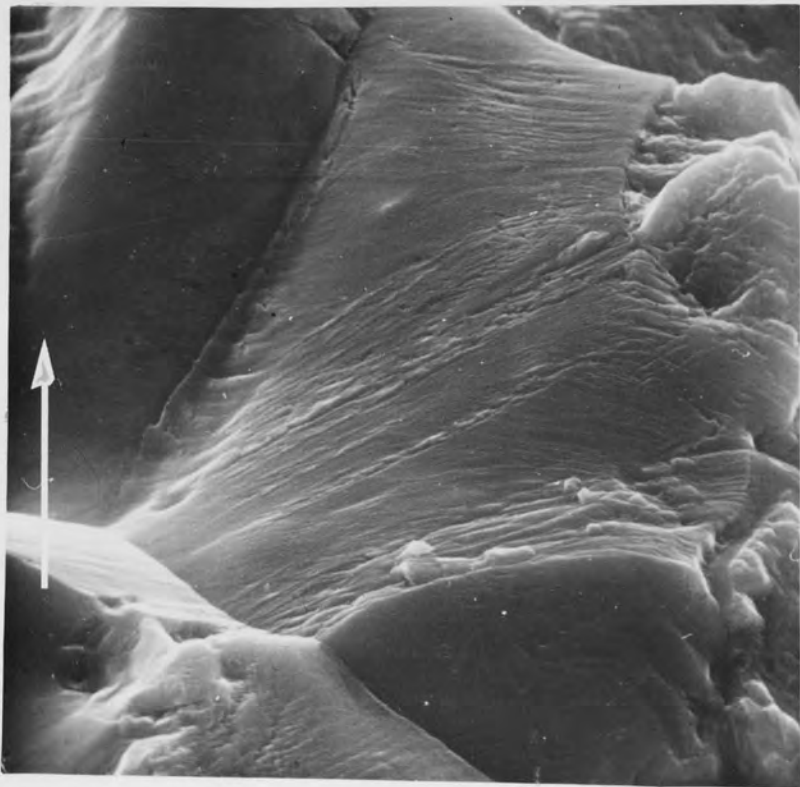
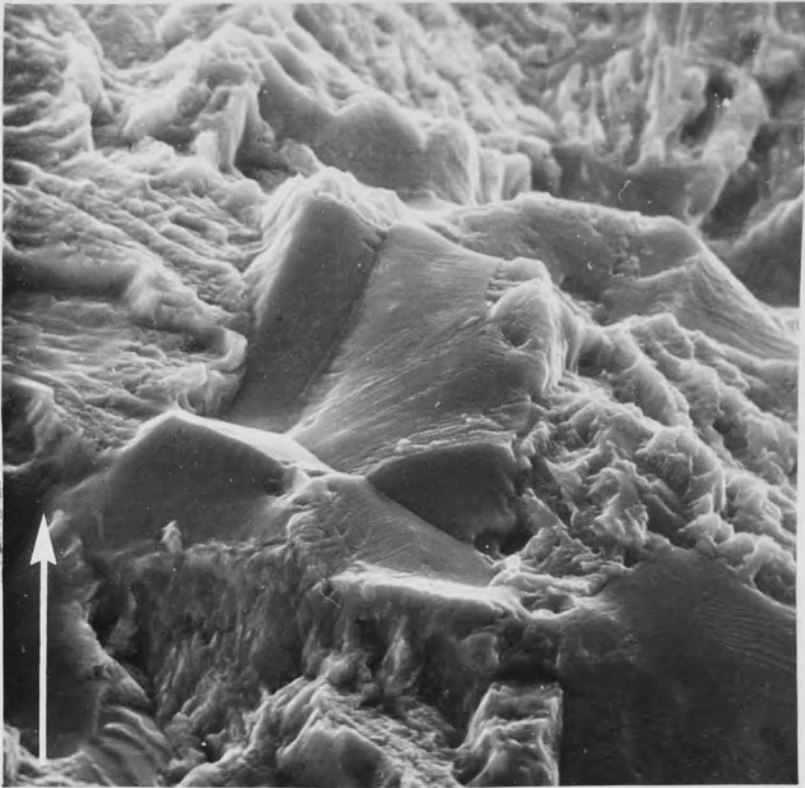


Fig. 31. Stage IIb Fracture.
x 500 Mag.
Operating Angle 45° .
(Neg. 233/34)

Fig. 32. Stage IIb Fracture
x 2000 Mag.
Operating Angle 45° .
(Neg. 233/32)

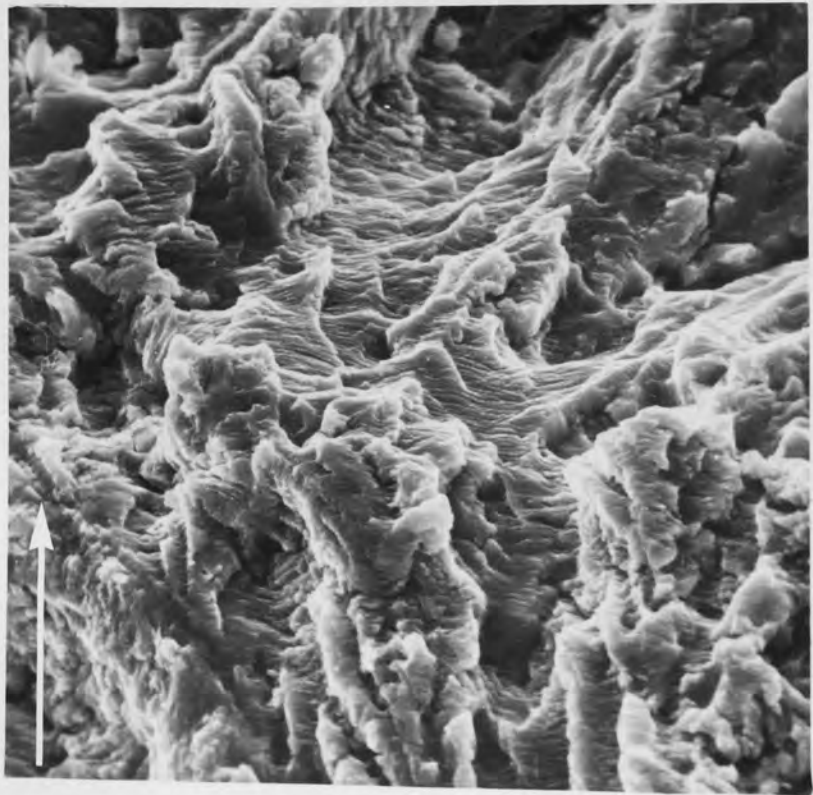
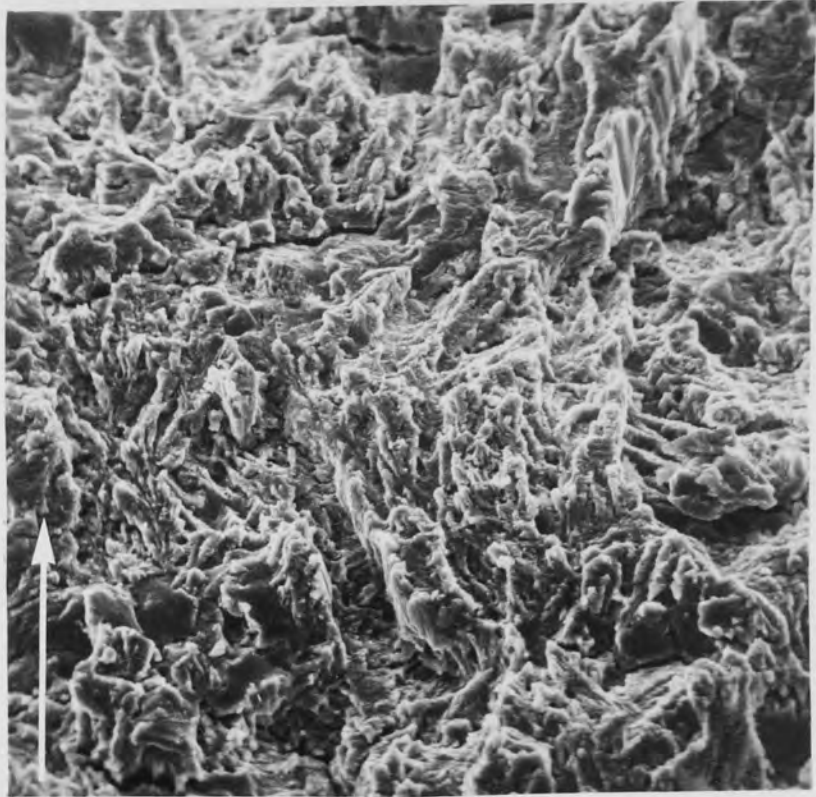


Fig. 33. Striations on Stage IIb Fracture
x 5000 Mag.
Operating Angle 45° .
(Neg. 233/31)

Fig. 34. Fracture Surface Batter
Labelled "D" on Stage IIb
Fracture.
x 5700 Mag.
Operating Angle 45° .
(Neg. 91/3)

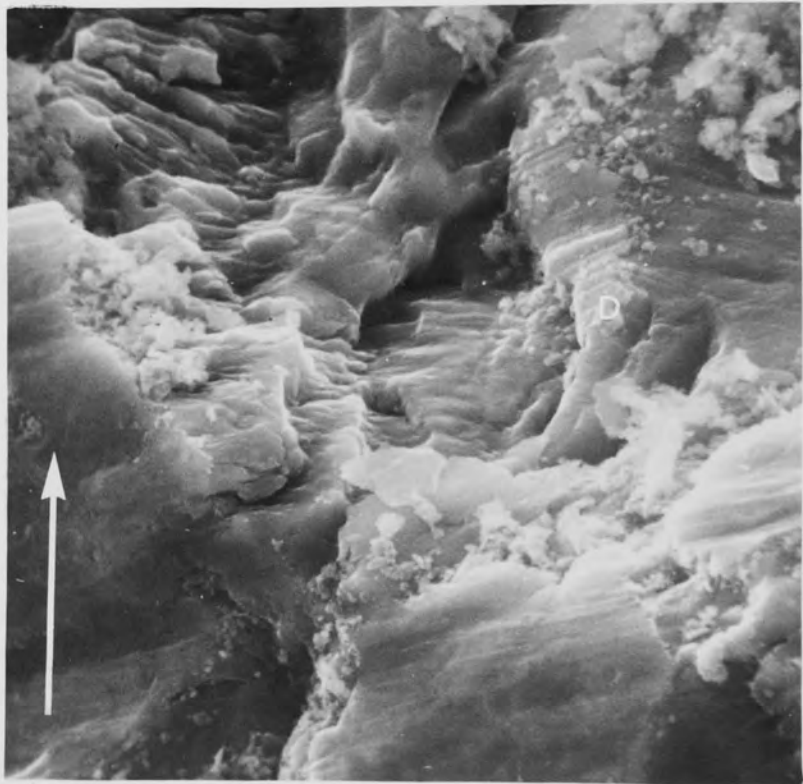
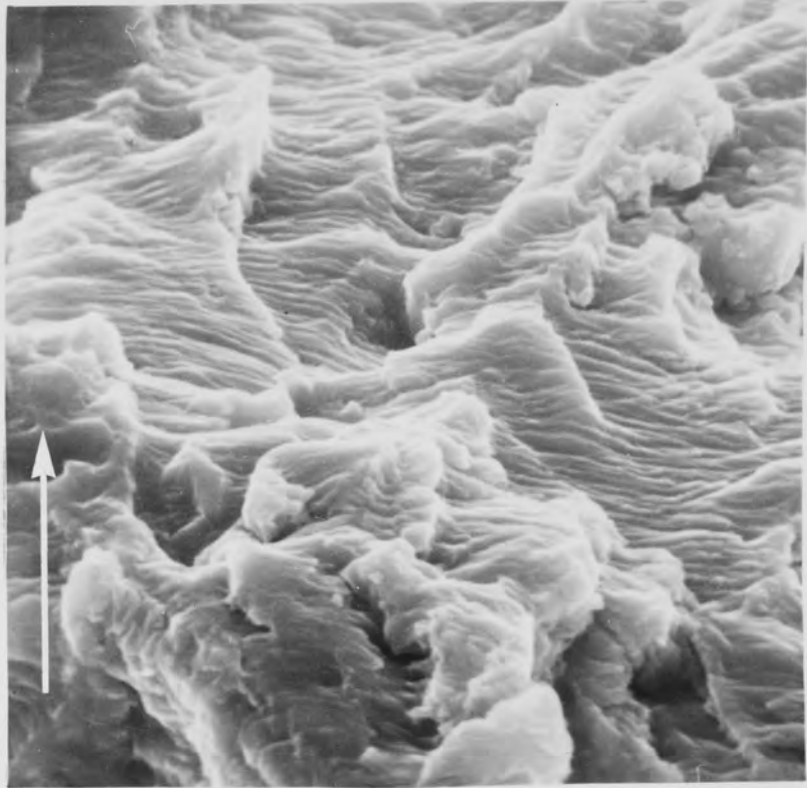


Fig. 35. Pearlite on Stage IIa Fracture.
100 Seconds Etching Time.
x 2400 Mag.
Operating Angle 45° .
(Neg. 48/11)

Fig. 36. Pearlite on Stage IIb Fracture.
100 Seconds Etching Time.
x 6000 Mag.
Operating Angle 45°
(Neg. 130/20A)

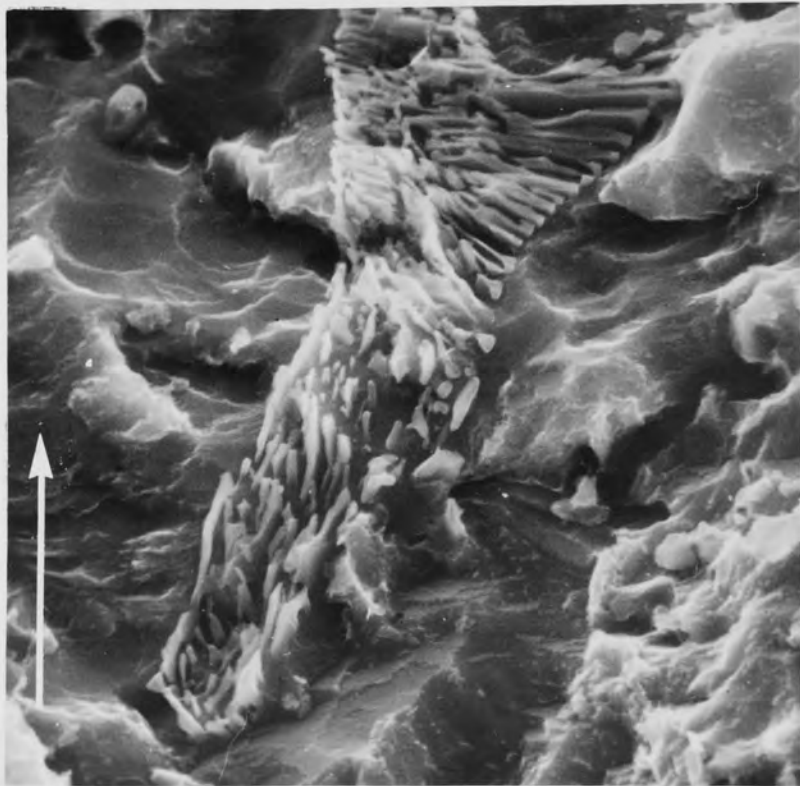
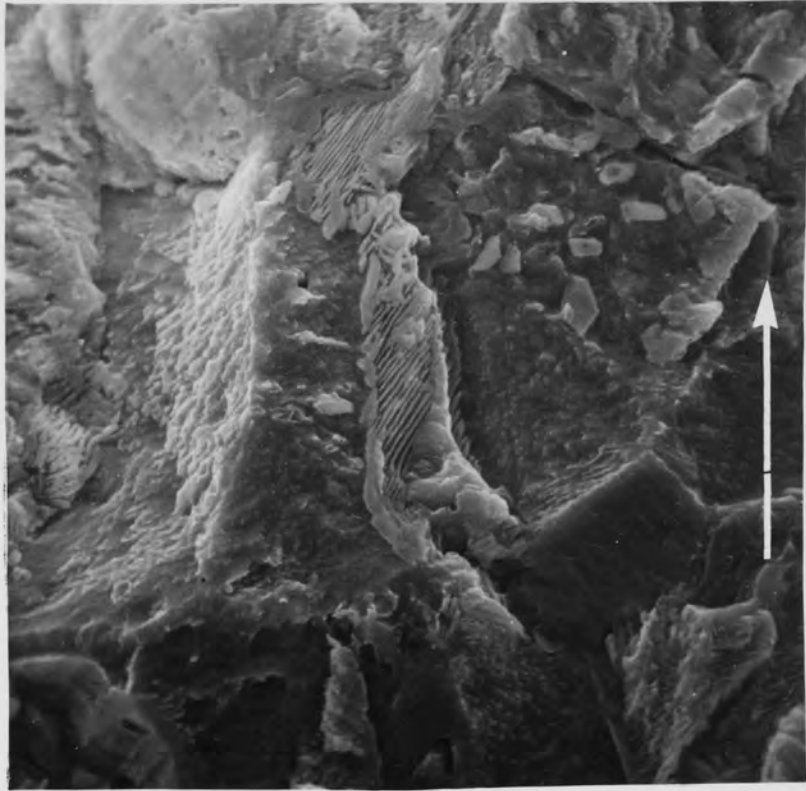


Fig. 37. Longitudinal Section Through
Stage IIa Fracture.
x 2500 Mag.
Operating Angle 45°
(Neg. 153/14)

Fig. 38. Longitudinal Section Through
Stage IIb Fracture.
x 5800 Mag.
Operating Angle 45° .
(Neg. 153/15)

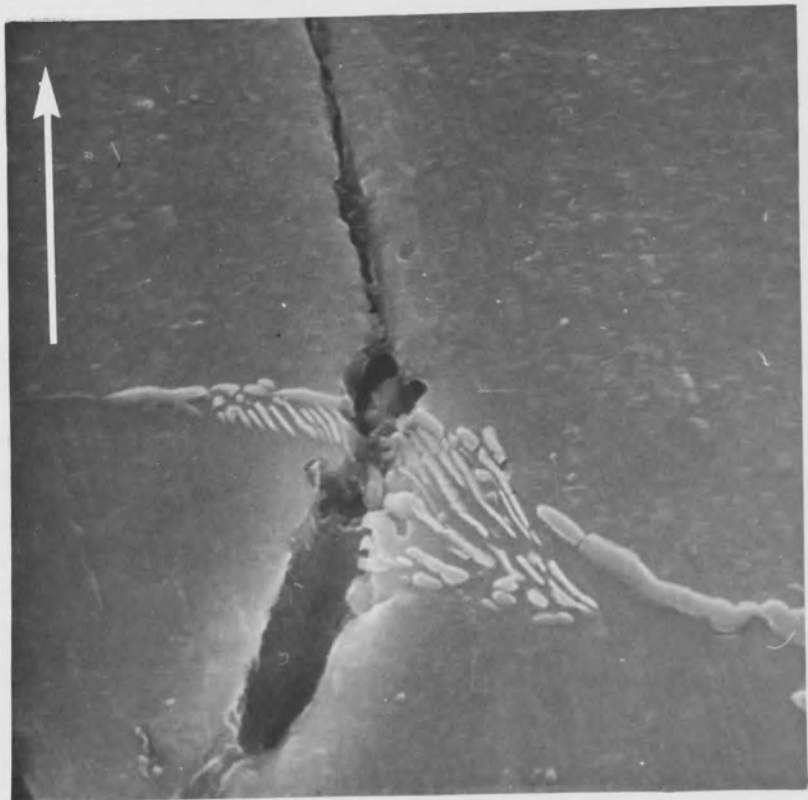
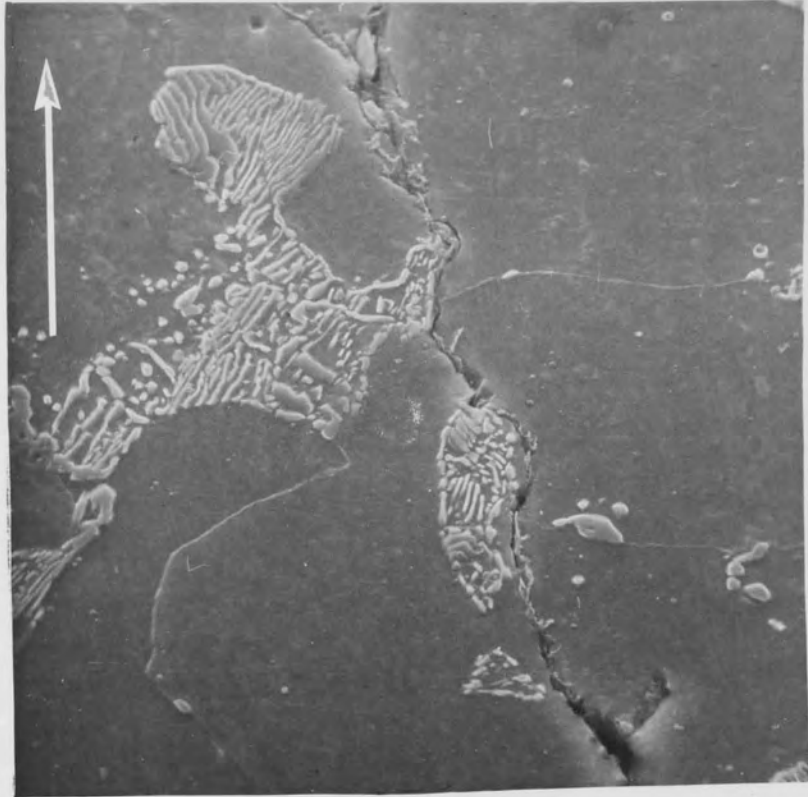


Fig. 39. Grain Boundary Fracture in
OFHC Copper.
x 600 Mag.
Operating Angle 45° .
(Neg. 182/5A)

Fig. 40. Stage IIb Fracture in
OFHC Copper.
x 500 Mag.
Operating Angle 45°
(Neg. 182/43)

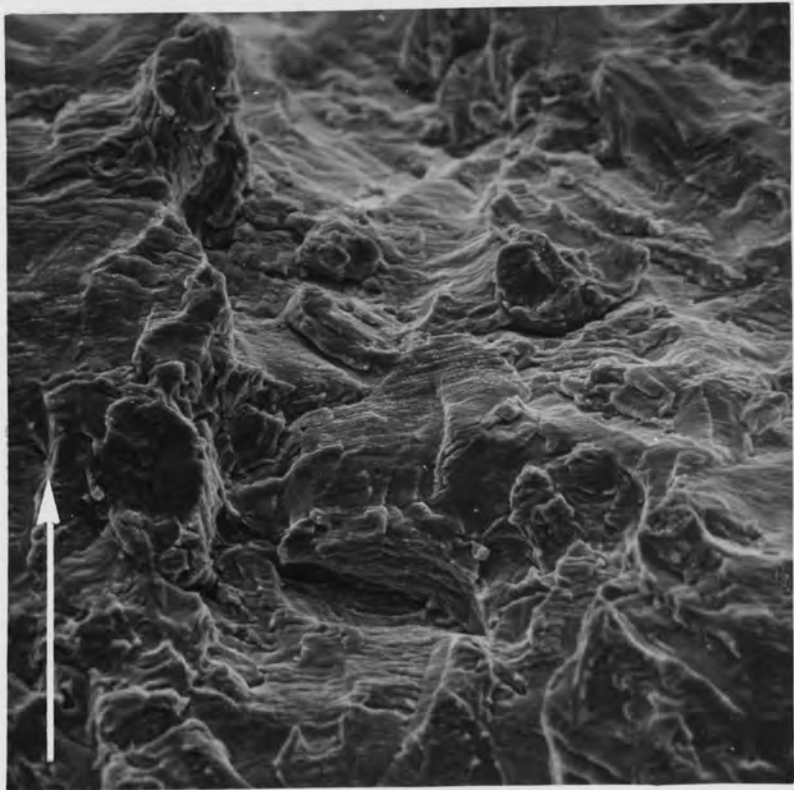
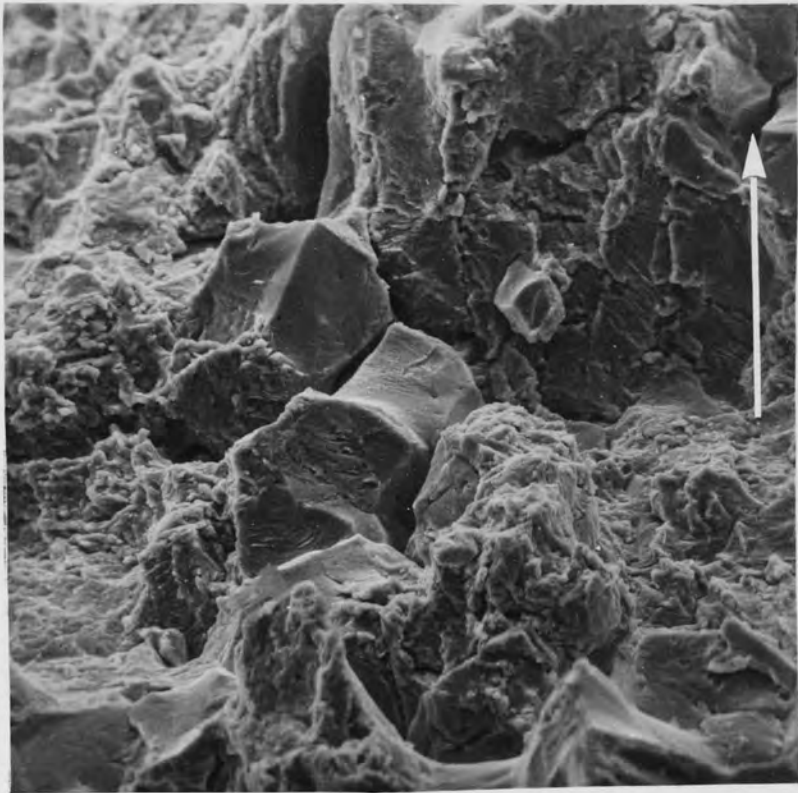
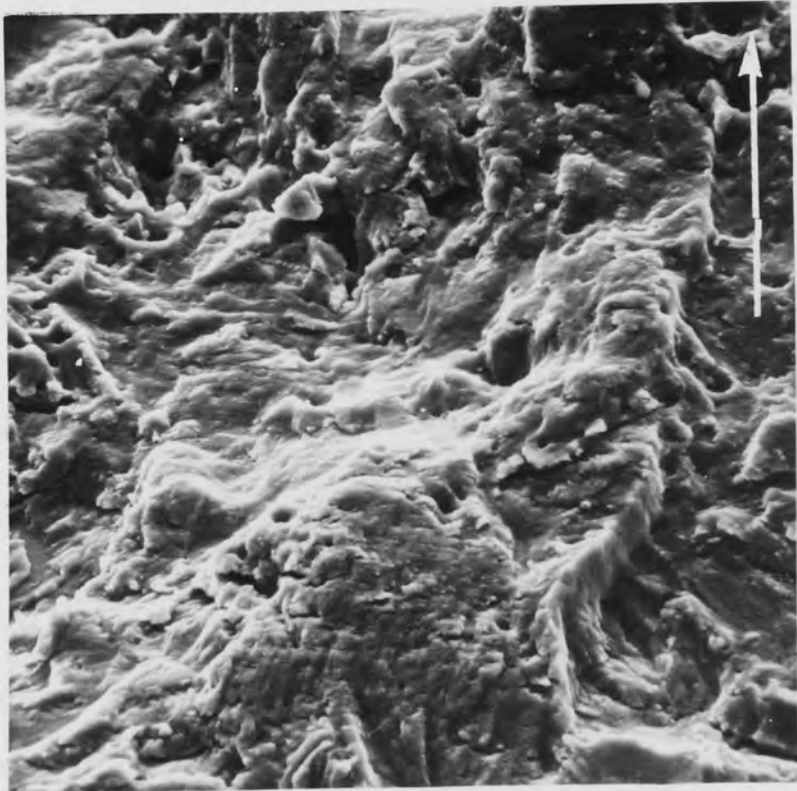
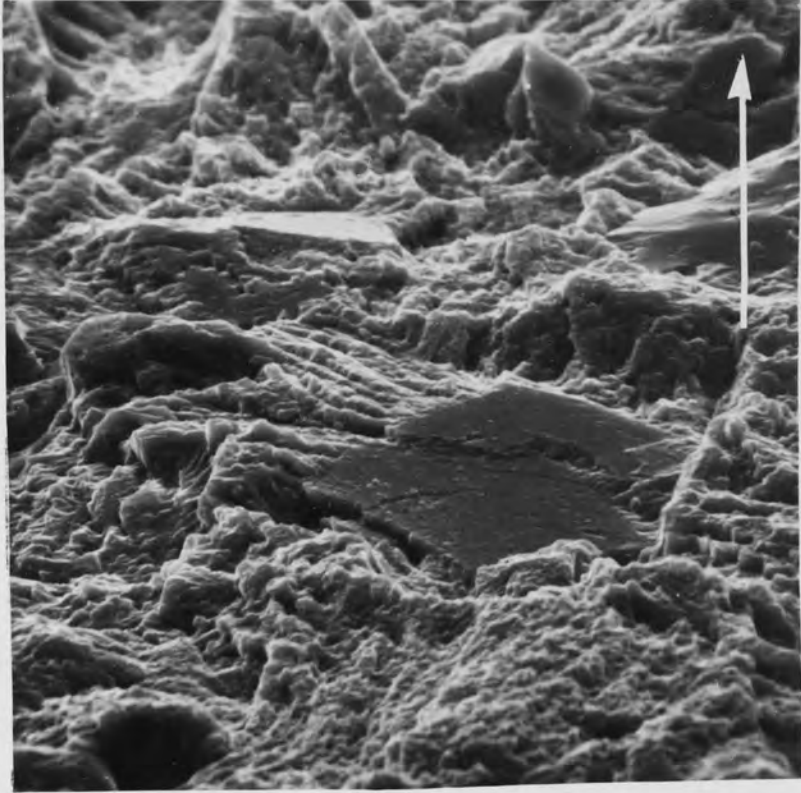


Fig. 41. Grain Boundary Facets in
18/8 Stainless Steel.
x 2200 Mag.
Operating Angle 45° .
(Neg. 236/35)

Fig. 42. Stage IIb in 18/8
Stainless Steel.
x 2200 Mag.
Operating Angle 45° .
(Neg. 236/36)



LIBRARY

4.2.5. Quantitative Aspects of Stage IIa and Stage IIb Fracture

The transition from IIa to IIb occurred very rapidly in specimens tested at high stresses, but at low stresses the transition period was longer and contained mixed fracture modes. Crack lengths at which the transition occurred were measured on both zero mean stress and three point bending specimens using the micrometer stage of the Stereoscan. The location of the transition was taken as the point at which the last well defined grain boundary facet appeared.

Six specimens were heated to between 900°C and 1200°C in vacuum to produce coarser grain sizes ranging from .0025 ins to .0045 ins. (67 to 115 μm). These were fatigue tested in three point bending and a record of the crack length-cycles relationship was taken in the usual way. Crack growth data was interpreted in terms of fracture mechanics and the transition from stage IIa to IIb was again measured on the Stereoscan. Table 7 gives details of the fracture transition. For the zero mean stress tests, the effective pulsating tension stress was calculated from the work of Gurney (25). This was then used to calculate the maximum stress intensity at the transition crack length.

For a constant grain size there is a critical stress intensity and hence a specific plastic zone size at which the transition occurs. This value of stress intensity factor remains constant with changes in alternating load level in both tension-tension and zero mean stress. Those specimens with coarser grain sizes show larger values of K_{max} at the transition, but the ratio of plastic zone size to mean grain diameter remains constant at about 4. The range of values quoted in table 7 is probably associated with inaccuracies in the determination of the crack length at the transition.

The effects of mean stress and loading mode on the stage IIa to stage IIb transition were also investigated. The results are shown in table 8 where it can be seen that the ratio of r_y/d is again in the region of 4.

SPECIMEN	GRAIN SIZE (d) ins (μ m)	YIELD STRESS tsi (MN/m ²)	K _{max} TRANSITION ksi ^{1/2} ins (MNm ^{-3/2})	TRANSITION PLASTIC ZONE RADIUS (r _y) ins (mm)	r _y /d
TR1	.0039 (100)	7.6 (117)	16.98 (18.66)	.014 (.356)	3.62
TR2	.0045 (115)	7.5 (116)	17.97 (19.75)	.016 (.406)	3.60
TR3	.0029 (74)	8.0 (124)	16.45 (18.08)	.012 (.305)	4.10
TR4	.0029 (73)	8.6 (133)	17.64 (19.38)	.012 (.305)	4.25
TR5	.0028 (72)	8.6 (133)	18.33 (20.14)	.013 (.330)	4.57
TR6	.0026 (67)	8.8 (136)	17.43 (19.15)	.011 (.279)	4.27
67	.00097 (25)	11.5 (178)	13.22 (14.53)	.0037 (.094)	3.81
77	.00097 (25)	11.5 (178)	13.38 (14.70)	.0038 (.097)	3.92
83	.00097 (25)	11.5 (178)	13.92 (15.30)	.0041 (.104)	4.23
21	.00097 (25)	11.5 (178)	13.16 (14.46)	.0037 (.094)	3.81
52	.00097 (25)	11.5 (178)	13.59 (14.93)	.0039 (.099)	4.02
50	.00097 (25)	11.5 (178)	12.85 (14.12)	.0035 (.089)	3.61

TABLE 7. TRANSITION FROM STAGE IIa TO STAGE IIb.

Table 9 shows the results of the fracture mechanics analysis of the coarse grained specimens. The m and C values do not appear to vary systematically with grain size when compared with the results of the .001" (25 μ m) grain size (see table 4).

4.2.6. Striation Spacing Measurements

It was shown in the literature review that many workers have correlated striation spacings with the macroscopic crack growth rate. Clearly this technique could be extremely useful for programmed loading studies, and with this in view striation spacings of several constant

SPECIMEN	MEAN LOAD lb (N)	MAX. TEST- ING LOAD lb (N)	STRESS RATIO R	K_{max} ksi \sqrt{ins} ($MNm^{-3/2}$)	r_y/d	LOAD MODE
135	376 (1673)	735 (3270)	0.02	13.20 (14.50)	3.81	3PB
136	376 (1673)	681 (3030)	0.10	13.91 (15.28)	4.23	3PB
140	314 (1397)	484 (2153)	0.30	13.00 (14.28)	3.71	TT
141	314 (1397)	627 (2789)	0.00	13.40 (14.72)	3.92	TT
142	314 (1397)	627 (2789)	0.00	13.54 (14.88)	4.02	TT
143	314 (1397)	484 (2153)	0.30	13.43 (14.76)	3.92	TT

Grain Size = .001" (25 μm) 3PB = Three Point Bending TT = Tension-Tension.

TABLE 8. EFFECT OF MEAN STRESS AND LOADING MODE ON THE STAGE IIa TO STAGE IIb TRANSITION

SPECIMEN	GRAIN SIZE		ALTERNATING LOAD		LIFE (CYCLES) $\times 10^5$	m	STANDARD ERROR OF FIT %	C IMP (SI)	STANDARD ERROR ON INDEX
	ins	μm	lb	N					
TR2	.005	115	305	1357	6.40	2.63	± 7.5	5.0×10^{-18} (7.7×10^{-12})	± 0.8
TR3	.003	74	305	1357	5.79	2.91	± 4.5	3.2×10^{-19} (3.3×10^{-12})	± 0.6
TR4	.003	73	305	1357	5.60	2.84	± 8.5	6.3×10^{-19} (4.1×10^{-12})	± 1.0
TR5	.003	72	305	1357	5.70	2.49	± 3.0	1.6×10^{-17} (9.5×10^{-12})	± 0.3
TR6	.003	67	305	1357	5.30	2.69	± 12.3	2.5×10^{-18} (5.8×10^{-12})	± 1.4

TABLE 9. FATIGUE TEST RESULTS OF COARSE GRAINED SPECIMENS

(MEAN LOAD = 448 lb, (1993 N))

amplitude fractures were examined in detail.

Striation spacings were measured at intervals along the fracture at magnifications in the region of 20,000 times. Crack lengths were selected on the basis of the macroscopically observed crack growth rates. The maximum value of crack growth rate varied depending on the loading mode and specimen size. Small specimens tested in three point bending showed a lower maximum crack growth rate than the same specimens tested in the push-pull mode, whilst the large specimens tested on the MTS machine produced the highest values. This is due to the inherent design characteristics of the Vibrophore which prevent the alternating load being maintained under conditions of high strain.

For given crack lengths, six or seven photographs of typical striations were taken on the scanning electron microscope, with the specimen positioned at 90° to the electron beam. Mean striation spacings were measured by laying a rule across the fractograph. All of the measurements were taken from the stage IIb fracture mode and the results are summarised in fig.43. Typical examples of striations are shown in figs. 44 and 45.

A constant striation spacing is observed up to crack growth rates of 7.9×10^{-6} ins (200 nm) per cycle. Beyond growth rates of 1.2×10^{-5} ins (300 nm) per cycle there is a tendency for the observed striation spacing to correlate with the macroscopic crack growth rate although pockets of small striations exist even at the fastest crack growth rates.

4.3 RESULTS OF PROGRAMMED LOADING TESTS

Having established reliable constant amplitude data it was then possible to proceed with the programmed loading aspect of the investigation, using three point bending tests. A systematic approach to the problem was adopted, starting with simple two level tests to investigate the effects of block size, sequence and load level. These then formed the basis for subsequent experiments.

In the following section and subsequent discussion the term block refers to a number of cycles at a discreet load level and sequence refers to a group of blocks which together make up the loading programme.

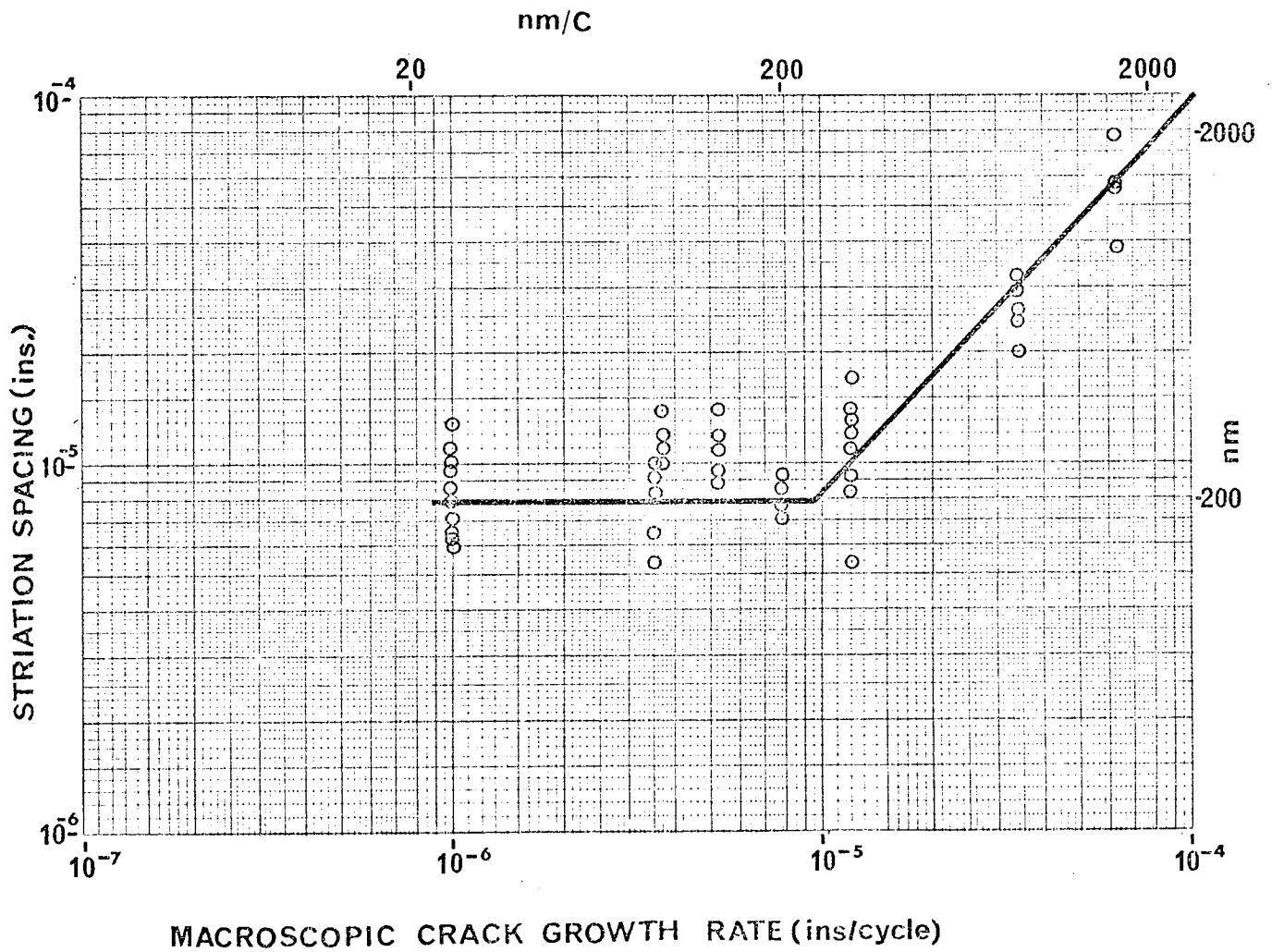
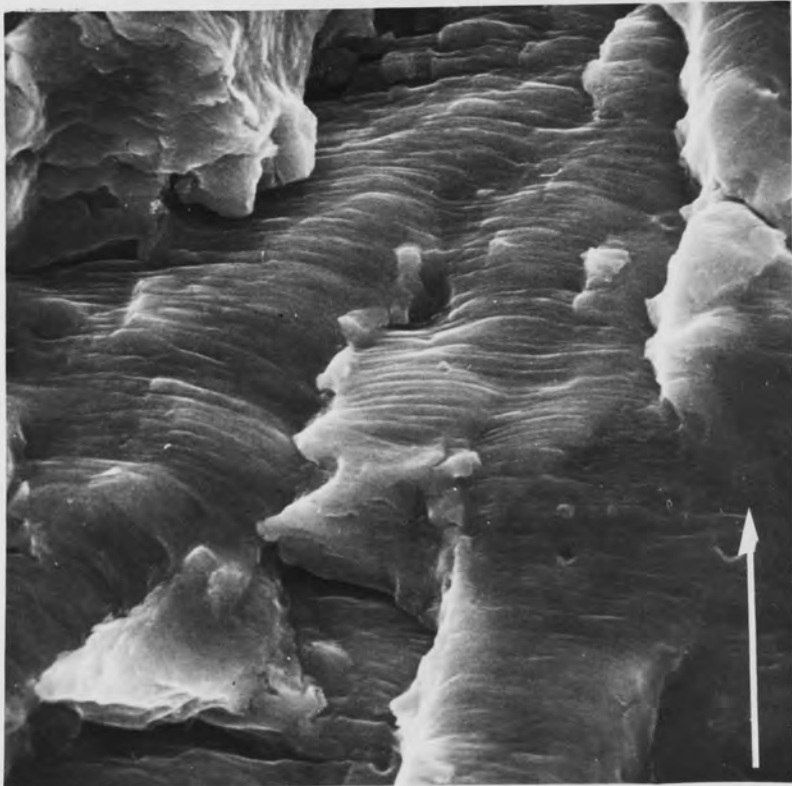
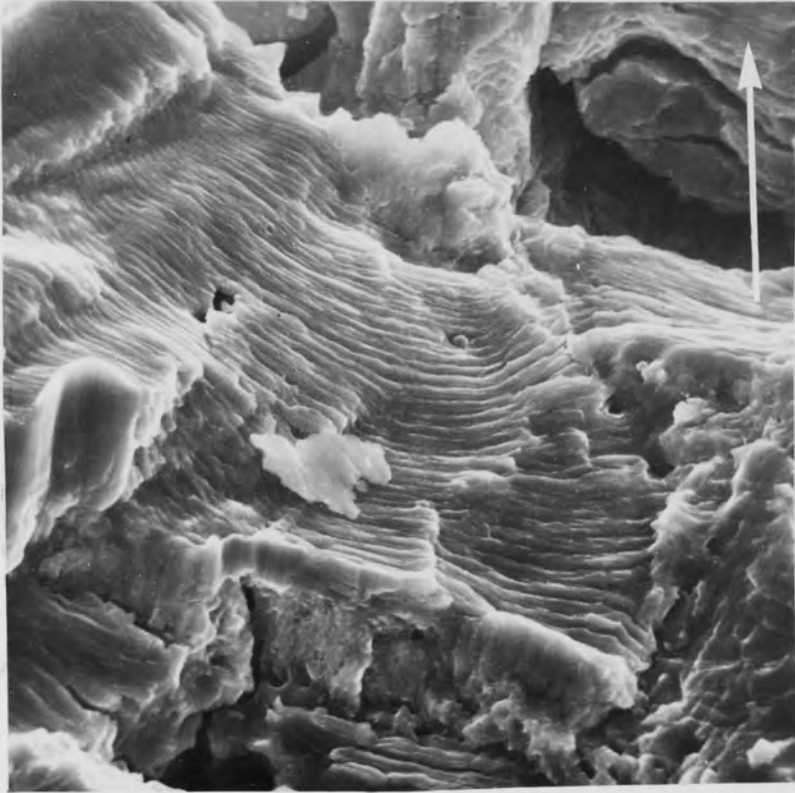


Fig. 43

Fig. 44. Striations in Stage IIb Fracture.
Average Spacing 3.9×10^{-5} ins.
(1000 nm).
Macroscopic Growth Rate
 5.2×10^{-5} ins. (1300 nm) per cycle.
x 2000 Mag.
Operating Angle 90° .
(Neg. 212/26)

Fig. 45. Striations in Stage IIb Fracture.
Average Spacing 1.0×10^{-5} ins.
(260 nm).
Macroscopic Growth Rate
 3.5×10^{-6} ins. (90 nm) per cycle.
x 5700 Mag.
Operating Angle 90° .
(Neg. 89/15)



The sequence is repeated at regular intervals until failure.

4.3.1. Two Level Tests

Two level repeated tests were carried out using the load levels investigated in the constant amplitude part of the investigation. The block size was initially fixed at 3.4×10^4 cycles to attain a compromise between providing a reasonable number of load level changes during the tests and maintaining the actual proportion of cycles involved in the load change to a small fraction of the total (approx. 2%).

Using the high to low sequence and a block size of 3.4×10^4 cycles, tests were carried out to investigate the effect of load level on the cumulative cycle ratio. In addition two tests were carried out from the highest stress to a level below the fatigue limit. (In this case the cumulative cycle ratio was calculated neglecting those cycles below the fatigue limit.) The effects of reversed sequence (low to high) and variation of block size in the range 5×10^3 to 6.8×10^4 cycles were also investigated. (The 5×10^3 block programme was applied manually).

Details of these two level programmes and the cumulative cycle ratio are given in table 10. Generally none of the variables investigated appeared to systematically affect $\sum \frac{n}{N}$, which remained within the narrow limits of 1.01 to 1.13.

SPECIMENS	LOAD PROG.	RESPECTIVE LOADS lb (N)	BLOCK SIZE $\times 10^3$ CYCLES	$\sum \frac{n}{N}$
94-98	Hi-Lo	439-233 (1953-1036)	34	1.05, 1.13, 1.11, 1.02, 1.10
102, 103	Hi-Lo	358-233 (1593-1036)	34	1.08, 1.03
100, 101	Hi-Lo	305-233 (1357-1036)	34	1.08, 1.01
107, 121	Hi-Lo	439-134 (1953-1036)	34	1.04, 1.05
105, 120	Lo-Hi	233-439 (1036-1953)	34	1.07, 1.09
104, 123	Hi-Lo	439-233 (1953-1036)	5	1.05, 1.04
108, 122	Hi-Lo	439-233 (1953-1036)	20	1.07, 1.05
106, 119	Hi-Lo	439-233 (1953-1036)	68	1.07, 1.10

TABLE 10. RESULTS OF TWO LEVEL TESTS

4.3.2. Multi-Level Tests

The next series of tests involved four load levels arranged in ascending and descending staircase sequences, which were repeated until failure. Table 11 gives the results in summary form. In the first group of tests the block size was constant for all load levels (3.4×10^4 cycles) and it is quite clear that the cumulative cycle ratio still lies within the range observed for the two level tests, irrespective of the direction of the staircase.

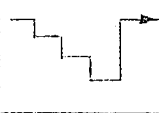

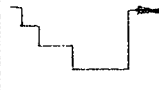
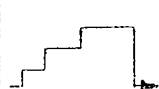
SPECIMEN	LOAD PROG.	RESPECTIVE ALTERNATING LOADS lb (N)	RESPECTIVE BLOCK SIZE ($\times 10^3$ CYCLES)	$\sum \frac{n}{N}$
111, 112, 117, 118		439, 358, 305, 233 (1953, 1593, 1357, 1036)	34, 34, 34, 34	1.07, 1.04, 1.07, 1.13
113, 114 115, 116		233, 305, 358, 439 (1036, 1357, 1593, 1953)	34, 34, 34, 34	1.09, 1.12, 1.10, 1.05
126, 146		439, 358, 305, 233 (1953, 1593, 1357, 1036)	15, 27, 55, 130	1.26, 1.21
147, 149		233, 305, 358, 439 (1036, 1357, 1593, 1953)	130, 55, 27, 15	1.51, 1.42

TABLE 11. SUMMARY OF MULTI-LEVEL PROGRAMMED LOADING TESTS

However, when the block size was reduced to 10% of the constant amplitude life for each respective load level a significant increase in the value of $\sum \frac{n}{N}$ occurred. For the repeated descending staircase programme $\sum \frac{n}{N}$ increased to 1.21 to 1.26 whilst the ascending staircase had an even larger effect from 1.42 to 1.51. Although the number of tests is limited, the ascending staircase appears to produce higher cumulative cycle ratios.

4.3.3. Crack Growth Data

Crack growth data obtained from optical measurements was plotted on linear scales and a typical example for a two level high to low test is shown in fig. 46. These curves were used in the first instance to accurately determine the number of cycles to reach the failure crack length, in order to calculate the cumulative cycle ratio.

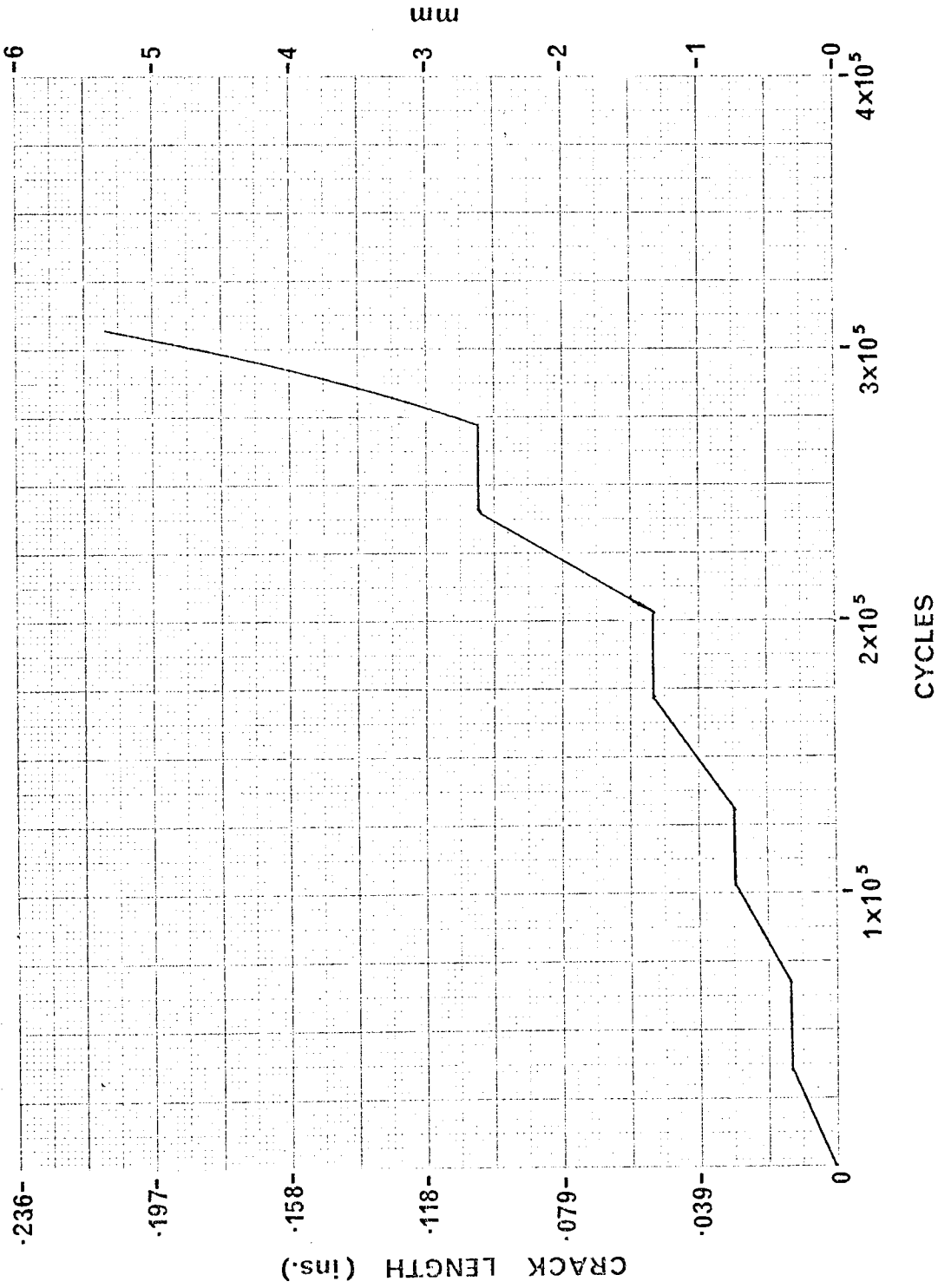


Fig.46 TYPICAL CRACK GROWTH CURVE FOR A TWO LEVEL TEST

10/10/50

The curves derived from the potential drop technique were very similar in form to fig. 46 and there was no conclusive evidence of crack arrest or acceleration at the load level changes.

4.3.4. Effect of Rate of Change of Load Level

It was emphasized in section 3.2. that the Amsler programmed loading device requires several hundred load cycles to change the load level. It was thought possible that the diffuse nature of such a load change might reduce its effect on fatigue life. Therefore a series of experiments were carried out in which the rate of change of load level was varied. For this work an MTS closed loop servo-hydraulic fatigue machine was employed. The machine available had a 42 ton load cell and therefore necessitated the use of much larger specimens. (The constant amplitude tests on these specimens have been presented in table 6). Two level high to low tests were carried out in two groups, the first simulating the Vibrophore situation to provide a standard for comparison with the small specimens and the second using instantaneous load changes.

The rate of load rise and fall in a Vibrophore test was determined by strain gauges attached to the Vibrophore dynamometer. This information was used to control the response of the servo-hydraulic machine and so provided an exact simulation of the Vibrophore loading conditions. In the limited number of tests carried out, the cumulative cycle ratio was unaffected by the rate of load change (see table 12).

4.4. FRACTOGRAPHIC RESULTS OF PROGRAMMED LOADING TESTS

4.4.1. Observations at Low Magnifications

One fracture from each type of test was examined in detail on the Stereoscan. The positions of load changes were clearly visible to the naked eye as a change in colour across the fracture. However, under the Stereoscan, the colour changes were difficult to see, and usually appeared as a slightly lighter band. On the microscopic scale the load changes were often more easily detected by a boundary between the stage IIa and stage IIb fracture modes.

SPECIMEN	LOAD PROG.	RESPECTIVE ALTERNATING LOADS tons (kN)	RESPECTIVE BLOCK SIZE $\times 10^3$	LIFE (to 32.5 mm crack length)	$\sum \frac{n}{N}$
K11	Hi-Lo VIB simulation	2.70 - 1.43 (26.9 - 14.3)	34 - 34	2.93×10^5	1.18
K13	Hi-Lo VIB simulation	2.70 - 1.43 (26.9 - 14.3)	34 - 34	2.78×10^5	1.08
K12	Hi-Lo Instantaneous	2.70 - 1.43 (26.9 - 14.3)	34 - 34	2.77×10^5	1.08
K14	Hi-Lo Instantaneous	2.70 - 1.43 (26.9 - 14.3)	34 - 34	2.77×10^5	1.08

TABLE 12. RESULTS OF VIBROPHORE SIMULATION AND INSTANTANEOUS LOAD CHANGES

4.4.2. Observations at High Magnifications

Attempts were made to measure the change in striation spacing across a load change. However, no significant alterations in the spacing were observed, even on the large specimens at fast crack growth rates where this technique should have been most feasible. Striation spacings were not therefore considered to be a useful technique with which to examine the programmed loading tests.

However, stage IIa was observed to occur after high to low changes, even though the maximum stress intensity for the low was greater than the transition K_{\max} of $13.5 \text{ ksi}\sqrt{\text{ins}}$ ($14.8 \text{ MNm}^{-3/2}$). Thus it was reasoned that the high to low transition was giving rise to residual compressive stresses that were acting in opposition to the applied load thereby reducing the effective stress intensity at the crack tip below $13.5 \text{ ksi}\sqrt{\text{ins}}$ ($14.8 \text{ MNm}^{-3/2}$). Fatigue fracture under these conditions is referred to as "unstable" stage IIa.

In all cases, the transition from "unstable" stage IIa back to stage IIb occurred at a point where the load returned to a higher level. In other words the block size was never long enough to permit complete decay of the residual stress. However it was possible to make an estimate of the level of the induced residual stress at the end of the low block by assuming that at this point the maximum effective stress intensity was not greater than $13.5 \text{ ksi}\sqrt{\text{ins}}$ ($14.8 \text{ MNm}^{-3/2}$). Subtracting this value from the actual stress intensity operative at the same point gave a minimum value of negative K_{\max} . Table 13 shows that surprisingly high values were present at long crack lengths, rising in some instances to at least $-10 \text{ ksi}\sqrt{\text{ins}}$ ($11 \text{ MNm}^{-3/2}$).

Residual compressive stresses were also estimated approximately from a knowledge of the actual crack growth rate during the low block of the two level tests. This was calculated by dividing the observed length of "unstable" stage IIa by the block size. The K_{\max} value corresponding to this actual crack growth rate was obtained from graphs of da/dN vs. K_{\max} .*

* Graphs of K_{\max} vs. da/dN were obtained from constant amplitude data.

The applied K_{\max} was calculated in the usual manner, using the crack length at the mid-point of the block and assuming a linear crack growth rate throughout the block. The difference between the two values of K_{\max} gave a value of $-K_{\max}$.

Reasonable agreement with the previously calculated results was obtained, $-K_{\max}$ falling in the region 1.0 - 10.0 $\text{ksi}\sqrt{\text{ins}}$ (1.1-11.0 $\text{MNm}^{-3/2}$). However these values were often slightly less than the minimum values estimated by the previous approach based on the reversion of unstable stage IIa at the load rise. This error was considered to be caused by the steep slope of the K_{\max} vs. da/dN curve at slow crack growth rates, small changes in da/dN giving large changes in K_{\max} .

4.4.3. The Extent of "Unstable" Stage IIa

Since the reversion of "unstable" stage IIa to stage IIb at the low stress was always assisted by a load rise in the programme sequence, it had not been possible to make any assessment of the extent of the residual stress effect or its decay rate with increasing stress intensity. With this in mind, a series of high to low repeated tests were carried out in which the crack was allowed to run out to failure at the low stress level immediately after a high to low load change. Table 14 gives full details of these tests. Fig.47 shows the relationship between the stress intensity immediately after the load drop and the subsequent extent of stage IIa. For the prevailing geometrical conditions, the difference in the rate of change of stress intensity across the zone of "unstable" stage IIa, at different crack lengths, is small and considered to exert only a second order effect on the extent of observed stage IIa. It can be seen that higher ΔK values are associated with shorter lengths of induced stage IIa.

The cumulative cycle ratios for all of these tests lies between 1.12 and 1.38 suggesting a strong residual compressive stress effect. Two of the points shown on fig. 47 (labelled X) include a proportion of stable stage IIa, since the load drop occurred to a stress intensity level at which stable stage IIa would normally occur. However, the fact that K_{\max}

for the reversion to stage IIb was observed to be greater than 13.5 ksi $\sqrt{\text{ins}}$ ($14.8 \text{ MNm}^{-3/2}$) suggests a prolonged residual stress effect.

4.5. RESIDUAL TENSILE STRESS EFFECTS

All the experiments carried out so far had strongly suggested an important influence of residual compressive stress. The run out tests (see Table 14) emphasized the effectiveness of a single load drop in producing significant levels of $-K_{\text{max}}$ and cumulative cycle ratios well in excess of unity. In order to make a preliminary assessment of any residual tensile stress effects, the two level high to low tests numbered 94-98 were examined in detail. Crack growth rates for each high block were measured manually on graphs of crack length against cycles, the crack growth rate throughout each block being assumed constant. A crack length was quoted for each result which corresponded to the mid-point of the block. This result was then compared with the crack length-crack growth rate data obtained from constant amplitude tests. Table 15 shows the results obtained. It can be seen that about 80% of the results of the programmed tests are slightly higher than the corresponding constant amplitude results.

Graphs of da/dN vs. K_{max} were constructed from the constant amplitude data. These were used to obtain estimates of residual tensile stress ($+K_{\text{max}}$) by comparing the differences in K_{max} obtained graphically from the programmed and constant amplitude da/dN values listed in table 15. Generally, $+K_{\text{max}}$ fell between +0.1 and +3.0 ksi $\sqrt{\text{ins}}$ (+0.11 and +3.3 $\text{MNm}^{-3/2}$). As a result of these observations, two programmed tests were carried out in which the load changes were always increased upwards. The sequence consisted of three stress levels arranged in an ascending staircase pattern starting with the lowest stress level. The block size was set at about 33% of the expected constant amplitude life for each respective load level. Table 16 details the results of these tests from which it can be seen that for the first time the cumulative cycle ratio has fallen below unity, and the computer predicted life (see section 4.6) is greater than the

SPECIMEN	PROGRAMME	BLOCK SIZE x10 ³ CYCLES	BLOCK IDENTITY	CRACK LENGTH AT LOAD CHANGE						EXTENT OF UNSTABLE Iia ins. (mm)	- K _{max} AT Iia to Iib ksi√ins (MN ^{-3/2})	
				EXTERNALLY OBSERVED		SEM Iib TO Iia		SEM Iia TO Iib				
				ins.	(mm)	ins.	(mm)	ins.	(mm)			
96	Hi-Lo	34	EH3 EL3	.0484	(1.23)	.0528	(1.34)	.0567	(1.44)	.0039	(0.10)	† .74 (0.81)
				.0484	(1.23)	.0957	(2.43)	.1020	(2.59)	.0063	(0.16)	
			EH4 EL4	.0921	(2.34)	.0571	(1.45)	.0630	(1.60)	.0059	(0.15)	† 3.55 (4.23)
				.0969	(2.46)	.0752	(1.91)	.0787	(2.00)	.0035	(0.09)	
101	Hi-Lo	34	EH7 EL7	.0528	(1.34)	.0949	(2.41)	.1008	(2.56)	.0055	(0.14)	† 3.52 (4.20)
				.0575	(1.46)	.1126	(2.86)	.1177	(2.99)	.0051	(0.13)	
			EH8 EL8	.0693	(1.76)	.1654	(4.20)	.1756	(4.46)	.0102	(0.26)	† 9.44 (10.37)
				.0744	(1.89)	.0496	(1.26)	.0587	(1.49)	.0091	(0.23)	
			EH9 EL9	.0933	(2.37)	.0776	(1.97)	.0831	(2.11)	.0055	(0.14)	† 2.59 (2.85)
				.0984	(2.50)							
			EH10 EL10	.1189	(3.02)							
				.1260	(3.20)							
			EH11 EL11	.1539	(3.91)							
				.1693	(4.30)							
			EH5 EL5	.0539	(1.37)							
				.0539	(1.37)							
EH6 EL6	.0772	(1.96)										
	.0772	(1.96)										

EH = End of High SEM = Scanning Electron Microscope
EL = End of Low

TABLE 13. OBSERVATION OF "UNSTABLE" STAGE Iia DURING BLOCK PROGRAMME TESTS

SPECIMEN	PROGRAMME	BLOCK SIZE x10 ³ CYCLES	BLOCK IDENTITY	CRACK LENGTH AT LOAD CHANGE						EXTENT OF UNSTABLE IIA ins. (mm)	- K _{max} AT IIA TO IIB ksi√ins (MNm ^{-3/2})
				EXTERNALLY OBSERVED		SEM IIB TO IIA		SEM IIA TO IIB			
				ins. (mm)	ins. (mm)	ins. (mm)	ins. (mm)	ins. (mm)	ins. (mm)		
107	Hi-Lo (Lo=below fatigue limit)	34	EH5 EL5	.1807	(4.59)	.1787	(4.54)	.1811	(4.60)	.0024 (0.06)	6.51(7.15)
				.1807	(4.59)						
105	Lo-Hi	34	EH3 EL4	.0579	(1.47)	.0606	(1.54)	.0669	(1.70)	.0063 (0.16)	1.45(1.59)
				.0579	(1.47)						
			EH4 EL5	.1221 .1260	(3.10) (3.20)	.1201	(3.05)	.1252	(3.18)	.0051 (0.13)	5.52(6.07)
104	Hi-Lo	5	- -	-	(-)	.0500	(1.27)	.0547	(1.39)	.0047 (0.12)	0.63(0.69)
				-	(-)						
				-	(-)	.0677	(1.72)	.0724	(1.84)		
108	Hi-Lo	20	EH6 EL6	-	(-)	.1410	(3.58)	.1433	(3.64)	.0024 (0.06)	6.89(7.57)
				-	(-)						
				.0898 .0898	(2.28) (2.28)	.0925	(2.35)	.0969	(2.46)		
108	Hi-Lo	20	EH7 EL7	.1323	(3.36)	.1402	(3.56)	.1461	(3.71)	.0591 (0.15)	7.03(7.73)
				.1402	(3.56)						

TABLE 13 (cont. (i))

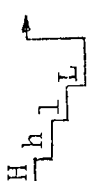
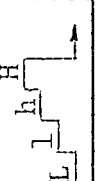
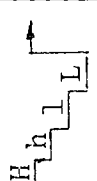
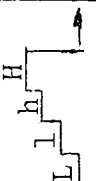

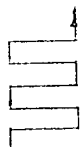
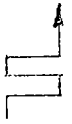


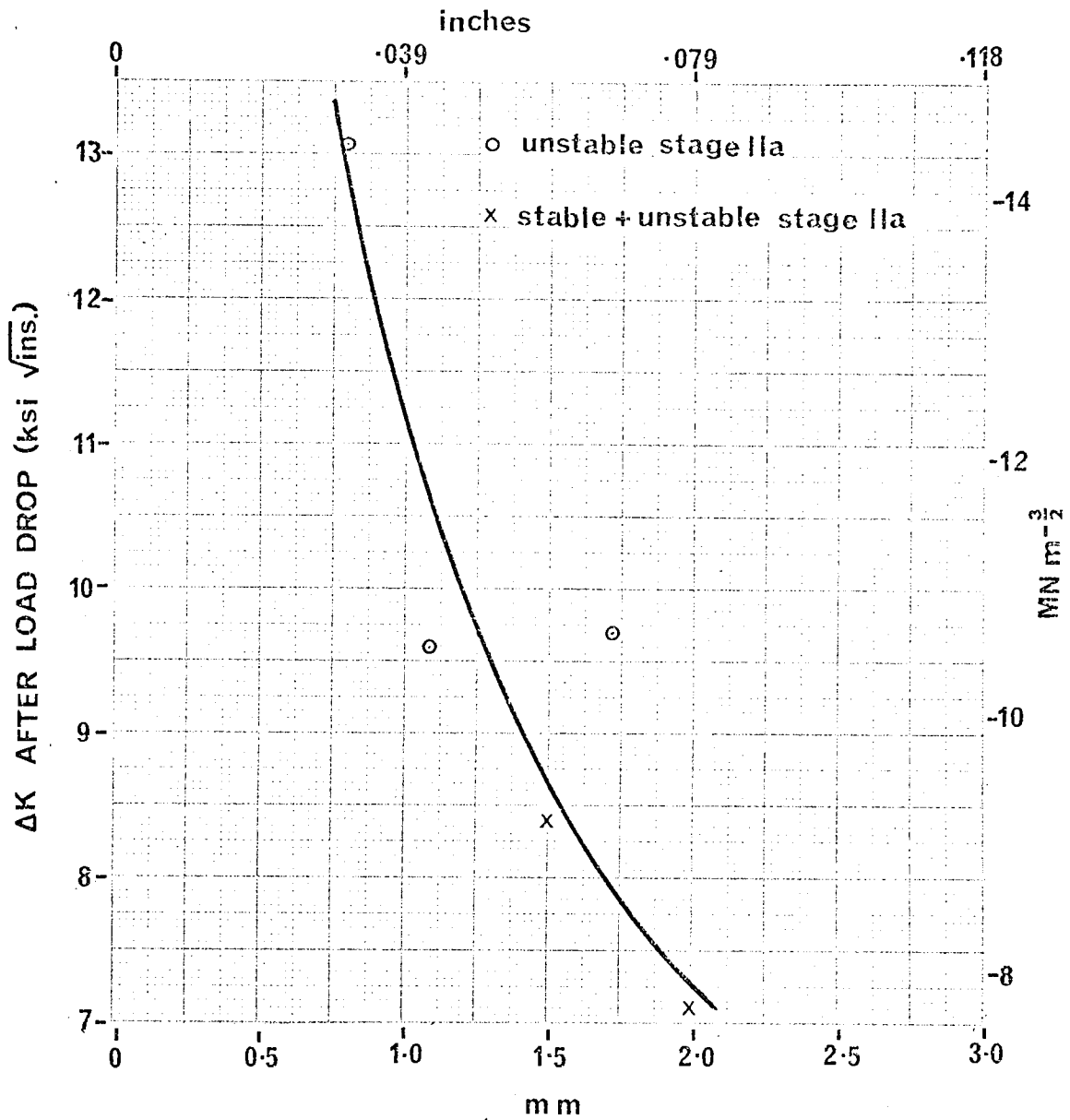
SPECIMEN	PROGRAMME	BLOCK SIZE x10 ³ CYCLES	BLOCK IDENTITY	CRACK LENGTH AT LOAD CHANGE				EXTENT OF UNSTABLE IIAa ins. (mm)	- K _{max} AT IIA to IIB ksi√ins (N/mm ^{3/2})			
				EXTERNALLY OBSERVED (mm)	SEM IIB TO IIAa (mm)	SEM IIA TO IIB ins. (mm)	SEM IIA TO IIB (mm)					
										ins.	ins.	ins.
106	Hi-Lo	68	Eh2 EL2	.1008 .1067	(2.56) (2.71)	.1039	(2.64)	.1122	(2.85)	.0083	(0.21)	4 4.59 (5.04)
111	Descending Staircase 	34	Eh2 Eh2	.0508 .0650	(1.29) (1.65)	.0512	(1.30)	.0618	(1.57)	.0106	(0.27)	4 3.80 (4.18)
113	Ascending Staircase 	34	EL2 EL2	.0732 .0768	(1.86) (1.95)	.0764	(1.94)	.0850	(2.16)	.0087	(0.22)	4 2.74 (3.01)
126	Descending Staircase 	10%	Eh3 EL3	.0673 .1087	(1.71) (2.76)	.0764	(1.94)	.1138	(2.89)	.0374	(0.95)	4 4.74 (5.21)
127	Ascending Staircase 	10%	Eh2 EL3	.0634 .0933	(1.61) (2.37)	.0669	(1.70)	.0886	(2.25)	.0138	(0.35)	4 4.71 (5.18)
			Eh3 EL4	.1665 .2429	(4.23) (6.17)	.1717	(4.36)	.1858	(4.72)	.0142	(0.36)	4 10.33 (11.35)

TABLE 13 (cont. (ii))

SPECIMEN	LOAD PROGRAMME	BLOCK SIZE x10 ³ CYCLES	LIFE (x10 ⁵ CYCLES)		$\sum \frac{n}{N}$	EXTENT OF STAGE Iia + UNSTABLE STAGE Iia	EXTENT OF UNSTABLE Iia	K _{max} AT REVERSION OF UNSTABLE Iia to IIb	EFFECTIVE - K _{max}
			EXPERIMENTAL	COMPUTER PREDICTED					
130		34	5.22	4.17	1.12	-	.031 (0.79)	21.39 (23.5)	-7.89 (-8.7)
131		34	9.50	6.77	1.29	-	.046 (1.16)	17.20 (18.9)	-3.70 (-4.1)
132		34	10.50	9.19	1.18	.058 (1.48)	.011 (0.28)	16.43 (18.1)	-2.93 (-3.2)
133		34	14.10	1.23	1.29	.078 (1.99)	.031 (0.79)	16.28 (17.9)	-2.78 (-3.1)
145		140	8.40	4.31	1.38	-	.061 (1.54)	18.39 (20.2)	-4.89 (-5.4)

High Load = ±439 lb (±1953 N)
Low Load = ±233 lb (±1036 N)
Mean Load = 448 lb (1993 N)

TABLE 14. DETAILS OF "RUN OUT" TESTS



EXTENT OF INDUCED STAGE IIa

LOAD DROP $\pm 439 - \pm 233 \text{ lb}$
 $(\pm 1953 - \pm 1036 \text{ N})$

Fig.47

SPECIMEN	BLOCK NUMBER	da/dN			
		PROGRAMMED		CONSTANT AMPLITUDE	
		ins./CYCLE	(nm/CYCLE)	ins./CYCLE	(nm/CYCLE)
94	H2	4.57×10^{-7}	(11.6)	3.94×10^{-7}	(10.0)
	H3	7.56×10^{-7}	(19.2)	6.69×10^{-7}	(17.0)
	H4	1.65×10^{-6}	(42.0)	1.52×10^{-6}	(38.5)
	H5	3.94×10^{-6}	(100.0)	3.90×10^{-6}	(99.0)
95	H2	3.15×10^{-7}	(8.0)	2.91×10^{-7}	(7.4)
	H3	5.98×10^{-7}	(15.2)	4.84×10^{-7}	(12.3)
	H4	1.22×10^{-6}	(31.1)	1.02×10^{-6}	(26.0)
	H5	2.60×10^{-6}	(66.0)	2.52×10^{-6}	(64.0)
	H6	6.30×10^{-6}	(160.0)	5.32×10^{-6}	(135.0)
96	H2	3.23×10^{-7}	(8.2)	3.74×10^{-7}	(9.5)
	H3	6.58×10^{-7}	(16.7)	6.30×10^{-7}	(16.0)
	H4	1.19×10^{-6}	(30.2)	1.30×10^{-6}	(33.0)
	H5	3.35×10^{-6}	(85.0)	3.35×10^{-6}	(85.0)
97	H2	6.69×10^{-7}	(17.0)	3.70×10^{-7}	(9.4)
	H3	8.90×10^{-7}	(22.6)	7.68×10^{-7}	(19.5)
	H4	1.81×10^{-6}	(46.0)	1.85×10^{-6}	(47.0)
	H5	3.62×10^{-6}	(92.0)	3.94×10^{-6}	(100.0)
98	H2	4.10×10^{-7}	(10.4)	3.74×10^{-7}	(9.5)
	H3	5.51×10^{-7}	(14.0)	6.50×10^{-7}	(16.5)
	H4	1.52×10^{-6}	(38.7)	1.46×10^{-6}	(37.0)
	H5	3.15×10^{-6}	(80.0)	3.58×10^{-6}	(91.0)

H = High

TABLE 15. PROGRAMMED AND CONSTANT AMPLITUDE CRACK GROWTH RATES

experimental life. This was therefore considered to be a clear indication of the presence of residual tensile stress during the ascending staircase sequence.

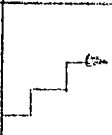
SPECIMEN	LOAD PROG.	RESPECTIVE BLOCK SIZE (x10 ³ CYCLES)	LIFE (CYCLES)		$\sum \frac{n}{N}$
			EXPERIMENTAL	COMPUTER	
150		420, 184, 20	6.20x10 ⁵	6.49x10 ⁵	0.78
151		420, 184, 27	6.31x10 ⁵	6.49x10 ⁵	0.83

TABLE 16. UNIDIRECTIONAL ASCENDING STAIRCASE TESTS

RESPECTIVE LOADS 233, 305, 439 lb (1036, 1357, 1953 N).

Using the constant amplitude S-N data it was possible to calculate the maximum value of tensile stress that would cause the observed difference in life between the computed and the experimental values. Estimates suggest a residual K_{max} of +0.3 ksi \sqrt{ins} (0.33MNm^{-3/2}), which is in good agreement with the values predicted from the data in table 15.

4.6. LIFE PREDICTION COMPUTER PROGRAMME

A computer programme was developed to predict the life of a load history by numerical integration of the constant amplitude fracture mechanics data. Each individual block of cycles was divided into 1000 cycle units and the crack growth increment for each was calculated on a cumulative basis using the equation:

$$\frac{da}{dN} = C(\Delta K)^m$$

The crack growth increment for the first unit of cycles was added on to the notch depth and the new stress intensity calculated, from which the crack growth increment for the next unit of cycles was calculated. This process was continued, m and C being varied according to the load level of the block considered, until the crack had reached a specified value. A correction based on experimental observations, was also made for the number of cycles to initiate the crack.

Although the same results can be obtained graphically, the computer

has the advantage of speed, accuracy and flexibility. The accuracy of the constant amplitude experimental m and C values was initially checked by inserting the appropriate values of m and C into the programme and carrying out a constant amplitude integration. Comparison of the predicted and experimental lives showed that the predicted life was always shorter. However small changes in m (within the experimental scatter) were found to have a large effect on the predicted life and the m values were therefore reduced slightly (e.g. from 3.23 to 3.215 and from 2.60 to 2.56) so as to ensure maximum accuracy in the programmed loading life predictions. Full details of the programme are given in appendix 6.

As expected the predicted lives of the variable load history experiments were always less than the experimental (see table 17), but in many instances were remarkably close.

In most of the loading programmes, both optical and potential drop techniques suggested that in the majority of the low load blocks (± 233 lb (± 1036 N)) crack growth was negligible. As a first approximation the computer programme was re-run, the results being calculated in such a manner that the contribution to the crack length was zero, the cycles still being included in the summation.

Table 18 shows the results of these predicted lives compared with the original experimental values. It can be seen that the general effect has been to increase the predicted life to a level often greater than the experimental life.

SPECIMEN	LOAD PROG.	RESPECTIVE ALT. LOADS lb (N)	RESPECTIVE BLOCK SIZE $\times 10^3$ CYCLES	ACTUAL LIFE	COMPUTER PREDICTED LIFE	$\sum \frac{n}{N}$ (EXP.)
94	Hi-Lo	439, 233 (1953, 1036)	34, 34	3.00×10^5	2.89×10^5	1.05
95	Hi-Lo		34, 34	3.37×10^5	2.87×10^5	1.13
96	Hi-Lo		34, 34	3.06×10^5	2.88×10^5	1.11
97	Hi-Lo		34, 34	2.90×10^5	2.87×10^5	1.02
98	Hi-Lo		34, 34	3.03×10^5	2.88×10^5	1.10
102	Hi-Lo	358, 233 (1593, 1036)	34, 34	5.55×10^5	5.00×10^5	1.08
103	Hi-Lo		34, 34	5.11×10^5	5.00×10^5	1.03
100	Hi-Lo	305, 233 (1357, 1036)	34, 34	8.26×10^5	7.64×10^5	1.08
101	Hi-Lo		34, 34	7.68×10^5	7.64×10^5	1.01
107	Hi-Lo	439, 134 (1953, 596)	34, 34	3.45×10^5	3.04×10^5	1.04
121	Hi-Lo		34, 34	3.47×10^5	3.04×10^5	1.05
105	Lo-Hi	233, 439 (1036, 1953)	34, 34	3.27×10^5	3.11×10^5	1.07
120	Lo-Hi		34, 34	3.32×10^5	3.13×10^5	1.09
104	Hi-Lo	439, 233 (1953, 1036)	5, 5	3.12×10^5	2.92×10^5	1.05
123	Hi-Lo		5, 5	3.07×10^5	2.92×10^5	1.04
108	Hi-Lo		20, 20	3.04×10^5	2.92×10^5	1.07
122	Hi-Lo		20, 20	2.93×10^5	2.92×10^5	1.05
106	Hi-Lo		68, 68	3.00×10^5	2.89×10^5	1.07
119	Hi-Lo		68, 68	3.03×10^5	2.89×10^5	1.10

TABLE 17. COMPARISON OF COMPUTER PREDICTED AND EXPERIMENTAL LIVES.

TABLE 17 (Continued)

SPECIMEN	LOAD PROG.	RESPECTIVE ALTERNATING LOAD lb (N)	RESPECTIVE BLOCK SIZE $\times 10^3$ CYCLES	ACTUAL LIFE	COMPUTER PREDICTED LIFE	$\sum_{N=1}^n$ (EXP.)
111	Rep. Desc. Staircase	439, 358, 305, 233	34, 34, 34, 34	3.32×10^5	3.09×10^5	1.07
112	"	(1953, 1593, 1357, 1036)	34, 34, 34, 34	3.23×10^5	3.11×10^5	1.04
117	"		34, 34, 34, 34	3.30×10^5	3.09×10^5	1.07
118	"		34, 34, 34, 34	3.55×10^5	3.08×10^5	1.13
113	Rep. Asc. Staircase	233, 305, 358, 439	34, 34, 34, 34	3.98×10^5	3.78×10^5	1.09
114	"	(1036, 1357, 1593, 1953)	34, 34, 34, 34	3.99×10^5	3.73×10^5	1.12
115	"		34, 34, 34, 34	3.96×10^5	3.74×10^5	1.10
116	"		34, 34, 34, 34	3.88×10^5	3.73×10^5	1.05
126	Rep. Desc. Staircase	439, 358, 305, 233	15, 27, 55, 130	7.13×10^5	5.70×10^5	1.26
146	Rep. Desc. Staircase	(1953, 1593, 1357, 1036)	15, 27, 55, 130	6.95×10^5	5.73×10^5	1.21
147	Rep. Asc. Staircase	233, 305, 358, 439	130, 55, 27, 15	9.45×10^5	6.45×10^5	1.51
149	Rep. Asc. Staircase	(1036, 1357, 1593, 1953)	130, 55, 27, 15	8.95×10^5	6.49×10^5	1.42

SPECIMEN	LIFE (CYCLES)	
	EXPERIMENTAL	PREDICTED
94	3.09×10^5	3.06×10^5
95	3.37×10^5	3.37×10^5
96	3.06×10^5	3.06×10^5
97	2.90×10^5	3.04×10^5
98	3.03×10^5	3.05×10^5
102	5.55×10^5	6.30×10^5
103	5.11×10^5	6.30×10^5
100	8.26×10^5	1.06×10^6
101	7.68×10^5	1.06×10^6
107	3.45×10^5	3.04×10^5
121	3.47×10^5	3.06×10^5
105	3.27×10^5	3.28×10^5
120	3.32×10^5	3.30×10^5
104	3.12×10^5	3.25×10^5
123	3.07×10^5	3.25×10^5
108	3.04×10^5	3.30×10^5
122	2.93×10^5	3.27×10^5
106	3.00×10^5	3.06×10^5
119	3.03×10^5	3.05×10^5
111	3.32×10^5	3.29×10^5
112	3.23×10^5	3.32×10^5
117	3.30×10^5	3.29×10^5
118	3.55×10^5	3.28×10^5
113	3.98×10^5	3.88×10^5
114	3.99×10^5	3.84×10^5
115	3.96×10^5	3.84×10^5
116	3.88×10^5	3.83×10^5
126	7.13×10^5	7.45×10^5
146	6.95×10^5	7.49×10^5
147	9.45×10^5	8.72×10^5
149	8.95×10^5	8.75×10^5

TABLE 18. COMPARISON OF EXPERIMENTAL AND COMPUTER PREDICTED LIVES AFTER THE OMISSION OF THE CRACK GROWTH CONTRIBUTION OF THE LOW STRESS.

5. DISCUSSION

5.1. CONSTANT AMPLITUDE RESULTS

5.1.1. Fracture Mechanics Data

The values of m obtained from the three point bending fracture mechanics analysis lie in the range 2.60 - 3.23. This result agrees quite well with the results of Pook et al (19) who re-analysed the earlier crack propagation data of Frost by the fracture mechanics approach. Pook et al found an m value of 3.3 for mild steel and also noted wide variations in m according to the material considered.

The experimental results presented in this study again emphasise the fact that no single value of m will apply to all materials. The fracture mechanics results of the coarse grain size specimens (table 9) show no significant difference from the results of the finer grain size specimens (table 4). In addition an increase of 10% in the pearlite content from 10% in the case of the vacuum melted steel to 20% for the EN 3B, does not exert a significant effect on the fatigue crack propagation data. This suggests that grain size is of secondary importance in fatigue crack propagation. However it should be remembered that the fracture mechanics approach to fatigue is not particularly sensitive to changes in micro-structure. Its principal advantage is that crack propagation behaviour in specimens of different geometry can be directly compared. For this reason it is well suited to life prediction studies.

5.1.2. Deviations in the Slope of the Fracture Mechanics Analysis

Examination of the three point bending fracture mechanics results for the small specimens (table 4) revealed a significant difference in the m values between the highest load tests and the remainder (3.23 as compared with 2.60 - 2.85). This effect is absent in the results of the larger specimens (see table 6) tested on the MTS machine, where the m values are within the same range as the lower load tests on the small specimens. The development of shear lips has been shown to exert very little effect on the fracture mechanics relationship and was not thought to be causing

the observed change in slope.

It was considered that changes in stress ratio with each change in load level could also be a possible cause, but re-analysis of the data using the Forman relationship did not change the differential, although all of the m values were reduced.

The higher m values in the highest load tests on the small specimens are considered to be due to a size effect associated with the increase in percentage of crack tip plasticity in the small specimens. Table 19 shows a comparison between the radius of the plastic zone and the half specimen thickness for the beginning and end of tests at various load levels. It can be clearly seen that the largest percentage of plasticity is associated with the smallest specimen tested at the highest stress.

TEST	$r_y/0.5b$ AT START $a/w = .056$	$r_y/0.5b$ AT END $a/w = .34$ (VIB) $a/w = .45$ (MTS)
High Stress (MTS)	0.6%	7.6%
High Stress (VIB)	4.6%	20.0%
Intermediate Stress (VIB)	1.8%	14.6%
Low Stress (MTS)	0.3%	4.2%
Low Stress (VIB)	1.8%	11.8%

TABLE 19. EXTENT OF CRACK TIP PLASTICITY

Increases in m value have been observed by other workers (26, 27) and have been predicted by the theoretical approach of Tomkins (16). Ductile dimples were observed to be associated with the fatigue mode at the highest stress level in the small specimens. These dimples were not as numerous on the fracture surfaces of the smaller specimens tested at the lower stress levels, nor on any of the larger specimens tested on the MTS machine. Therefore it was concluded that the observed increase in m was

principally associated with crack acceleration effects caused by ductile tearing occurring in addition to the fatigue mode as the general yield condition was approached. However, yielding was observed to occur on the back face of the specimen at the point of contact of the central loading bar and this effect may have also contributed to the increase in m value.

5.1.3. Scatter in Results

The problems associated with specimen alignment are well demonstrated in the results of the zero mean stress tests. The scatter associated with the S-N curve and fracture mechanics data is exceptionally large for notched specimens. The fact that fracture surface battering was observed on some specimens and not others is a further indication of the variability of the experimental conditions. The column of the Vibrophore is quite flexible in one direction and it is likely that this permitted flexing of the specimen on the compressive portion of the cycle, thereby inducing unwanted bending stresses which would be superimposed on to the applied load and cause the observed variations in life. Furthermore, the Vibrophore push-pull grips are designed in such a manner that it is extremely difficult to accurately centralise a specimen and ensure that the location is retained during the tightening sequence.

The dramatic improvement in the consistency of the results under three point bending conditions is a positive indication of the absence of alignment problems with this loading mode. The principal disadvantage of this technique is the more restricted crack growth rate range over which data can be collected for the same design of specimen. The increase in scatter of the m values for the coarse grained small specimens was caused by errors in the crack length observations, due to surface rumpling effects associated with the coarse grain size.

5.2. CONSTANT AMPLITUDE FRACTOGRAPHY

5.2.1. Stage IIa and Stage IIb Fracture Criteria

Two modes of fracture were described in the experimental results and were designated stage IIa and stage IIb. This designation is a subdivision

of Forsyth's definition of stage II, since both stage IIa and stage IIb occur at 90° to the tensile axis. However it could be argued that stage IIa resembles Forsyth's definition of stage I, since both are sensitive to microstructure. Although crystallographic modes of fatigue fracture were discussed in the literature survey there do not appear to be any observations similar in character to the stage IIa mode observed in this work.

The experimental results show conclusively that for a given grain size the externally applied value of K_{\max} is the parameter governing the transition from stage IIa to stage IIb. For a specific grain size the value of K_{\max} is constant with changes in alternating load in bending and zero mean stress tests. It also remains constant with changes in mean stress in the bending tests. K_{\max} in turn controls the radius of the plastic zone r_y and it is the ratio of the plastic zone size to grain diameter that ultimately governs the point of transition.

This behaviour suggests that when the plastic zone is small, extending over only one or two grains ahead of the crack tip, constraint is high and a restricted number of slip systems are available. This causes specific planes in the ferrite to fracture and gives rise to the "hill and valley" structure. Under these conditions of high constraint, cracking along favourably oriented grain boundaries will also occur. It could be argued that this effect is due to the presence of residual impurities in the steel that segregate to the grain boundaries during the solidification process. Elements such as arsenic, antimony and tin have been held responsible for grain boundary fracture in higher strength steels (99). However, the strength level of the experimental material was well below that of the materials quoted in reference 99 and indeed there is evidence (72) to suggest that the proportion of intergranular fracture decreases as the strength level is increased by the addition of carbon. Grain boundary carbide films are not considered to be a potential cause of intergranular fracture in the present work since they were not detected on the fracture

surface. It is possible therefore, that intergranular fracture is a much more common feature of fatigue fracture than has been previously appreciated. The appearance of stages IIIa and IIIb in copper and stainless steel (figs. 39 - 42) certainly reinforces this view.

It may also be argued that the presence of structure sensitive fatigue fracture is due to the atmospheric testing environment, since moisture has been shown to promote grain boundary fracture in higher strength steels (98). However the tests were carried out in humidities varying from 25% to 80%, and little effect on the transition stress intensity was observed. It would appear therefore that the variations in the testing environment are having little influence on the occurrence of stage IIIa fracture. It may well be that there is a threshold level of water vapour and pressure below which stage IIIa will not occur. The discolouration of the beach markings associated with the periods of slow crack growth on the programme loaded specimens is thought to be caused by an environmental reaction with the freshly exposed fracture surfaces. At low magnifications, the Stereoscan revealed the slow growth band to be slightly lighter in colour than the surrounding fracture, suggesting the presence of a thin film of less conducting material (oxide) on the fracture surface.

As the plastic zone increases in radius, beyond about 4 grains ahead of the crack tip, the degree of elastic constraint is reduced and slip in the grains ahead of the crack tip can occur more easily. The crack therefore begins to propagate into a much larger pre-deformed zone and the fracture path becomes less crystallographic giving rise to stage IIIb fracture. This theory also explains the observation that the transition is much quicker at high applied stress levels since the radius of the plastic zone is increasing much faster. The value of 4 for the ratio of r_y/d may not be important since it is dependent on the accuracy of the plastic zone calculation. Nevertheless a critical level of plasticity ahead of the crack tip is essential before the transition from stage IIIa to stage IIIb will occur. Stage IIIb fracture is typical of many observations

in the literature and is characterised by an absence of micro-structural detail. This fracture mode remains consistent with increased levels of plasticity ahead of the crack tip and does not change its basic form over a wide range of crack growth rates.

It is also interesting to note that no distinct change occurs in the crack length versus cycles curve at the transition from stage IIIa to stage IIIb and it is therefore not possible to say whether the structure sensitive mode is more "fatigue resistant". Certainly, it is in this field that micro-structural control of fatigue crack propagation should be most effective.

It would be useful to determine the crystallographic orientation of the features of stage IIIa, but the irregular nature of the fracture surface makes this extremely difficult. Etch pitting techniques were not successful and the grain size was too small for conventional X-ray analysis. The X-ray micro-beam technique could be useful here, irradiating a single grain of a coarse grained specimen and employing the Laue technique of analysis.

5.2.2. The Nature of Crack Front Movement

The literature survey showed that much emphasis has been placed on the correlation of striation spacings with macroscopic crack growth rate under conditions of high strain, particularly in aluminium alloys. The fracture surfaces of ferrous materials have received much less attention, particularly at slow crack growth rates.

The present experimental work has shown that there is a tendency towards a surprisingly large minimum striation spacing in mild steel and that until a crack growth rate of at least 1.2×10^{-5} ins. (300 nm) per cycle is exceeded, there is no possibility of correlating striation spacings with the externally observed crack growth rate. Therefore a situation can arise in which the macroscopic crack growth rate is less than the observed striation spacing and this is interpreted as an indication that the crack does not move forward on a single front. Instead it is thought that it progresses in a discontinuous manner, with localised areas of crack front propagating at different instants in time.

The reason for the minimum striation spacing of about 7.9×10^{-6} ins. (200 nm) is not clear, but it would seem reasonable to assume that a critical strain energy is necessary for crack extension to occur on every cycle. At slow crack growth rates the strain energy input per cycle is below the critical level and a number of cycles must therefore elapse before the critical strain energy level is achieved. This accumulation of strain energy probably occurs in the form of plastic deformation and hardening at the crack tip prior to crack extension.

Between 7.9×10^{-6} and 1.2×10^{-5} ins. (200-300 nm) per cycle, larger lengths of crack front begin to move forward at a given instant until, at crack growth rates in excess of 1.2×10^{-5} ins. (300 nm) per cycle, the strain energy input is sufficient to ensure complete crack front extension on every cycle. In addition any excess strain energy may be consumed in producing greater crack extension (i.e. larger striation spacings) and hence a one to one correlation between macroscopic crack growth rate and one striation spacing per cycle is observed.

The concept of the crack front moving forward in an irregular manner is supported by the evidence presented in figs. 44 and 45. Fig. 44 shows striations formed under conditions where there is a one to one correlation between striation spacing and macroscopic crack growth rate. Fig. 45 is typical of the slower crack growth rates where discontinuous crack advance is occurring. It will be noticed that the striations in the former case are wider and less interrupted, as would be expected if the crack front was moving more as a single line.

The precise mechanisms of striation formation probably depend upon the extent of plasticity ahead of the crack tip. At very slow crack growth rates (where stage IIa is predominant), it is likely that the mechanism of striation formation will be based on a crystallographic mechanism (91). However, as the amount of crack tip plasticity increases and the stage IIb mode occurs, the Laird-Smith mechanism probably becomes predominant.

The literature has always inferred that striations are more readily

observed in aluminium alloys than in steels. However there appears to have been very little fractographic work carried out at slow crack growth rates on aluminium and its alloys and it may well be that under these conditions the striations become much less regular even in those materials.

5.3. PROGRAMMED LOADING

5.3.1. The Consistency of the Cumulative Cycle Ratio

The most significant observation in this part of the investigation is the consistency of the cumulative cycle ratio. For load histories containing a mixture of load rises and falls, $\sum \frac{n}{N}$ is always greater than unity and the Palmgren-Miner hypothesis therefore provides a safe and satisfactory method of estimating the fatigue crack propagation life of low carbon steels. This means that computer integration of the fracture mechanics data using the relevant load sequence can provide a reliable estimate of life for design purposes.

The consistency of these results is in direct contrast to much of the previously published work and it should be emphasised that the removal of residual stress caused by machining etc. before testing is an important factor controlling these results. In practice, however large residual stresses may be present in finished components and the designer must take full account of their effects before attempting to use the Palmgren-Miner hypothesis.

Apart from the consistency of the results, it is also noteworthy that the cumulative cycle ratio is always very close to unity and the concepts of residual stresses discussed in the literature review (38, 63) can be used to explain this effect.

In the simple two level tests, the cumulative cycle ratio lay between 1.01 and 1.13. It was also noted that the effects of load level, block size and sequence were not exerting any significant effect and this was initially attributed to the symmetrical nature of the programmes. In other words there was a tendency for the residual compressive stresses (induced by load drops) to be cancelled out by residual tensile stress effects

(induced by load rises). However since $\sum \frac{n}{N}$ was always greater than unity it was concluded that the total compressive contribution was always dominant.

The purpose of the multi-level tests was to introduce some imbalance into the loading sequence. However whilst the block size remained constant for each load level (34,000 cycles), the cumulative cycle ratio still fell within the same limits as the two level tests, irrespective of the load sequence.

At this point it was considered possible that the cycles of the highest stress were taking too large a proportion of the total life and so the block size for each level was adjusted to 10% of the respective constant amplitude life. The 4 level staircase programmes were then repeated. In both directions a significant change in the cumulative cycle ratio occurred. The ascending staircase gave a larger value (1.42 - 1.51) than the descending staircase (1.21 - 1.26). In both cases it was noteworthy that $\sum \frac{n}{N}$ had increased significantly above the values previously obtained.

Before attempting to explain this effect, it is necessary to examine the results of the run out tests. Fig. 47 shows clearly that the extent of unstable stage IIa decreases with increasing ΔK . In other words the rate of decay of residual stress is greater at higher stress intensity levels. This occurs even though the stress intensity drop increases at higher ΔK levels. On a mechanistic basis (discussed in the next section) the increase in stress intensity drop should extend the amount of stage IIa. Clearly the level of ΔK is the most influential factor.

In both of the staircase programmes with the 10% block size, the observed increase in $\sum \frac{n}{N}$ is almost certainly related to the increasing predominance of compressive stresses and this situation arises because the proportion of high stress cycles is decreasing, thereby prolonging the decay period.

The larger value of $\sum \frac{n}{N}$ obtained for the ascending staircase

(1.42 - 1.51) compared with the descending staircase (1.21 - 1.26) may be explained by similar reasoning. In the former case the large load drop in the sequence is followed immediately by a low stress block, thereby prolonging the stability of the residual compressive stress effect.

However, in the descending staircase sequence, although the residual compressive stresses are still dominant their effectiveness is reduced because the load drop occurs in three discrete steps and the effectiveness of the lowest block is offset by the load rise (and consequent tensile stresses) back to the highest stress block of the sequence.

A similar explanation applies to the results of the two level tests and staircase tests with the 34,000 cycle block size, where the cumulative cycle ratio was particularly close to unity (1.01 - 1.13). In this case a large proportion of the total crack propagation life was occupied by the highest stress level, which therefore promoted rapid decay of compressive stresses.

5.3.2. Mechanisms of Residual Stress Formation and Decay

Throughout this work it has become obvious that residual compressive stresses have a greater influence than the residual tensile stresses. This lends support to the plastic zone concepts discussed in the literature review. Tensile stresses would only be expected to be operative after a load rise, whilst the plastic zone enlarges to a size characteristic of the new stress level. After a load drop a situation arises in which the plastic zone is too large for the new stress level and is therefore forced into compression, causing a reduction or arrest in crack growth.

On this basis the mechanism of decay of residual compressive stress might be expected to be based simply on the crack cutting the non-equilibrium plastic zone in half, thereby permitting stress relief. However table 20 shows that the extent of "unstable" stage IIa is well in excess of the theoretical plastic zone radius at the load drop and thus the situation is not quite as simple as the model would suggest.

SPECIMEN	RADIUS OF PLASTIC ZONE AT LOAD DROP		EXTENT OF INDUCED STAGE IIa	
	ins.	(mm)	ins.	(mm)
130	.013	(0.33)	.031	(0.79)
131	.007	(0.18)	.046	(1.16)
132	.005	(0.13)	.058	(1.48)
133	.004	(0.10)	.078	(1.99)
145	.007	(0.18)	.061	(1.54)

TABLE 20. COMPARISON OF r_y AT LOAD DROP WITH THE EXTENT OF "UNSTABLE" STAGE IIa.

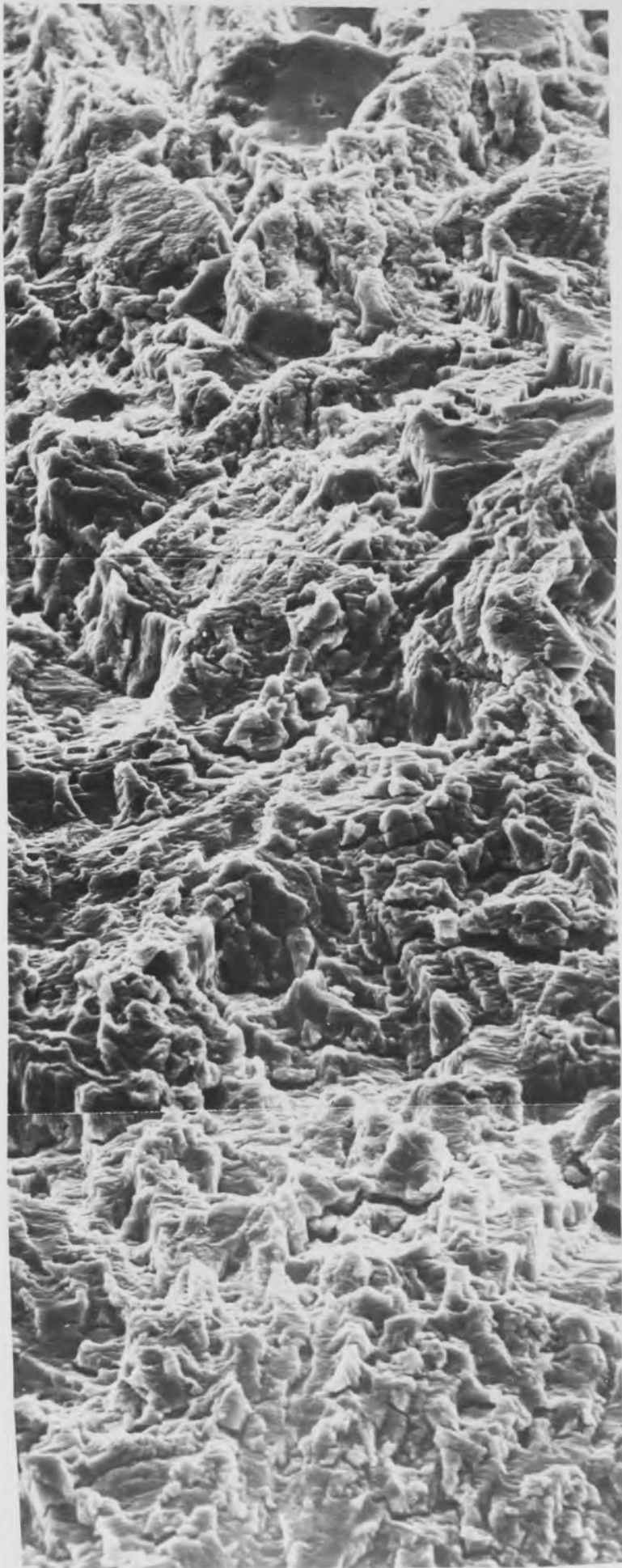
Observations of plastic zones in static loading (107) have shown well defined "ears" to develop ahead of the crack tip. In fatigue this effect may occur on a smaller scale, and the "ears" stretching in front of the crack tip could be responsible for the observed extension of residual stress.

Fig. 48. shows the appearance of unstable stage IIa fracture after a high to low load change. A band of intensified branch cracking is often observed at the load drop before the reversion to stage IIa.

Fig. 49 shows one of these branch cracks in detail. Striations are observed to run into the mouth of the crack and it is concluded that the load change is inducing multiple initiation of secondary fatigue cracks. Longitudinal sections through the fracture indicated that these cracks did not extend very far below the fracture before terminating.

Rice (108) has argued that residual compressive stresses are unlikely to be developed at the crack tip after high to low load changes, since reversed plastic flow at the crack tip will rapidly annihilate any effects of this type. He suggests instead that at high stresses the crack tip is more blunted, and on changing to a lower stress, crack front arrest occurs until the crack tip resharpenes to a new characteristic root radius. This mechanism infers that the load change will not exert any long range effect

Fig. 48. Composite Fractograph
of a Reversion from
Stage IIb to "Unstable"
Stage IIa After a Load Drop.
x 1200 Mag.
Operating Angle 45° .
(Negs. 248/8, 9, 11)

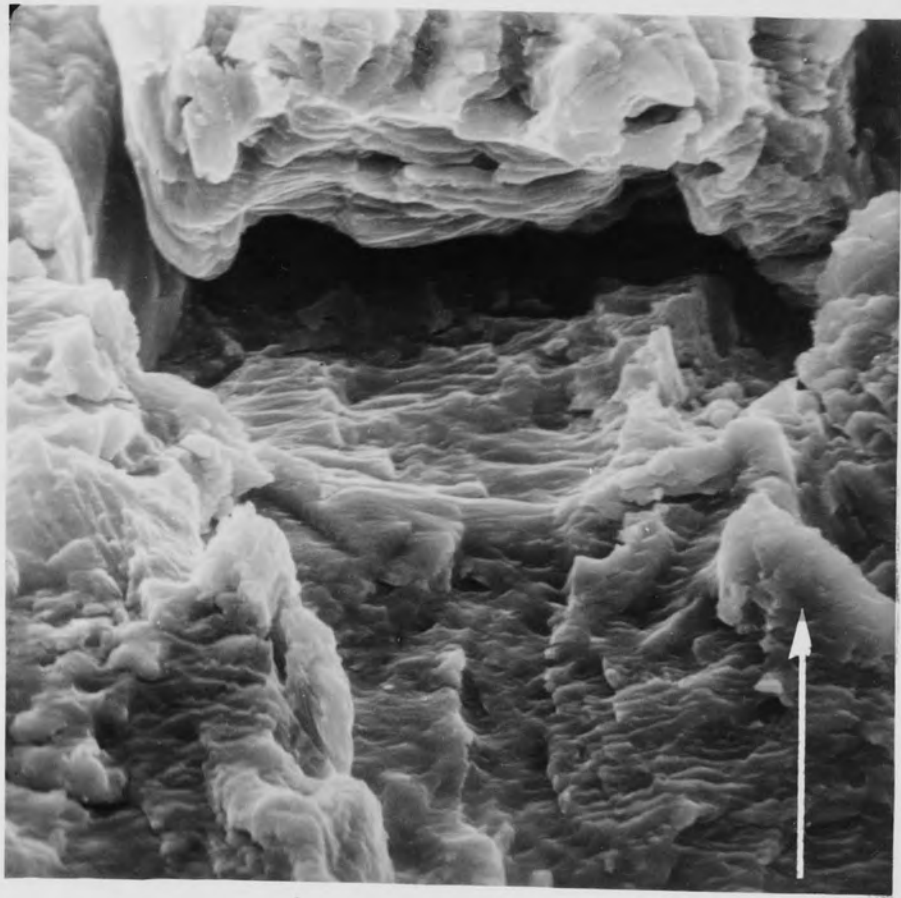


↑
STAGE IIa

—
↑
BAND OF
CRACKING
↓
—

STAGE IIb

Fig. 49. Typical Branch Crack
at Load Change.
x 3500 Mag.
Operating Angle 45° .
(Neg. 258/10)



ahead of the crack tip and is in direct conflict with the observations of "unstable" stage IIa in this study.

5.3.3. The Magnitude of Residual Stress

Residual compressive stresses appear to be dominant under programmed loading conditions. Although exact values cannot be evaluated from the results of this work, the estimates based on the fractographic observations of "unstable" stage IIa suggest that the level of compressive stress can be considerable ranging from 1.0 - 10.0 ksi $\sqrt{\text{ins}}$. (1.1 - 11.0 MNm^{-3/2}).

Estimates of residual tensile stresses suggest $+K_{\text{max}}$ levels of 0.1 - 3.0 ksi $\sqrt{\text{ins}}$ (0.11 - 3.3 MNm^{-3/2}). Although considerably less than the compressive stress levels, they are often greater than would be expected from a model based simply on the enlargement of the plastic zone. This further emphasises the complexity of the situation at the crack tip.

These comments are important when considering the effect of the rate of change of load level. The tests carried out to examine this effect were balanced with an equal number of load changes in each direction. It may well be that the rate of change of load level will exert a more drastic effect on $\sum \frac{n}{N}$ in tests where load changes occur in one direction only. This aspect of the problem should receive more attention, since it could be important under random loading conditions.

5.3.4. The Validity of the Palmgren-Miner Hypothesis

The foregoing discussion has explained, from residual stress considerations, the experimental observation that the Palmgren-Miner hypothesis is both a safe and reliable method of estimating fatigue crack propagation life in low carbon steels. The theories put forward should apply to both ferrous and non-ferrous ductile materials.

The fact that residual compressive stresses appear to be the dominating factor in mixed load histories is extremely encouraging from the designer's viewpoint. Smith (61) showed that treating both broad and narrow band random loading signals on an rms basis, produced cumulative cycle ratios in excess of unity. This suggests that the effects observed

in this study will also apply to the random loading situation and that some simple approximations may enable accurate life prediction for design purposes.

- 6.1. In the programmed loading tests containing a mixture of load rises and falls, the cumulative cycle ratio was always slightly greater than unity irrespective of block size, load level, rate of load change or sequence. The Palmgren-Liener hypothesis is therefore considered to be a satisfactory life prediction relationship for the crack propagation situation in this material.
- 6.2. In programs containing only load rises, the cumulative cycle ratio fell below unity.
- 6.3. The consistency of the cumulative cycle ratio was discussed in terms of residual tensile and compressive stresses induced at load rises and load drops respectively.
- 6.4. Under constant amplitude loading, the fracture mechanics analysis provides a satisfactory method of data correlation, provided the effects of material and experimental variables are fully appreciated. However, a single value of slope of the log stress intensity-log crack growth rate relationship will apply to all materials and conditions.
- 6.5. Under programmed loading conditions, computer integration of the constant amplitude fracture mechanics data provides a safe and accurate means of life prediction in terms of stress and crack length.
- 6.6. Two distinct modes of fatigue fracture were observed to occur. The first (designated stage IIa) was structure sensitive, exhibited grain boundaries and trans-granular cracking through specific fracture planes. The second (designated stage IIb) was more typical of previous observations in the literature being irregular in nature and not showing a dependence on microstructure.

6. CONCLUSIONS

This study of the effects of variable amplitude loading history on fatigue crack propagation in low carbon steel has provided the following conclusions.

- 6.1. In the programmed loading tests containing a mixture of load rises and falls, the cumulative cycle ratio was always slightly greater than unity irrespective of block size, load level, rate of load change or sequence. The Palmgren-Miner hypothesis is therefore considered to be a satisfactory life prediction relationship for the crack propagation situation in this material.
- 6.2. In programmes containing only load rises, the cumulative cycle ratio fell below unity.
- 6.3. The consistency of the cumulative cycle ratio was discussed in terms of residual tensile and compressive stresses induced at load rises and load drops respectively.
- 6.4. Under constant amplitude loading, the fracture mechanics analysis provides a satisfactory method of data correlation, provided the effects of material and experimental variables are fully appreciated. However, no single value of slope of the log stress intensity-log crack growth rate relationship will apply to all materials and conditions.
- 6.5. Under programmed loading conditions, computer integration of the constant amplitude fracture mechanics data provides a safe and accurate means of life prediction in terms of stress and crack length.
- 6.6. Two distinct modes of fatigue fracture were observed to occur. The first (designated stage IIa) was structure sensitive, exhibiting grain boundaries and trans-granular cracking through specific ferrite planes. The second (designated stage IIb) was more typical of previous observations in the literature being irregular in nature and not showing a dependence on microstructure.

- 6.7. The transition from stage IIa to stage IIb occurred when the radius of the plastic zone ahead of the advancing crack reached a value of approximately 4 times the mean grain diameter. The presence of stage IIa was therefore associated with conditions of high constraint at the crack tip and was possibly dependent on environmental conditions.
- 6.8. After a drop in load, stage IIa fracture was often observed to occur, even though the prevailing stress intensity was at a level which would produce stage IIb in a single stress level test. It is suggested that substantial residual compressive stresses were reducing the effective stress intensity at the crack tip. The extent of "unstable" stage IIa suggested that the decay of residual stress was faster at higher stress intensities than at low.
- 6.9. Fracture surfaces revealed fatigue striations at all crack growth rates. However a one to one correlation between striation spacing and crack growth rate was only observed above macroscopic crack growth rates of 1.2×10^{-5} ins (300 nm) per cycle. Below this value, an average minimum spacing of 7.9×10^{-6} ins. (200 nm) was observed. This effect was explained in terms of discontinuous movement of the crack front.
- 6.10. Striation spacing measurements at load level changes did not reveal any changes in "microscopic" crack growth rate. In addition neither the optical nor potential drop crack monitoring techniques were sufficiently sensitive to detect the effects of residual stresses on the macroscopic crack growth rate.
- 6.11. Grain size variations in the range .001 ins (25 μ m) to .005 ins (115 μ m), and increases in pearlite content from 10-20% did not appear to significantly affect the fatigue crack growth characteristics.
- 6.12. Under reversed loading conditions, specimen flexing causes extensive scatter in the results. The three point bending loading mode produces much improved consistency due to the absence of alignment problems.

7. SUGGESTIONS FOR FURTHER WORK

- 7.1. In extending the work towards random loading histories, it will be instructive to study the effect of progressively reducing the block size to the situation of isolated impulse loads. As an approximation for design purposes it would also be useful to carry out random loading tests calculating the cumulative cycle ratio on an rms basis.
- 7.2. Any study of fatigue in steels which is biased towards assisting the designer to predict life in real components must ultimately deal with the problem of residual stresses due to manufacturing processes. This is a very complex problem and needs detailed examination if the results obtained under laboratory conditions are to be directly applicable to the service environment.
- 7.3. It is important to know whether the Palmgren-Miner relationship is applicable to other steels under similar loading conditions.
- 7.4. Further work is needed to examine the individual effects of the rate of load rise and fall on the cumulative cycle ratio. Use should be made of loading programmes in which all load changes are in one direction, thereby avoiding any possible balancing effect between residual tensile and compressive stresses.
- 7.5. More accurate information is needed concerning the exact magnitude of the induced residual stress. Strain control tests using unnotched specimens to simulate notch root conditions can provide such information, thereby enabling realistic adjustments of the computer programme to be made.
- 7.6. It would be useful to determine the influence of environment on the presence and extent of stage IIa fracture, particularly the effect of humidity. At the same time it would be instructive to determine the orientation of the "hill and valley" facets, using an X-ray micro-beam technique.

8. REFERENCES

- (1) H.F. Moore. Bull. 165 Ill. Univ. Engng. Exp. Stn. (1927).
- (2) A.V. de Forrest. J. Appl. Mech. 3 p. A23 (1936).
- (3) J.A. Bennett. Proc. Am. Soc. Test. Mater. 46 p. 693 (1946).
- (4) N.E. Frost and D.S. Dugdale. J. Mech. Phys. Solids. 5 p. 182 (1957).
- (5) A.K. Head. Phil. Mag. 44 p. 925 (1953).
- (6) N.E. Frost and D.S. Dugdale. J. Mech. Phys. Solids. 6 p. 92 (1958).
- (7) A.J. McEvily and W. Illg. NACA T.N. 4394 (1958).
- (8) P.C. Paris, M.P. Gomez and W.E. Anderson. Trend Engng. Univ. Wash. 13 p. 9 (1961).
- (9) P.C. Paris and F. Erdogan. J. Bas. Engng. 85 p. 528 (1963).
- (10) G.R. Irwin. J. Appl. Mech. 24 p. 361 (1957).
- (11) W.F. Brown Jr. and J.E. Srawley. Am. Soc. Test. Mater. STP. 410 p. 1 (1966).
- (12) P.C. Paris. Proc. 10th Sagamore Army Materials Research Conf. New York. p. 107 (1963).
- (13) J. Weertman. Proc. 1st Int. Conf. on Fracture 1 p. 153, Sendai (1965).
- (14) R.W. Lardner. Phil. Mag. 17 p. 71 (1968).
- (15) B.A. Bilby and P.T. Heald. Proc. Roy. Soc. 305 p. 429 (1968).
- (16) B. Tomkins. Phil. Mag. 18 p. 1041 (1968).
- (17) N.E. Frost and K. Denton. Natn. Engng. Lab. Rep. 260. East Kilbride, Glasgow (1966).
- (18) N.E. Frost. Proc. Instn. Mech. Engrs. 173 p. 811 (1959).
- (19) L.P. Pook, N.E. Frost and K. Denton. Natn. Engng. Lab. Rep. Z2/1/69 East Kilbride, Glasgow (1969).
- (20) J. Schijve. Am. Soc. Test. Mater. STP. 415 p. 415 (1967).
- (21) D. Broek and J. Schijve. Natn. Aerospace Res. Inst. NLR Rep. TN M2111. Amsterdam (1963).
- (22) R. Roberts and F. Erdogan. J. Bas. Engng. 89 p. 885 (1967).
- (23) R.G. Forman, V.E. Kearney and R.M. Engle. *ibid.* p. 459 (1967)
- (24) C.M. Hudson and J.T. Scandina. Engng. Fract. Mech. 1 p. 429 (1969).

- (25) T.R. Gurney. Welding Inst. Rep. E18/12/68 Cambridge (1968).
- (26) W.G. Clark Jr. Engng Fract. Mech. 1 p.385 (1968).
- (27) C.M. Carman and J.M. Katlin. J. Bas. Engng. 88 p.792 (1966).
- (28) A.J. Brothers and S. Yukawa. J. Bas. Engng. 89 p.19 (1967).
- (29) G.R. Irwin. J. Bas. Engng. 82 p.417 (1960).
- (30) H.W. Liu. Appl. Mater. Res. 3 p.229 (1964).
- (31) A.R. Rosenfield, P.K. Dai and G.T. Hahn. Proc. 1st Int. Conf. on Fracture 1 p.223 Sendai (1965).
- (32) D.P. Wilhelm. Am. Soc. Test. Mater. STP. 415 p.363 (1967).
- (33) S.R. Swanson, F. Cicci and W. Hoppe. Am. Soc. Test. Mater. STP. 415 p.312 (1967).
- (34) A.J. McEvily and T.L. Johnston. Proc. 1st Int. Conf. on Fracture 2 p.515 Sendai (1965).
- (35) N.E. Frost and K. Denton. J. Mech. Engng. Sci. 3 p.295 (1961).
- (36) W.E. Anderson and P.C. Paris. Metal Engng. Quart. 1 p.33 (1961).
- (37) R.W. Hertzberg and P.C. Paris. Proc. 1st Int. Conf. on Fracture 1 p.459 Sendai (1965).
- (38) C.M. Hudson and H.F. Hardrath. NASA TN D960 (1961).
- (39) C.M. Hudson. NASA TN D2331 (1964).
- (40) C.M. Hudson. NASA TN D2743 (1965).
- (41) B.M. Linder. M.S. Thesis. Lehigh University, Pennsylvania (1965).
- (42) R.P. Wei, P.M. Talda and Che-Yu Li. Am. Soc. Test. Mater. STP. 415 p.460 (1967).
- (43) S.J. Maddox. Welding Inst. Rep. E/29/69. Cambridge (1969).
- (44) S.J. Maddox. ibid. E/36/70 Cambridge (1970).
- (45) A. Hartman. Int. J. Fract. Mech. 1 p.167 (1965).
- (46) F.J. Bradshaw and C. Wheeler. Appl. Mater. Res. 5 p.112 (1966).
- (47) R.P. Wei. Engng. Fract. Mech. 1 p.633 (1970).
- (48) N.E. Frost. Appl. Mater. Res. 3 p.131 (1964).
- (49) G.W.J. Waldron, A.E. Inckle and P. Fox. Proc. 3rd A. Scanning Electron Microscope Symp. p.297 Chicago (1970).

- (50) S. Pearson. Nature, Lond. 211 p.1077 (1966).
- (51) A. Palmgren. Z. Ver. dt. Ing. 68 p.339 (1924).
- (52) M.A. Miner. J. Appl. Mech. 12 p. A159 (1945).
- (53) F.E. Richart and N.H. Newmark. Proc. Am. Soc. Test Mater. 48 p.767 (1948).
- (54) S.M. Marco and W.L. Starkey. Trans. Am. Soc. Mech. Engrs. 76 p.627 (1954).
- (55) L. Kaechele. Rand Corp. Mem. No. RM-3650-PR (1963).
- (56) S.S. Manson. Int. J. Fract. Mech. 2 p.327 (1966).
- (57) H.J. Grover. Am. Soc. Test. Mater. STP. 274 p. 120 (1960).
- (58) R.R. Gatts. J. Bas. Engng. 83 p.529 (1961).
- (59) R.H.W. Brook and J.S.C. Parry. J. Mech. Engng. Sci. 11 p.243 (1969).
- (60) P.C. Paris. Am. Soc. Mech. Engrs. Paper 66-Met-3 p.1 (1962).
- (61) S.H. Smith. Acoustical Fatigue in Aerospace Structures. Ed. W.J. Trapp and D.M. Forney p.331. Dayton, Ohio (1964).
- (62) P.R. Edwards. R.A.E. Tech. Rep. 69237 Farnborough (1969).
- (63) J. Schijve. Natn. Aerospace Res. Inst. NLR. Rep. MP178. Amsterdam (1959).
- (64) C.R. Smith. Proc. Soc. Exp. Stress Analysis 12 p.21 (1954).
- (65) E.J. Pattinson and D.S. Dugdale. Metallurgia 66 p.228 (1962).
- (66) D. Rosenthal and G. Sines. Proc. Amer. Soc. Test. Mater. 51 p.593 (1951).
- (67) P.G. Forrest. Proc. Internat. Conf. on Fatigue of Metals. Instn. Mech. Engrs. and Am. Soc. Mech. Engrs. p.171 (1956).
- (68) T.H. Topper, J. Morrow and R.M. Wetzell. Am. Soc Test. Mater. STP 462 p.74 (1970).
- (69) T.H. Topper, B.I. Sandor and J. Morrow. J. Mater. 4 p.189. (1969).
- (70) P.J.E. Forsyth. Crack Propagation Symp. 1 p.76 Cranfield (1961).
- (71) J.C. McMillan and R.W. Hertzberg. Am. Soc. Test. Mater. STP 436 p.89 (1968).
- (72) P. Fox. M. Phil. Thesis. British Railways Research Dept. Derby (1970).

- (73) G. Jacoby. *Expl. Mech.* 5 p.65 (1965).
- (74) C.A. Zapffe and C.O. Worden. *Trans. Am. Soc. Metals* 43 p.958 (1951).
- (75) P.J.E. Forsyth and D.A. Ryder. *Aircr. Engng.* 32 p.96 (1960).
- (76) C. Crussard. *Proc. Internat. Conf. on Fatigue of Metals.* Inst. Mech. Engrs. and Am. Soc. Mech. Engrs. p.784 (1956).
- (77) G.A. Miller. *Trans. Am. Soc. Metals.* 62 p.651 (1969).
- (78) J. Schijve. *Natn. Aerospace Res. Inst. NLR Rep. M2122.* Amsterdam (1964).
- (79) R.M.N. Pelloux. *Trans. Am. Soc. Metals.* 57 p.511 (1964).
- (80) R.C. Bates and W.G. Clark. *ibid.* 62 p.380 (1969).
- (81) W.A. Spitzig and R.P. Wei. *ibid.* 60 p.279 (1967).
- (82) D.A. Meyn. *ibid.* 61 p.42 (1968).
- (83) D.A. Meyn. *ibid.* 61 p.52 (1968).
- (84) W.J. Plumbridge and D.A. Ryder. *Metals and Materials* 3 p.119 (1969).
- (85) G. Jacoby. *N.A.T.O. AGARD Rep. 541 Paris* (1966).
- (86) A.J. McEvily, R.C. Boettner and T.L. Johnston. *Proc. 10th Sagamore Army Materials Research Conf.* p.95 New York (1963).
- (87) C.A. Stubbington and P.J.E. Forsyth. *J. Inst. Metals* 90 p.347 (1961).
- (88) P.J.E. Forsyth. *Acta Metall.* 11 p.703 (1963).
- (89) C. Laird and G.C. Smith. *Phil. Mag.* 7 p.847 (1962).
- (90) C. Laird. *Am. Soc. Test. Mater. STP 415* p.131 (1967).
- (91) R.W. Hertzberg. *ibid.* p.205 (1967).
- (92) R.M.N. Pelloux. *Trans. Am. Soc. Metals* 62 p.281 (1969).
- (93) D. Broek and C.Q. Bowles. *Natn. Aerospace Res. Inst. NLR Rep. TR 69048 U.* Amsterdam (1969).
- (94) H.D. Williams and G.C. Smith. *Phil. Mag.* 13 p.835 (1966).
- (95) M.E. Ashton. *British Railways Research Dept. Rep. E626 Derby* (1970).
- (96) D.I. Golland and P.L. James. *Metal Sci. J.* 4 p.113 (1970).
- (97) D.W. Hoepfner. *Am. Soc. Test. Mater. STP 415* p.486 (1967).
- (98) E.P. Dahlberg. *Trans. Am. Soc. Metals* 53 p.46 (1965).
- (99) P.R.V. Evans, N.M. Madhava and T.G. Chart. *Czech. J. Phys.* B19 p.381 (1969).

- (100) J.C. McMillan and R.M.N. Pelloux. Am. Soc. Test. Mater. STP 415 p.505 (1967).
- (101) R.E. Petersen. Stress Concentration Design Factors. Wiley (1953).
- (102) D.M. Gilbey and S. Pearson. R.A.E. Tech. Rep. 66402 Farnborough (1966).
- (103) A.E. Inckle. J. Mater. Sci. 5 p.86 (1970).
- (104) G. Birkbeck, A.E. Inckle and G.W.J. Waldron. J. Mater. Sci. 6 p.319 (1971).
- (105) F.A. McClintock and G.R. Irwin. Am. Soc. Test. Mater STP 381 p.84 (1965).
- (106) E.F. Walker and M.J. May. BISRA Open Rep. MG/E/307/67 (1967).
- (107) A.R. Rosenfield, P.K. Dai and G.T. Hahn. Proc. 1st Int. Conf. on Fracture 1 p.223 Sendai (1965).
- (108) J.R. Rice. Am. Soc. Test. Mater. STP 415 p.247 (1967).
- (109) G. Wallgren. FFA Rep. No. 28. Stockholm (1949).
- (110) H.F. Hardrath and E.C. Utley Jr. NACA TN 2798 (1952).
- (111) H.T. Corten, G.M. Sinclair and T.J. Dolan. Proc. Am. Soc. Test. Mater. 54. p.737 (1954).
- (112) A.M. Freudenthal and R.A. Heller. J. Aero/Space Sci. 26 p.431 (1959).
- (113) J. Schijve and F.A. Jacobs. Natn. Aerospace Res. Inst. NLR. Rep. M1982. Amsterdam (1955).
- (114) H.F. Hardrath, E.C. Utley, and D.E. Guthrie. NASA TN D210 (1959).
- (115) R. Spitzer and H.T. Corten. Proc. Am. Soc. Test. Mater. 61 p.719 (1961).
- (116) S.S. Manson, A.J. Nachtigall, C.R. Ensign and J.C. Freche. J. Engng. Ind. 87 p.25 (1965).
- (117) S.R. Swanson. UTIA Rep. 84 Inst. of Aerophysics, University of Toronto (1963).
- (118) K.J. Marsh. Natn. Engng. Lab. Rep. 263. East Kilbride, Glasgow (1966).
- (119) H.J. Grover, S.M. Bishop and L.R. Jackson. NACA TN 2324 (1951).

- (120) W.H. Erickson and C.E. Work. Proc. Am. Soc. Test. Mater. 61 p.704 (1961).
- (121) K.J. Marsh and J.A. Mackinnon. Natn. Engng. Lab. Rep. 234. East Kilbride, Glasgow (1966).
- (122) U. Rosetti. Proc. 3rd Conf. on Dimensioning and Strength. p.701 Budapest (1968).
- (123) H. Yeomans. R.A.E. Tech. Note 327 Farnborough (1963).
- (124) E.C. Naumann. NASA TN D1522 (1962).
- (125) K. Heyer. Lilienthal Gessellschaft fur Luftfahrtforschung Bericht 152 (1943).
- (126) W.A.P. Fisher. R.A.E. Tech. Note 236 Farnborough (1958).
- (127) R.A. Carl and T.J. Wegeng. Proc. Am. Soc. Test. Mater. 54 p.903 (1954).
- (128) C.R. Smith. Proc. Soc. Exp. Stress Analysis 16 p.9 (1958).
- (129) J. Schijve. Full Scale Testing of Aircraft Structures. Ed. F.J. Plantema and J. Schijve. p.41 Pergammon Press (1961).
- (130) J. Schijve and D. Broek. Aircr. Engng. 34 p.314 (1962).
- (131) J. Schijve, F.A. Jacobs and P.J. Tromp. Natn. Aerospace Res. Inst. NLR TR Rep. 68117u Amsterdam (1968).
- (132) W.T. Kirkby and P.R. Edwards. Proc. 4th ICAF Symp. 1965. Ed. E. Gassner and W. Schutz. Published Pergammon (1969).
- (133) J.D. Harrison, T.R. Gurney and B. Smith. Proc. Conf. on Fatigue of Welded Structures p.292 Brighton (1970).
- (134) E.C. Naumann, H.F. Hardrath and D.E. Guthrie. NASA TN D212 (1959).
- (135) W.H. Munse, J.R. Fuller and K.S. Petersen. Bull. Am. Rly. Engng. Ass. June/July (1958).
- (136) K.J. Marsh and J.A. Mackinnon. J. Mech. Engng. Sci. 10 p.48 (1968).
- (137) K. Hatanaka, H. Kawabe and M. Tanaka. Tech. Rep. Osaka Univ. 19 p.619 (1969).

9. ACKNOWLEDGMENTS

I would like to thank my supervisors Dr. H.D. Williams and Dr. G.W.J. Waldron for helpful discussions throughout this project. Thanks are also due to Dr. G. Birkbeck for his suggestions and encouragement; to Dr. G.S. Lane who wrote the computer programmes used in this work; to Mrs. J. Hick for her painstaking care in producing the photographs; to Mr. M. Brzozowski for machining the specimens to the high standard of precision required; to Mrs. V. Soar who typed the thesis and to the British Railways Board for making available the facilities to carry out this study and granting permission to submit the results for a higher degree.

APPENDIX 1

SURVEY OF THE EXPERIMENTAL RESULTS OF PROGRAMMED LOADING TESTS IN THE LITERATURE

This appendix details the published results of variable load history experiments in terms of the cumulative cycle ratio. The examples cited are typical of work carried out over the past 30 years, principally in the high cycle fatigue region. For ease of interpretation the tables have been divided into ferrous and non-ferrous notched and unnotched specimens and where possible details of the specimen condition prior to testing have been included.

UNNOTCHED SPECIMENS

Tables 21 and 22 clearly demonstrate the lack of consistency in the results. The loading mode may influence the cumulative cycle ratio, but the evidence is far from conclusive.

The effect of sequence is also unclear. Schijve and Jacobs (113) considered that in 2024 aluminium alloy with axial loading conditions and stress ratio equal to zero, high to low unrepeated sequence was more beneficial than the reverse. Corten et al (111, 115), using rotating bend two level repeated tests on 7075-T6 aluminium alloy, found the reverse effect to Schijve and a slight coxing effect could possibly have been responsible. Grover, Bishop and Jackson (119) found virtually no sequence effect under axial loading conditions with the same alloys and stress ratios midway between those of Corten and Grover et al, their value of cumulative cycle ratio being scattered about unity.

In steels, available data tends to suggest that low to high sequence is more beneficial, again possibly due to coxing effects. However coxing effects depend on the block size and it is therefore difficult to generalise.

NOTCHED SPECIMENS

From the quantity of results cited in table 23 it is clear that this section has received by far the most attention, principally in connection

with aircraft structures. Unless specifically stated, the following discussion refers to mildly notched specimens (i.e. $K_t < 3$) where a significant proportion of the life is spent initiating the crack.

In table 23 the effect of stress ratio (R) and loading mode on non-ferrous materials appears to be fairly consistent. When R is equal to or greater than zero, the cumulative cycle ratio usually exceeds 1. Smaller R values seem to be associated with cumulative cycle ratios below unity. The effect may also be present in ferrous materials, although the results in table 24 are less conclusive.

Sequence effects are conflicting. Schijve (129) found that in rivetted joints of 2024 and 7075 aluminium alloys, an ascending staircase programme followed by a sharp load drop to the lowest level was more beneficial than the reverse. Also in two level repeated tests on notched specimens the high to low sequence was more beneficial. Schijve also found that decreasing block size reduced the sequence effect.

The results of Naumann et al (134) conflicted with those of Schijve, the ascending staircase being less beneficial than the reverse. The reason for this is not clear, but the difference in K_t and R between the two types of specimens and the higher stress levels used by Naumann et al must be significant.

In more sharply notched specimens when the majority of the life is spent in crack propagation, sequence effects are more consistent. As discussed previously in section 1.3.3. Schijve (63) and Hudson (38) found that load transitions from high to low caused crack arrests, whilst the reverse sequence had little effect. Thus the cumulative cycle ratio will tend to exceed unity to an extent that depends on the stability of the induced residual stress.

The influence of peak positive stresses on both mildly and sharply notched specimens depends on the level of applied stress. Schijve (129) showed that in rivetted joints, a peak positive load tended to increase the cumulative cycle ratio and had an even larger effect if repeated at

regular intervals. Clearly there is a limiting value of peak stress beyond which the damage induced becomes greater than the beneficial contribution of the residual stress. More recently Schijve et al (131) demonstrated that the omission of peak positive loads from a random load spectrum could reduce the cumulative cycle ratio during the crack propagation stage.

RESIDUAL STRESS EFFECTS

Edwards (62) has suggested that the level of tensile mean stress in a mildly notched specimen may be reduced in the vicinity of the stress raiser after the application of the peak load of the spectrum (see also section 1.3.3.). He has also proposed that at zero mean stress there is a greater likelihood of localised compressive yield raising the mean stress into the tensile region, thereby causing the cumulative cycle ratio to fall below unity.

Furthermore many rotating bend tests show scatter which is often caused by specimen preparation techniques influencing the nature of the surface. In certain instances, particularly in test pieces that are not stress relieved after final machining, residual stresses may significantly affect the results.

In crack propagation tests, sequence effects are clearly interpreted in terms of residual stress. The crack arrests observed by Schijve (63) and Hudson (38) after a high to low transition are almost certainly associated with the residual compressive stress induced in the plastic zone ahead of the crack tip. Little emphasis has been placed on residual stress in the past but clearly it is an extremely important factor and probably goes a long way towards explaining the inconsistencies in many results.

FATIGUE STRESSES BELOW THE FATIGUE LIMIT

The Palmgren-Miner summation takes no account of stresses below the fatigue limit and experimental observations concerning this problem are not conclusive. Generally, programmed load spectra reduce the effective

fatigue limit. Marsh (118) has suggested that in notched bars of mild steel and brass, stresses 20% below the constant amplitude fatigue limit may be contributory, whilst for unnotched specimens it may be as low as 40%. Marsh observed no effect in aluminium alloys, which conflicted with the findings of Schijve (129) and Wallgren (109) who both found that including stresses below the fatigue limit significantly reduced the value of cumulative cycle ratio. Clearly the level and number of cycles applied is important.

MATERIAL AND CONDITION	SPECIMEN DESIGN	LOAD MODE	STRESS RATIO	LOAD PROGRAMME	$\sum \frac{L}{N}$	REF.
Clad 24ST Aluminium	Hour glass	RB	-1	Multi-level repeated.	0.8 - 1.5	52
24ST	Parallel sided sheet	Axial	> 0	Manoeuvre spectrum, continuous staircase.	0.8 - 1.3	109
24ST4	Hour glass	RB	-1	Sinusoidal spectrum, Exponential spectrum.	0.9 0.6	110
75ST6 Aluminium	Hour glass	RB	-1	Two level repeated, Lo-Hi.	5% Hi = 2-3.5 * 50% Hi = 0.5-1.15	111
76ST61 Aluminium	Hour glass	RB	-1	Repeated descending staircase. Repeated ascending staircase.	0.6 - 0.9 1.5	54
2024 Aluminium	Hour glass	Vertical RB	-1	6 step repeated, random sequence.	Always < 1	112

RB = Rotating Bending Hi, Lo = High, Low Repeated Loading. Hi, L = High, Low Unrepeated Loading.

TABLE 21. NON FERROUS UN-NOTCHED

MATERIAL AND CONDITION	SPECIMEN DESIGN	LOAD MODE	STRESS RATIO	LOAD PROGRAMME	$\sum \frac{1}{N}$	REF.
24ST Aluminium	Flat waisted	Axial	0	Two level unrepeated.	H-L 1.9 L-H 0.8	113
7075-T6 Aluminium	Hour glass	RB	-1	Continuously varying cycles, sinusoidal and exponential.	Usually < 1	114
7075-T6	Wire	RB	-1	Repeated 2 level Hi-Lo and Lo-Hi.	0.8	115
5450 H311 As rec.	Hour glass	RB	-1	High stress + a low stress below fatigue limit.	0.7	116
2024 Aluminium	Round parallel gauge length	Axial	> -1	Random.	0.1	117
Leaded Brass As rec.	Round parallel gauge length	RB	-1	Triangular, continuously varying.	Usually < 1	118
24ST 75ST Aluminium	Flat waisted	Axial	> -1	Two step unrepeated.	H-L 0.97-2.36 L-H 1.01-2.04 H-L 1.09-1.52 L-H 1.14-1.44	119

TABLE 21 (Continued) NON FERROUS UN-NOTCHED

MATERIAL AND CONDITION	SPECIMEN DESIGN	LOAD MODE	STRESS RATIO	LOAD PROGRAMME	$\sum \frac{n}{N}$	REF.
ASTM A7 Normalised 4340 Hardened & tempered	Hour glass	RB	-1	Two step unrepeatd.	H-L 0.8 L-H 0.6-1.5	53
	Hour glass	RB	-1	Two step repeated	H-L 0.1-1.2 Hi-Lo 0.8-1.2 Lo-Hi 1.2-1.5	
X 4130 Normalised	Round parallel gauge length	RB	-1	Two step unrepeatd.	H-L 1.2 L-H 1.2-1.6	3
4340	Hour glass	Vertical RB	-1	6 step repeated, random sequence.	Always < 1	112
4340 Hardened & tempered	Hour glass	RB	-1	2 step unrepeatd.	H-L 0.6-0.98 L-H 1.0-1.4	120
Mild steel A/R + stress relief after m/c	Hour glass	Axial	-1	White noise through electromagnetic vibrator.	0.1-0.8	121
Mild steel. As above	Large hour glass	RB	-1	As above.	0.1-0.7	121
Med. carbon steel Patented	Wire Ropes	Axial	> 0	Ascending staircase.	0.74-1.17	122

TABLE 22. FERROUS UN-NOTCHED

MATERIAL AND CONDITION	SPECIMEN DESIGN	LOAD MODE	STRESS RATIO	LOAD PROGRAMME	$\sum \frac{1}{N}$	REF.
BS L65 Aluminium	Bolted joint greased and dry.	Axial	> 0	Simulated gust spectrum.	Always > 1	123
2024-T3 Aluminium	Double edge notched plate $K_t = 4$	Axial	-1 > 0	8 step random (sequence).	0.65 1.0 - 1.8	124
7075-T6 Aluminium	As above	Axial	-1 > 0	As above.	0.9 - 1.1 1.9 - 2.4	124
Al-Cu-Mg Al-Zn-Mg Al-Cu	Lug with hole and notched round bar.	Axial	0	Two step unrepeated	1.0 - 3.4	125
24ST Clad Aluminium	Round bar, keyhole notch	Axial	0	Two step repeated.	Hi-Lo 1.7-5.4 Lo-Hi 1.1-1.3	113
DTD 363A (\equiv 7075) Solution treated and aged.	Double edge notched sheet	Axial	0	Gust and manoeuvre spectrum.	1.0 - 1.5	126
7075-T6 Aluminium	Centre notched panel, $K_t = 5$	Axial	> 0	Broad & narrow band random loading	1.1-4.5 (rms basis)	61

TABLE 23. NON-FERROUS NOTCHED

MATERIAL AND CONDITION	SPECIMEN DESIGN	LOAD MODE	STRESS RATIO	LOAD PROGRAMME	$\sum \frac{R}{N}$	REF.
7075-T6 Aluminium	Wing structure $K_t=3$	Bending	> 0	Manoeuvre spectrum.	1.3 - 1.6	127
7075-T6	Centre notched panels, rivetted joints.	Axial	> 0	Preload + manoeuvre spectrum.	4.9 < 1, low preload > 1, high preload	128
2024-T3 Aluminium 7075-T6	Rivetted lap joints.	Axial	> 0	Multi-level repeated steps, flight simulation spectra.	2024 always >1 7075, 0.5-1.1	129
2024-T3	Centrally notched panels	Axial	> 0	Multi-level repeated gust spectrum simulation.	2.0 - 3.7	130
2024-T3 No heat treatment after precracking.	Precracked centrally notched panels.	Axial	> -1	Multi-level descending staircase, gust simulation.	3.4	131
2024-T3 7075-T6	Centrally notched panels	Axial	> 0	Two step unrepeated, H-L, L-H.	Always >1	38
BS 2L65 Aluminium	Double ended lug.	Axial	> 0	White noise, gust simulation	1.7 - 5.1	132
Leaded Brass AS rec.	Parallel gauge length	RB	-1	Continuously varying, triangular.	0.4 - 1.4	118

TABLE 23 (Continued) NON-FERROUS NOTCHED

MATERIAL AND CONDITION	SPECIMEN DESIGN	LOAD MODE	STRESS RATIO	LOAD PROGRAMME	$\sum \frac{N}{N}$	REF.
Al-Zn-Mg Aged 6 weeks	Plate with fillet welded stiffeners	Axial	0 0.5, -1	Multi-level staircase spectrum	4 0.5 - 2.5	133
2024-T3 Aluminium 7075-T6 Aluminium	Double edge notched panels $K_t = 4$	Axial	< 0	Multi-level gust spectrum simulation	Ascending staircase 0.72. Descending staircase 1.7. Ascending staircase 0.5. Descending staircase 2.3.	134

TABLE 23 (Continued) NON-FERROUS NOTCHED

MATERIAL AND CONDITION	SPECIMEN DESIGN	LOAD MODE	STRESS RATIO	LOAD PROGRAMME	$\sum \frac{h}{N}$	REF.
X 4130 Normalised	Round parallel gauge length	RB	-1	2 step unrepeated.	H-L 0.9 L-H 1.07	3
ASTM A7 Structural Steel Normalised.	Flat parallel gauge lengths; central hole	Axial	> 0	2 step unrepeated.	H-L 0.8-1.2 L-H 0.9-2.1	53
Low alloy Cr-Mo steel As rolled	Flat parallel gauge lengths; central hole	Axial	> 0 < 0	Manoeuvre spectrum. Gust spectrum	0.9 - 1.0 0.5 - 1.0	109
ASTM A7 Structural Steel	Bolted lap joints	Axial	> 0	2 level varying sinusoidally	< 1	135
Mild steel Normalised, stress relief after machining	Parallel gauge length round	RB	-1	2 step repeated.	0.6 - 0.9	113
Mild steel Normalised, stress relief after machining	Parallel gauge length, round	Axial	> -1	Multi-level	0.6 - 1.16	136

TABLE 24. FERROUS NOTCHED

MATERIAL AND CONDITION	SPECIMEN DESIGN	LOAD MODE	STRESS RATIO	LOAD PROGRAMME	$\sum \frac{n}{N}$	REF.
Mild steel Normalised, stress relief after machining	Parallel gauge length round	Axial	> -1	Filtered white noise	0.1 - 0.6	136
18/8 stainless steel (unstabilised) Solution treated 1100°C + W.Q.	-	RB	-1	Two step repeated	Hi-Lo 0.7 - 2.1 Lo-Hi 0.6 - 1.5	137

TABLE 24 (Continued) FERROUS NOTCHED

APPENDIX 2

NOTCH CUTTING PROCEDURE

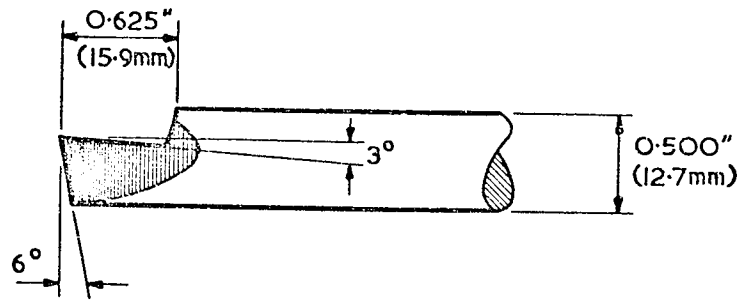
A sharp notch was essential to ensure that a minimum porportion of life was spent in initiating the fatigue crack. The profile adopted had a 45° included angle and a .002" (.05mm) root radius giving a theoretical K_t value of 10. A circular cutter profiled to this accuracy was not commercially available and a single point tool was therefore used. The principal disadvantage of this technique is the rapid rate of tool wear and strict control must be maintained over the cutting procedure in order to ensure that consistent notches are produced.

Eclipse high speed tool steel bar (0.5" (12.7 mm) in diameter) was ground to the form illustrated in Fig. 50. This procedure produced a notch tip radius of less than .0001" (.003 mm) and the required radius was subsequently produced manually using a fine carborundum stone and a projection microscope at x425 magnification.

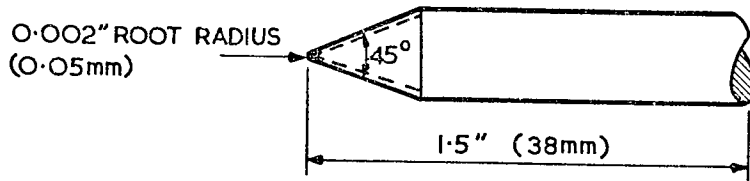
Machining was carried out on only 4 specimens at one time using a cutting speed of 115 r.p.m. and a feed rate of $7/16$ " (11 mm) per minute. Soluble oil cutting fluid was used throughout. The required notch depth of .040" (1 mm) was attained in five successive passes, the first three removing a .010" (.25 mm) per pass, the fourth .008" (.20 mm) and the fifth .002" (.05 mm). The cutting tool was then re-ground and profiled before further use.

It was important to locate the tool accurately in the holder so that the material was removed evenly at each cut. During the cutting stroke excessive elastic deflection of the tool caused an undulating effect along the root of the notch. This effect was minimised by restricting the maximum protrusion of the tool from the holder to .750" (19 mm).

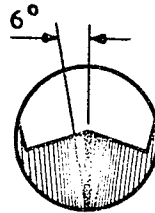
It is considered that the excellent agreement between replica three point bending tests was a reflection of the consistency of the notch profile.



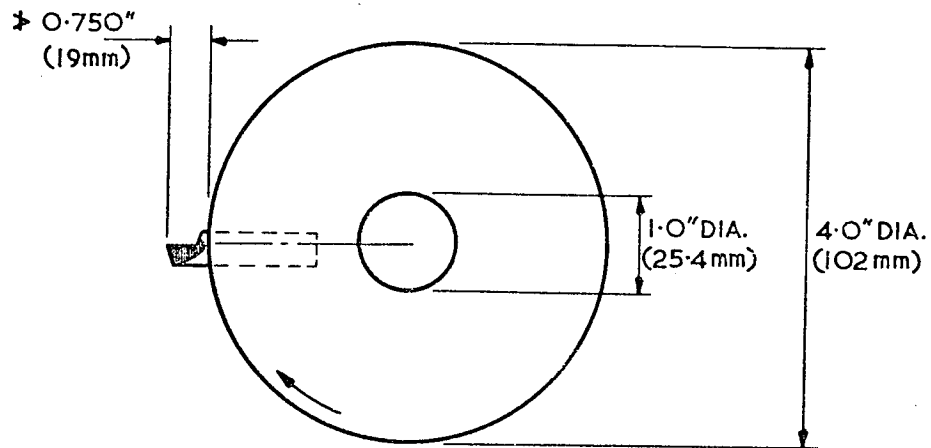
SIDE VIEW



TOP VIEW



FRONT VIEW



TOOL HOLDER

FIG. 50. DETAILS OF NOTCH CUTTING TOOL

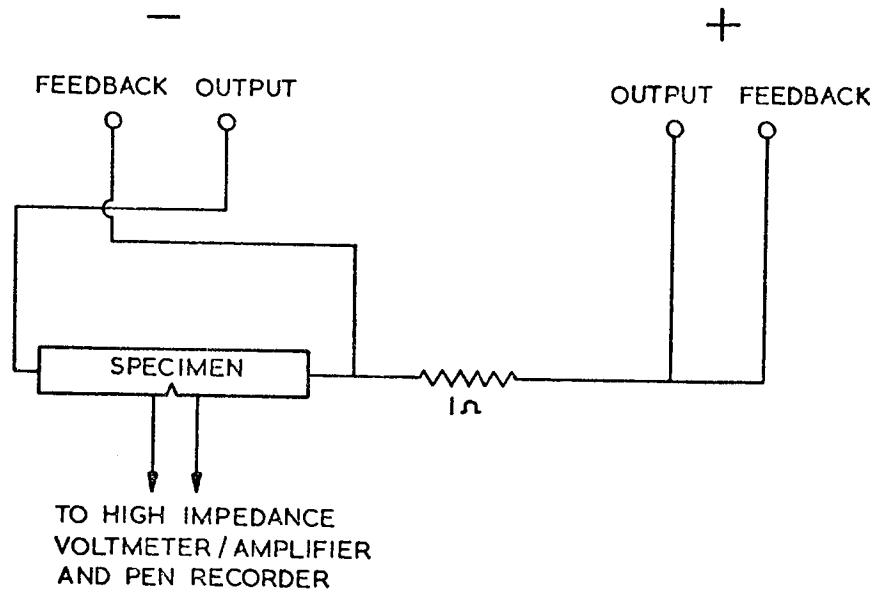
APPENDIX 3

THE POTENTIAL DROP CRACK GROWTH MEASUREMENT TECHNIQUE

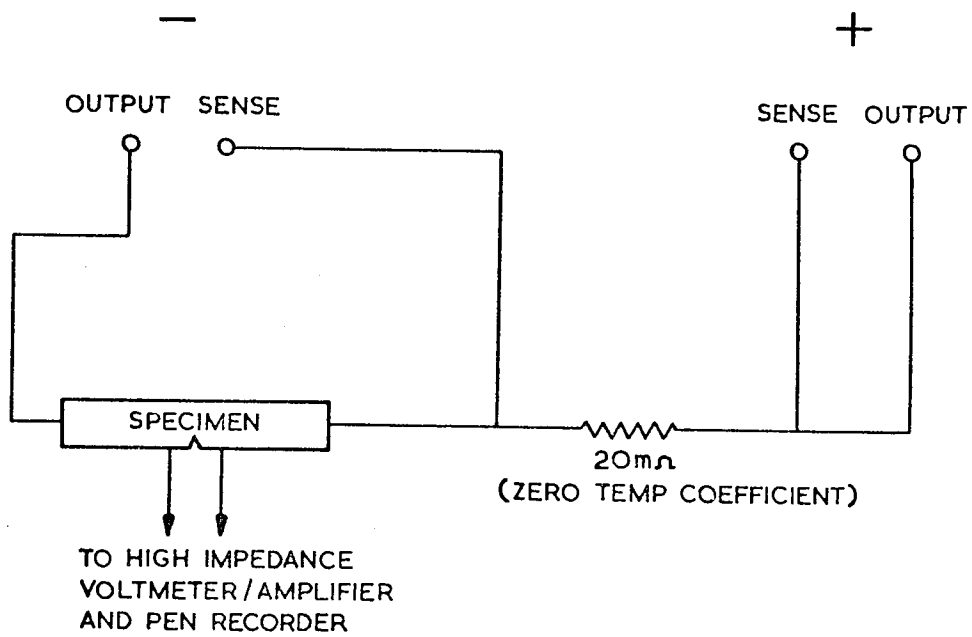
The technique, which is based on the work of Gilbey and Pearson (102), consists of passing a constant electric current through a specimen by means of probes attached to each end and measuring the change in potential drop across the crack as it grows. For convenience, this change in potential drop was calibrated directly with the optical microscopes.

It was important to ensure that the current supply was held constant throughout the test. For the small specimens 5 amps was adequate, but 50 amps was necessary for the large specimens. Details of the power supply connections are given in Fig. 51 whilst Fig. 52 shows the general arrangement for the small specimens on the 2 ton Vibrophore. The probes consisted of 36 swg iron wires which were spot welded either side of the notch, on the edge of the specimen. Connections from these probes were led to a Comark high impedance voltmeter - amplifier, the output of which was fed to a pen recorder. The time-scale of the pen recorder was assumed proportional to the cycles elapsed.

On the Vibrophore, it was found essential to screen the leads from the potential probes to reduce inductive pick-up from the electro-magnet. Even so, some instability was observed on the output trace, and this was probably caused by eddy currents induced in the specimen by the high frequency cycling. This effect limited the sensitivity of the technique.



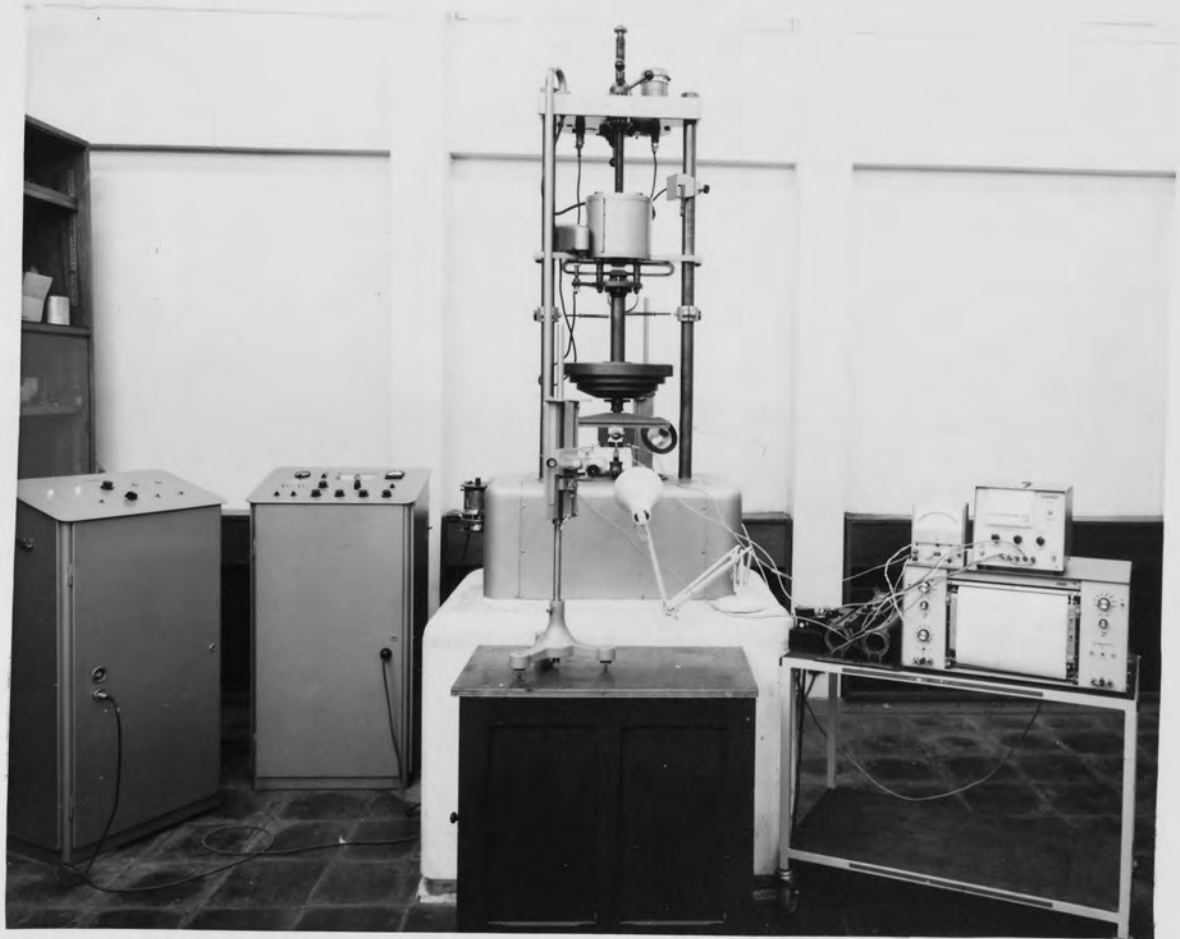
FARNELL L30 POWER SUPPLY
(SMALL SPECIMENS 5 AMPS)



COUTANT ASA / 5000 POWER SUPPLY
(LARGE SPECIMENS 50 AMPS)

FIG. 51. DETAILS OF CONSTANT CURRENT SUPPLY CONNECTIONS FOR POTENTIAL DROP TECHNIQUE

Fig. 52. General Arrangement of the
Potential Drop Equipment on
the Two Ton Vibrophore.
(Neg. 3684)





Aston University

**Content has been removed for
copyright reasons**

Etching of Tensile Surfaces

In the course of a fractographic investigation of fatigue in 4340 steel, it was found that a technique necessary to develop a fracture surface that would enable the principal features of the fracture surface to be related to the conditions of crack propagation.

In addition to conventional metallographic etching techniques, a technique was suggested. The fracture was prepared in a solution of 20% picric acid in water stained for generally revealing a fine etch was then treated on a 10% picric acid solution stained with methylene blue. A comparison of comparative photographs of sections of the fracture surface prepared in a picric acid solution and in a picric acid solution stained with methylene blue.

It was found that the picric acid stained fracture surface revealed features that were not apparent in the picric acid stained fracture surface.

28

It was observed in the fractographic features that after 20% picric acid stain the surface revealed features that were not apparent in the picric acid stained fracture surface.

The fracture was stained with a 10% picric acid solution stained with methylene blue before etching, and Fig. 10 and 11 show the surface after etching with 20% picric acid solution. The primary feature of Fig. 10 and 11 is a sharp line in the middle of the fracture.

Table 10
Etching time in picric acid solution stained with methylene blue

Etching time in picric acid solution stained with methylene blue	Number of features revealed in picric acid solution	Number of features revealed in picric acid solution stained with methylene blue
10	1	1
15	1	1
20	1	1
25	1	1
30	1	1
35	1	1
40	1	1
45	1	1
50	1	1
55	1	1
60	1	1
65	1	1
70	1	1
75	1	1
80	1	1
85	1	1
90	1	1
95	1	1
100	1	1

APPENDIX 5EXPERIMENTAL ERRORS

Standard deviations in the stress-life data were assessed on the assumption of a normal distribution using the relationship:

$$\bar{\sigma} = \sqrt{\frac{1}{n} \sum x^2 - \frac{(\sum x)^2}{n}}$$

where $\bar{\sigma}$ is the standard deviation, n the number of data points, x.

The straight line fit to the fracture mechanics data was calculated from the relationships:

$$y = ax + b$$

where $y = \log da/dN$ and $x = \log \Delta K$,

$$a = \frac{n \sum xy - \sum x \sum y}{n \sum x^2 - (\sum x)^2} = m$$

$$\text{and } b = \frac{\sum y \sum x^2 - \sum x \sum xy}{n \sum x^2 - (\sum x)^2} = c$$

Standard errors on a and b were obtained from the relationships:

$$\frac{\alpha_a^2}{n} = \frac{\alpha^2}{n \sum x^2 - (\sum x)^2}$$

$$\text{and } \alpha_b^2 = \frac{\alpha^2 \sum x^2}{n \sum x^2 - (\sum x)^2}$$

$$\alpha^2 = \frac{\sum d^2}{n-2}$$

where $d = ax + b - y$

An IBM 360 computer was used to carry out the above calculations.

Errors in the fracture mechanics data arise from three sources.

- 1) Measurement of the alternating load ΔP which is proportional to ΔK .

This error arises on both the Vibrophore and M.T.S. because of inherent design characteristics and amounts to approximately 1%.

- 2) Measurement of crack length gives rise to certain errors which influence ΔK through the Y function and also as a square root term. However, the

crack length - cycles data points are smoothed manually. Thus any errors due to local variations in the crack length will be negligible.

- 3) The most significant source of error occurs in the measurement of da/dN . This error will vary depending on the individual measuring the results, so that care should be exercised in comparing data from different sources. However table 25 shows the deviations in da/dN by measuring the same slopes on 6 identical curves. The agreement observed is reasonable and at worst amounts to $\pm 6\%$ about the mean.

All of these errors will be combined with the inherent deviation from linearity when the computer fits a straight line to a group of $\log \Delta K, \log da/dN$ points. Closer evaluation of the experimental scatter may be obtained by comparing the mean and standard deviations of a series of identical tests.

Errors quoted for stress life relationships also include statistical variations due to fatigue and experimental errors as described above. The average error in life was $\pm 2.6\%$ for three point bending, and it has been assumed that this error will be the same in the programmed loading tests.

CRACK LENGTH mm	CRACK GROWTH RATE $\frac{da}{dN}$							% DEVIATION FROM MEAN
	1	2	3	4	5	6	MEAN	
0.5	16	16	17	16	16	17	16.3	± 6.5
1.0	29	28	29	28	28	29	28.5	± 1.1
1.5	39	39	39	39	41	39	39.3	± 1.6
2.0	48	47	48	48	46	48	47.5	± 1.9
2.5	57	57	57	57	57	58	57.2	± 2.3
3.0	67	68	67	67	67	67	67.2	± 2.7
3.5	77	78	79	80	81	81	79.3	± 3.1
4.0	95	94	93	96	101	98	96.2	± 3.8
4.5	124	123	120	126	122	117	122.0	± 4.8
5.0	157	147	152	152	151	150	151.5	± 6.0

TABLE 25. DEVIATION IN CRACK GROWTH RATE MEASUREMENTS

APPENDIX 6

LIFE PREDICTION COMPUTER PROGRAMME

Full details of the integration programme listing are given in this appendix. The integration procedure consisted of dividing each block of the loading sequence into 1000 cycle units. The crack growth increment for each unit was then calculated from the relationship:

$$\frac{da}{dN} = C(\Delta K)^m$$

using the experimentally determined values of m and C . The increment was initially added onto the notch depth and the new stress intensity calculated from which the next crack growth increment was obtained and so on until the specified failure crack length was attained. The m and C values were varied according to the applied load level.

Before applying this approach to the programmed loading tests, integration was carried out for the constant amplitude situation using the appropriate m and C values for each load level. In all cases, deviations from the experimentally observed life occurred. However, slight adjustments of m value were found to bring the predicted life very close to the experimental value and the adjusted values were therefore used for the subsequent programmed loading calculations. Table 26 shows the effects of varying the m value on the constant amplitude life and also indicates the values selected.

This table also gives the number of cycles to initiate the crack for each load level based on experimental observations. This number of cycles was simply deducted from the first block of the programmed loading sequence before application in the computer programme and added back onto the computer predicted life so as to compare directly with the experimental values.

ALTERNATING LOAD lb (N)	C IMP. (SI)	EXPERIMENTAL LIFE	CYCLES TO INITIATE CRACK	m	COMPUTER PREDICTED LIFE
± 439 (1953)	2.1×10^{-20} (1.9×10^{-12})	1.69×10^5	12,000	3.20	1.83×10^5
				3.21	1.65×10^5
				3.215*	1.57×10^5
				3.22	1.50×10^5
				3.23	1.36×10^5
				3.24	1.23×10^5
± 358 (1593)	1.6×10^{-18} (5.2×10^{-12})	3.27×10^5	12,000	2.74	3.88×10^5
				2.75	3.54×10^5
				2.76*	3.22×10^5
				2.77	2.94×10^5
				2.78	2.68×10^5
± 305 (1357)	7.1×10^{-18} (8.9×10^{-12})	5.53×10^5	15,000	2.57	6.67×10^5
				2.58	6.08×10^5
				2.59*	5.55×10^5
				2.60	5.06×10^5
				2.61	4.62×10^5
± 233 (1036)	4.0×10^{-18} (6.2×10^{-12})	1.26×10^5	40,000	2.54	1.47×10^6
				2.55	1.34×10^6
				2.56*	1.22×10^6
				2.57	1.12×10^6
				2.58	1.02×10^6

* m value selected.

TABLE 26. ADJUSTMENT OF m VALUE

PROGRAMME LISTING

```

0001 DIMENSION AC(100),N(100),C(100),G(100),P(100)
0002 COMMON/PLK/E(5),R,M,TTF,AFAIL,ANOTCH
0003 READ(5,502)ATEST,NTEST,NBLOCK,NCODE,IJK
0004 IF(NBLOCK.EQ.0) GO TO 300
0005 READ(5,503)ANOTCH,AFAIL,R,W
0006 IF(IJK.EQ.0) GO TO 120
0007 READ(5,504)E,TTF
0008 GO TO 130
0009 CONTINUE
0010 E(1)=1.53
0011 E(2)=-3.07
0012 E(3)=14.53
0013 E(4)=-25.11
0014 E(5)=25.8
0015 TTF=6.0
0016 CONTINUE
0017 WRITE(6,551)ATEST,NTEST
0018 NT=0
0019 IF(NCODE-2)10,40,40
0020 NC=0
0021 WRITE(6,552)
0022 NC=NC+1
0023 IF(NC.GT.NBLOCK) GO TO 200
0024 READ(5,505)V(NC),C(NC),G(NC),P(NC)
0025 IF(NC.EQ.1)AT=ANOTCH
0026 IF(NC.GT.1)AT=AC(NC-1)
0027 CALL CRACK(AT,AC(NC),N(NC),C(NC),G(NC),P(NC),I,NK)
0028 NT=NT+N(NC)
0029 NT=NT-N(NC)
0030 CRA=AC(NC)-ANOTCH
0031 WRITE(6,553)NC,NT,CRA
0032 IF(CRA.LT.AFAIL)GO TO 20
0033 JA=NBLOCK-NC
0034 IF(JA.EQ.0)GO TO 110
0035 DO 30 J=1,JA
0036 LA=NC+J

```

```

00000020
00000030
45
50
00000070
75
00000090
81
82
83
84
85
86
87
88
89
90
99
00000100
00000110
00000120
00000130
00000140
150
00000160
00000170
00000180
00000190
00000200
00000205
00000210
00000215
00000220
00000225
00000230
00000235
00000240

```

```

0037 READ(5,505)N(LA),C(LA),G(LA),P(LA)
0038 CONTINUE
0039 GO TO 110
0040 CONTINUE
0041 NLEVEL=NCODE
0042 NCG=NBLOCK/NLEVEL
0043 WRITE(6,554)NCG,NLEVEL
0044 NC=2
0045 NC=0
0046 NC=NG+1
0047 DO 90 I=1,NLEVEL
0048 NC=(NC-1)*NLEVEL+I
0049 IF(NG.GT.1)GO TO 60
0050 READ(5,505)N(I),C(I),G(I),P(I)
0051 CONTINUE
0052 NT=NT+N(I)
0053 NTA=NT-N(I)
0054 IF(NC.EQ.1)AI=ANOTCH
0055 IF(NC.GT.1)AI=AC(NC-1)
0056 CALL CPACK(AI,AC(NC),N(I),C(I),G(I),P(I),I,NK)
0057 CRA=AC(NC)-ANOTCH
0058 WRITE(6,555)NC,NG,NT,CRA
0059 IF(NC.CF.NBLOCK)GO TO 200
0060 JF(CRA-AFAIL)GO,110,110
0061 CONTINUE
0062 GO TO 50
0063 CONTINUE
0064 IF(NC.EQ.1)RC=ANOTCH
0065 IF(NC.GT.1)RC=AC(NC-1)
0066 IF(NCODE.EQ.1)I=NC
0067 IF(NCODE.GT.1)I=NC-(NC-1)*NLEVEL
0068 CALL CRACK(RC,AZ,N(I),C(I),G(I),P(I),O,N7)
0069 I TOTAL=NTA+N7
0070 WRITE(6,556)ITOTAL
0071 WRITE(6,560)NZ
0072 FORMAT(1P5,20X,1H(,19,2X,22HCYCLES IN FINAL BLOCK))

```

```

00000245
00000250
00000255
00000260
00000270
00000280
00000290
00000300
00000310
00000320
00000330
00000340
00000350
00000360
00000370
00000380
00000395
00000400
00000410
00000420
00000430
00000440
00000450
00000490
00000500
00000510
00000515
00000520
00000530
00000535
00000540
00000550
00000740
00000743
00000746

```

```

0073 WRITE(6,557)ATEST,NTEST 750
0074 WRITE(6,558)B,N,ANOTCH,AFAIL 00000770
0075 WRITE(6,602) 771
0076 IF(NCODE.NE.2) WRITE(6,601)(N(LB),C(LB),G(LB),P(LB),LR=1,NBLOCK) 771
0077 IF(NCODE.EQ.2) WRITE(6,601)(N(LC),C(LC),G(LC),P(LC),LC=1,NLEVEL) 772
0078 GO TO 100
0079 FORMAT(1H,20X,37HELECTURE MECHANICS PREDICTION OF LIFE/1H,20X,3200000780
551 1H,MULTI-LEVEL FATIGUE TEST NUMBER ,A7,I3) 300
552 FORMAT(//1H+,20X,17HRANDOM BLOCK TEST//1H,20X,12HBLOCK NUMBER,5X,0000000810
553 16HCYCLES,6X,24HCRACK LENGTH (IN.) AT END OF BLOCK) 000000020
554 FORMAT(1H,20X,I3,I1X,I8,6X,E7.4) 000000030
555 FORMAT(//1H,20X,21HPROGRAMMED BLOCK TEST/1H,10X,6HUP TO ,I3,2X,20000000840
556 12HBLOCKS WITH ,I3,2X,21HSTRESS LEVELS IN EACH//1H,17X,10000000850
557 22HBLOCK NUMBER,5X,12HGROUP NUMBER,5X,6HCYCLES,5X,34HCRACK LENGTH (0000000860
3IN.) AT END OF BLOCK) 000000070
558 FORMAT(1H,20X,I3,I1X,I3,I1X,I9,6X,E7.4) 000000090
559 FORMAT(///1H,20X,17HPREDICTED LIFE = ,I9,2X,6HCYCLES) 000000090
560 FORMAT(1H,20X,1TEST NUMBER ,A7,I2/1H,20X,1TEST AND SPECIMEN DET 000
561 AILS') 000
562 FORMAT(//1H,20X,6HDEPTH = ,I3,56.3,I3,3HIN./1H,20X,8HWIDTH = ,5000000920
563 16.3,I3,3HIN./1H,20X,14HNOTCH DEPTH = ,F6.3,I3,3HIN./1H,20X,16HFA000000930
564 21HUP CRACK = ,F6.3,I3,3HIN.) 000000040
565 FORMAT(A7,I3,6I5) 050
566 FORMAT(4E10.0) 040
567 FORMAT(4E10.0) 070
568 FORMAT(110,3E10.0) 020
569 CONTINUE 000000000
570 WRITE(6,550) 00001000
571 WRITE(6,557)ATEST,NTEST 1003
572 WRITE(6,558)B,N,ANOTCH,AFAIL 00001005
573 WRITE(6,602) 1006
574 IF(NCODE.NE.2) WRITE(6,601)(N(LB),C(LB),G(LB),P(LB),LR=1,NBLOCK) 1010
575 IF(NCODE.EQ.2) WRITE(6,601)(N(LC),C(LC),G(LC),P(LC),LC=1,NLEVEL) 1011
576 GO TO 100 00001020
577 CONTINUE 00001070

```



```

0100          559  FORMAT(//IHO,55)FAILURE CRACK NOT REACHED IN SPECIFIED NUMBER OF 300001000
0101          601  1LOCKS)
0102          602  FORMAT(IHO,I0X,I13,I5X,I10,510,3,15X,F6.3,15X,F8.2)
0103          603  FORMAT(IHC,I0X,'BLOCK DETAILS',IHO,I0X,'NO. OF CYCLES',16X,'C-VALU
0104          604  I5,I7X,'M-VALUE',16X,'LOAD RANGE (LRF.)')
0105          605  STOP
0106          606  END
0001          SUBROUTINE CRACK(AI,AF,M,C,G,P,K,NK)
0002          607  DIMENSION A(1000),Y(1000),F(1000)
0003          608  COMMON/PLK/E(5),P,W,ITE,AFAIL,ANOTCH
0004          609  IF(M.FO.0)GO TO 005
0005          610  DN=Y/000.0
0006          611  A(I)=AI
0007          612  I=1
0008          613  Y(I)=E(1)+E(2)*(A(I)/h)+E(3)*(A(I)/W)**2+E(4)*(A(I)/W)**3+E(5)*(A(
0009          614  I)/h)**4
0010          615  F(I)=C*(ITE*Y(I)+P*SORT(A(I)))/(3*W)**G
0011          616  A(I+1)=A(I)+F(I)*DN
0012          617  IF(A(I+1).GE.W) GO TO 004
0013          618  IF(K.EC.1)GO TO 002
0014          619  IF(A(I+1).GL.(AFAIL+ANOTCH))GO TO 003
0015          620  CONTINUE
0016          621  NK=0
0017          622  I=I+1
0018          623  IF(I.LT.1000)GO TO 001
0019          624  IF(I.EQ.1000)AF=A(1000)
0020          625  GO TO 006
0021          626  NK=(I-1)*DN
0022          627  AF=A(I)
0023          628  GO TO 006
0024          629  NK=0
0025          630  AF=A(I)
0026          631  GO TO 006
0027          632  AF=AI
0028          633  NK=0
0029          634  CONTINUE
0030          635  RETURN
0031          636  END
0001110
00001120
00001130
00001140
00001150
00001160
00001170
00001180
00001190
00001200
00001210
00001220
00001230
00001240
00001250
00001260
00001270
00001280
00001290
00001300
00001310
00001320
00001330
00001340
00001350
00001360
00001370
00001380
00001390
00001400
00001410
00001420
00001430

```